

THE SEISMIC STRUCTURES OF THE U.S. PACIFIC NORTHWEST AND THE
SCALING AND RECURRENCE PATTERNS OF SLOW SLIP EVENTS

by

HAIYING GAO

A DISSERTATION

Presented to the Department of Geological Sciences
and the Graduate School of the University of Oregon
in partial fulfillment of the requirements
for the degree of
Doctor of Philosophy

March 2011

DISSERTATION APPROVAL PAGE

Student: Haiying Gao

Title: The Seismic Structures of the U.S. Pacific Northwest and the Scaling and Recurrence Patterns of Slow Slip Events

This dissertation has been accepted and approved in partial fulfillment of the requirements for the Doctor of Philosophy degree in the Department of Geological Sciences by:

Eugene Humphreys	Chairperson
David Schmidt	Member
Ray Weldon	Member
James Isenberg	Outside Member

and

Richard Linton	Vice President for Research and Graduate Studies/Dean of the Graduate School
----------------	--

Original approval signatures are on file with the University of Oregon Graduate School.

Degree awarded March 2011

© 2011 Haiying Gao

DISSERTATION ABSTRACT

Haiying Gao

Doctor of Philosophy

Department of Geological Sciences

March 2011

Title: The Seismic Structures of the U.S. Pacific Northwest and the Scaling and Recurrence Patterns of Slow Slip Events

Approved: _____
Dr. Eugene D. Humphreys

The Pacific Northwest of the United States has been tectonically and magmatically active with the accretion of the Farallon oceanic terrane “Siletzia” ~50 Ma. The accretion of Siletzia terminated the flat-slab subduction of the Farallon slab and initiated the Cascadia subduction zone. In this dissertation, I focus on both the large-scale tectonic structures preserved seismically in the crust and upper mantle, and the small-scale, short-term aseismic processes on the plate interface.

I measure the shear-wave splitting trends around eastern Oregon with a dataset of ~200 seismometers from 2006-2008 to analyze the upper-mantle anisotropy. The delay times between splitted shear-waves range from 0.8 s to 2.7 s. In the High Lava Plains, the fast polarization direction is approximately E-W with average delay time ~1.8 s. I infer that there must be significant active flow in a roughly E-W direction in the asthenosphere beneath this area. The splitting pattern is more variable and complicated in NE Oregon, where the crust and mantle lithosphere may be a significant contribution.

In terms of the imaged seismic velocity structures, I infer that the Eocene sedimentary basins in south-central Washington lie above a magmatically underplated crust of extended Siletzia lithosphere. Siletzia thrusts under the pre-accretion forearc, and its southeast termination is especially strong and sharp southeast of the Klamath-Blue Mountains gravity lineament. Magmatic intrusion has increased upper crustal velocity as in the less active Washington Cascades, but the higher temperatures beneath the magmatically active Oregon Cascades have a dominating effect.

To better understand the physical mechanism of slow slip events on the plate interface, I explore the scaling relationships of various source parameters collected mainly from subduction zones worldwide and also other tectonic environments. The source parameter scaling relationships of slow slip events highlight the similarities and differences between slow slip phenomena and earthquakes. These relationships hold implications for the degree of heterogeneity and fault healing characteristics. The recurrence statistics of northern Cascadia events behave weakly time predictable and moderately anti-slip predictable, which may indicate healing between events.

This dissertation includes co-authored materials both previously published and submitted for publication.

CURRICULUM VITAE

NAME OF AUTHOR: Haiying Gao

PLACE OF BIRTH: People's Republic of China

GRADUATE AND UNDERGRADUATE SCHOOLS ATTENDED:

University of Oregon, Eugene
Ocean University of China, Qingdao, P.R. China

DEGREES AWARDED:

Doctor of Philosophy, Geophysics, 2011, University of Oregon
Master of Science, Geophysics, 2005, Ocean University of China
Bachelor of Science, Geology, 2002, Ocean University of China

AREAS OF SPECIAL INTEREST:

Seismology
Tectonics

GRANTS, AWARDS, AND HONORS:

Graduate Teaching Fellowship, Geological Sciences, 2005 to present

Thayer Scholarship, University of Oregon, 2006

President of Chinese Scholar and Student Association, University of Oregon,
2007

Waiser Awards, the Graduate School, University of Oregon, 2010

PUBLICATIONS:

Gao, H., D. A. Schmidt, and R. J. Weldon (2011), Scaling relationships of source parameters for slow slip phenomena, submitted for review.

- Gao, H., E. D. Humphreys, H. Yao, and R. D. Van der Hilst (2011), Crustal and lithosphere structure of the Pacific Northwest with ambient noise tomography: Terrane accretion and Cascade arc development, *Earth Planet. Sci. Lett.* doi:10.1016/j.epsl.2011.01.033.
- Schmidt, D. A., and H. Gao (2010), Source parameters and time-dependent slip distributions of slow slip events on the Cascadia subduction zone from 1998 to 2008, *J. Geophys. Res.* 115, B00A18, doi:10.1029/2008JB006045.
- Long, M. D., H. Gao, A. Klaus, L. S. Wagner, M. J. Fouch, D. E. James, E. Humphreys (2009), Shear wave splitting and the pattern of mantle flow beneath eastern Oregon, *Earth Planet. Sci. Lett.* 288, 359-369, doi:10.1016/j.epsl.2009.09.039.

ACKNOWLEDGMENTS

There are so many people that I wish to express my sincere appreciation. First, I'd like to thank my two PhD advisors, Eugene Humphreys and David Schmidt, for providing the opportunities and projects for me. I enjoy working with them so much and benefit from their patience, generosity, willingness to assist students, and breadth of knowledge in seismology and tectonics. I'd also like to thank Pat Ryan, a field technician, who was in charge of the field work and taught me a lot about instrument deployment. Thank you to Ray Weldon, the collaborator in the Cascadia project, with whom I benefit the discussion.

In addition, special thanks are due to Dr. van der Hilst in MIT and Dr. Huajian Yao in UCSD, who provided the methodology of ambient noise tomography. I benefit the discussion with them.

I need to thank my officemates Leland O'Driscoll and Brandon Schmandt, who are both great friends and colleagues. I need to thank my wonderful roommate, Isolde Belien, who always has been so helpful and friendly in many aspects. And thank you to many others who have helped me during my study here and had lots of fun together.

Finally, I would like to show my deep appreciation to my family, who is the best wealth for me in my life. Thank you for being supporting my study in the United States, and always being patient whenever I need a listener.

For my parents, who are the mentors of my life and always support me.

TABLE OF CONTENTS

Chapter	Page
I. INTRODUCTION.....	1
II. SHEAR WAVE SPLITTING AND THE PATTERN OF MANTLE FLOW BENEATH EASTERN OREGON.....	6
1. Introduction.....	6
2. Tectonic, Geologic, and Geophysical Setting.....	9
3. Date and Methods.....	13
4. Results	18
5. Interpretation.....	26
5.1. Distinguishing between Lithospheric and Asthenospheric Anisotropy....	26
5.2. Implications for Mantle Flow.....	29
5.3. The Source of the Large Delay Times.....	31
5.4. Explaining Lateral Variations in Delay Times in the HLP.....	34
5.5. Implications for the Tectonic Evolution of Eastern Oregon.....	35
6. Outlook and Summary.....	36
III. CRUST AND LITHOSPHERE STRUCTURE OF THE NORTHWESTERN U.S. WITH AMBIENT NOISE TOMOGRAPHY: TERRANE ACCRETION AND CASCADE ARC DEVELOPMENT	40
1. Introduction.....	40
2. Geological Setting.....	43
3. Date and Methods.....	46

Chapter	Page
4. Results	51
4.1. Siletzia Terrane.....	55
4.2. Western Columbia Basin	56
4.3. Cascade Mountain Range.....	56
4.4. Columbia River Basalt Source Area.....	57
5. Discussion.....	58
5.1. Distribution of Siletzia Lithosphere within North America.....	59
5.2. Rifting Origin of the Western Columbia Basin.....	61
5.3. Cascades.....	63
5.4. Columbia River Basalt Source Area.....	64
6. Conclusions.....	65
IV. SOURCE PARAMETERS AND TIME-DEPENDENT SLIP DISTRIBUTIONS OF SLOW SLIP EVENTS ON THE CASCADIA SUBDUCTION ZONE FROM 1998-2008	67
1. Introduction.....	67
2. GPS Data	71
3. Time-Dependent Inversions.....	73
4. Inversion Results.....	76
4.1. July 1998 Event	77
4.2. August 1999 Event	79
4.3. December 1999 Event.....	79

Chapter	Page
4.4. December 2000 Event.....	80
4.5. April 2001 Event	80
4.6. February 2002 Event.....	80
4.7. February 2003 Event.....	81
4.8. January 2004 Event.....	82
4.9. May 2004 Event	82
4.10. July 2004 Event	82
4.11. April 2005 Event	83
4.12. September 2005 Event.....	83
4.13. December 2005 through January 2006 Event Sequence.....	84
4.14. January 2007 Event.....	85
4.15. July 2007 Event	85
4.16. May 2008 Event.....	85
4.17. Other Poorly Resolved Events.....	86
5. Discussion.....	87
5.1. Event Statistics	90
5.2. Implications for Slow Slip Processes.....	93
6. Conclusions.....	95
V. SCALING RELATIONSHIPS OF SOURCE PARAMETERS FOR SLOW SLIP PHENOMENA.....	97
1. Introduction.....	97

Chapter	Page
2. Slow Slip Data Set.....	98
3. Empirical Scaling Laws of SSEs.....	99
3.1. Fault Length versus Width.....	99
3.2. Seismic Moment versus Fault Area.....	100
3.3. Seismic Moment versus Event Duration.....	103
3.4. Average Rupture Velocity versus Seismic Moment.....	104
3.5. Rupture Duration versus Rise Time	107
3.6. Recurrence Statistics.....	108
4. Conclusions.....	111
VI. CONCLUSIONS	113
REFERENCES CITED.....	118

LIST OF FIGURES

Figure	Page
2.1. Geologic Map of Eastern Oregon	7
2.2. Map of Stations Used in This Study.....	14
2.3. Map of Earthquake Distribution	16
2.4. An Example of a High-quality (“Good”) Measurement	19
2.5. Splitting Result for All Stations.....	20
2.6. Examples of Detailed Splitting Patterns.....	22
2.7. Histogram of Splitting Pattern.....	25
2.8. Map of Average Splitting Parameters	26
2.9. A Horizontal Slice.....	32
3.1. Geological Structures of the U.S. Pacific Northwest.....	42
3.2. The Station Distribution Used in This Study.....	47
3.3. Inversion Result at One Grid Point.....	50
3.4. Fundamental-mode Rayleigh-wave Phase Velocity	52
3.5. Shear-wave Velocity Variation.....	53
3.6. Imaged Shear-wave Velocity Anomaly Model.....	54
3.7. Vertical Cross Section along the Cascade	54
3.8. Cartoon Cross Section.....	59
4.1. A Map of the Cascadia Subduction Zone.....	69
4.2. Detrended GPS Time Series	72
4.3. Seasonal Trends	74

Figure	Page
4.4. The Estimated Slip Distribution for 16 Slow Slip Events.....	78
4.5. Cumulative Slip Pattern.....	88
4.6. Plot of Source Parameters.....	91
5.1. The Relationship of Along-strike Fault Length versus Downdip Fault Width	100
5.2. The Logarithmic Relationship of Seismic Moment versus Fault Area.....	102
5.3. The Relationship of Seismic Moment with Event Duration.....	104
5.4. The Relationship of Average Rupture Velocity with Seismic Moment.....	106
5.5. The Relationship of Event Duration versus Rise Time.....	109
5.6. Recurrence Statistics for Slow Slip Events	110

CHAPTER I

INTRODUCTION

Accretion of the Farallon oceanic terrane “Siletzia” to the Pacific Northwest of the United States ~50 Ma causes a westward jump in subduction to the modern-day Cascadia subduction zone. At this latitude and time, the contractional and anmagmatic Laramide orogeny ended, intense post-Laramide lithospheric extension and magmatism within Siletzia and adjacent North America began, and soon thereafter, the Cascade volcanic arc was established across Siletzia. The distribution of the oceanic Siletzia terrane is well constrained west of the Cascades in terms of the sampled outcrops and the magnetic anomaly. However, east of the Cascades because of the wide coverage of the erupted Columbia River Flood Basalt in northern Oregon and most of Washington, the distribution of Siletzia is unclear. Most of eastern Washington lies at low elevation and acts as a rigid block in term of the clockwise rotation pattern from the GPS analysis. Moreover, this area is surrounded by active magmatism in northeastern Washington and most of Idaho ~50 Ma. This anomalous behavior in the western U.S. is expected for the accretion of the subducted oceanic lithosphere into the continent. Thus, a better image of the sub-surface distribution of the oceanic lithosphere will help to understand the subduction and accretion process.

With the deployment of the EarthScope USArray Transportable Array in the western United States since 2006, in conjunction with many other flexible projects at the same time period, the large-scale upper-mantle structure of the U.S. Pacific Northwest has been well imaged and constructed, especially with the improvement of seismological

methods. However, a joint study of the crustal velocity structure with the tectonics of the U.S. Pacific Northwest has not been done. A high-resolution crustal velocity model is required which, for example, is important for the resolution and precision of teleseismic body-wave tomography.

In recent years, slow slip and tremor events have been discovered on subduction zones worldwide, including Cascadia, Nankai, Hikurangi, Aleutian, and Middle American. The location of this phenomenon has been proposed to be downdip of the transition zone providing a good opportunity to study the faulting processes on a region of the plate interface. Fluid is thought to be critical for its occurrence. The occurrence of slow slip events on subduction zones may accumulate and release the strain downdip of the transition zone regularly. However, whether the occurrence of this phenomenon increases or decreases the probability of next mega-earthquake is still an enigma, therefore, imposing a need to better understand its physical mechanism. Also, slow slip and tremor events have been proposed to be a candidate to study the rupture mechanics of faults considering their short-term recurrence intervals compared to the sparse historical records of large earthquakes. Thus, it is important to explore the similarities and differences between slow slip events and earthquakes.

With the deployment of more geodetic and seismic instruments by PASSCAL (Program for Array Seismic Studies of the Continental Lithosphere) and UNAVCO (University NAVSTAR Consortium) since 2005 in the Pacific Northwest, much progress has been made in understanding the newly-discovered slow slip and non-volcanic tremor events on the Cascadia subduction zone. Some features appear to be very complex, for example, propagation reversals to the major trend along strike, updip migration faster

than the along-strike propagation, and fast-then-slow rupture pattern along strike have been reported for non-volcanic tremor. The precise location of the tremor source, whether above or on the fault interface, is still on debate, as well as the causal relationship of transient slip with tremor. The unresolved issues with slow slip prompts further study of the role of fluid, the faulting processes, numerical simulations, as well as the laboratory experiments. Additionally, the physical mechanism of the slow slip and tremor phenomenon is still not well understood although hypothesis have been proposed (e.g., shear slip on faults, the remote-triggering of surface-waves, and the periodic tidal loading).

In this dissertation the tectonic features of the Pacific Northwest of the United States since the Cenozoic, especially the accretion of oceanic Siletzia terrane and the development of the Cascade arc, are reconstructed in terms of the seismic images, in conjunction with the tectonic histories in Chapters II and III. I start by analyzing the upper-mantle anisotropy with SKS-splitting method beneath eastern Oregon and its surroundings (Chapter II). A very subtle anisotropy pattern is observed in NE Oregon where the Columbia River Flood Basalt eruption occurred in comparison with the nearly E-W splitting pattern of the High Lava Plains. The origin of the approximately E-W fast polarization direction as well as the large delay times between splitted shear-waves (~ 1.8 s on average) in the High Lava Plains are proposed and discussed. I apply fundamental-mode Rayleigh-wave ambient noise tomography to solve the layered seismic velocity structures of the U.S. Pacific Northwest (Chapter III). In this study I construct a 3D shear-wave velocity model of the crustal and uppermost mantle of the U.S. Pacific Northwest. The accretion of the Siletzia and the development of the Cascade arc are

reinterpreted in terms of the tomography results. In general, the results presented in these two chapters provide a general pattern of the upper-mantle anisotropy in eastern Oregon and its surroundings, and a high-resolution 3D velocity structure of the U.S. Pacific Northwest

In Chapters IV and V, the characteristics of slow slip events on the Cascadia subduction zone have been resolved and the general scaling relationships of worldwide slow slip events have been explored to understand better the physical mechanism. In Chapter IV, I process GPS daily time series from 1998 to 2008 to invert for the time-dependent slip distributions of 16 slow slip events on the Cascadia subduction zone. The slip patterns of individual events are described. Following this work, I explore the general scaling relationships of source parameters for slow slip phenomena and discuss the implications of these scaling laws for the physical mechanisms (Chapters V).

I am the first author on Chapters III and V in this dissertation, and the second author on Chapters II and IV. I am responsible for the data analysis, the development of the methodologies and the interpretations of the results in each chapter. Chapter II has been published in *Earth and Planetary Science Letters* in 2010 and coauthored with 6 others, Dr. Maureen Long (the primary author, Yale University), Amanda Klaus (Scripps College), Dr. Lara Wagner (University of North Carolina), Dr. Matthew Fouch (Arizona State University), Dr. David James (Carnegie Institution of Washington), and my advisor, Dr. Eugene Humphreys. All assisted in the editorial process, and Dr. Maureen Long and I are responsible for the data analysis of the SKS-splits. Chapter III has been published by *Earth and Planetary Science Letters* in 2011. This manuscript is coauthored with my advisor, Eugene Humphreys, and Dr. Huajian Yao (SCRIPPS, UCSD) and Dr. Robert

van der Hilst (MIT). All coauthors assisted with the editorial process, and Pat Ryan, the field technician, aided with instrument deployment and data collection in the field. Dr. Huajian Yao and Dr. Robert van der Hilst provided the initial ambient noise tomography programs. Chapter IV has been published in the *Journal of Geophysical Research* in 2010. This manuscript is coauthored with my advisor, David Schmidt (who is the first author). I assisted with the editorial process, and I am responsible for data processing, running the time-dependent inversions, and analyzing the results with the guidance of David Schmidt. Chapter V has been submitted for review, and is coauthored with my advisor David Schmidt and committee member Ray Weldon. All collaborators assisted in the editorial process. Chapter VI is a synthesis of the work discussed in the previous chapters.

CHAPTER II
SHEAR WAVE SPLITTING AND THE PATTERN OF MANTLE FLOW
BENEATH EASTERN OREGON

This work was published in volume 288 of *Earth and Planetary Science Letters* in October, 2009. Coauthors Maureen Long (the first author), Amanda Klaus, Lara Wagner, Matthew Fouch, David James, and Eugene Humphreys aided in the editorial process. I performed the work on the northern part of the studied area and was the second author.

1. Introduction

Varied tectonic and geological terranes comprise the Cascadian backarc of eastern Oregon, including the volcanically active High Lava Plains (HLP) and the older Mesozoic accreted terranes of the Blue and Wallowa Mountains. The region is bounded by the Columbia River Basalt group to the north, the arc volcanoes of the Cascades to the west, and Precambrian North America to the east, and it transitions into extensional Basin and Range to the south (Fig. 2.1). The region's recent geological history is dominated by voluminous intraplate magmatism, with the appearance of the Columbia River and Steens flood basalts along the western margin of the North American craton at ~17–15 Ma followed by a still ongoing period of bimodal (basaltic and silicic) volcanism in both the High Lava Plains and Snake River Plain to the east. The causes of this ongoing tectonomagmatic activity and its relationship to other tectonic processes, such as the uplift of the Wallowa Mountains in northeastern Oregon, are not well understood. A variety of models for the widespread volcanism has been proposed, which variously

invoke the inferred Yellowstone plume (e.g., Camp and Ross, 2004), rollback and steepening of the Cascadia slab (e.g., Carlson and Hart, 1987), lithospheric extension related to the Basin and Range to the south (e.g., Cross and Pilger, 1978), localized lithospheric delamination (Hales et al., 2005), or a combination of these processes. A consensus on which model best explains the current range of geological, geochemical, petrological, and geophysical data, however, has not been forthcoming.

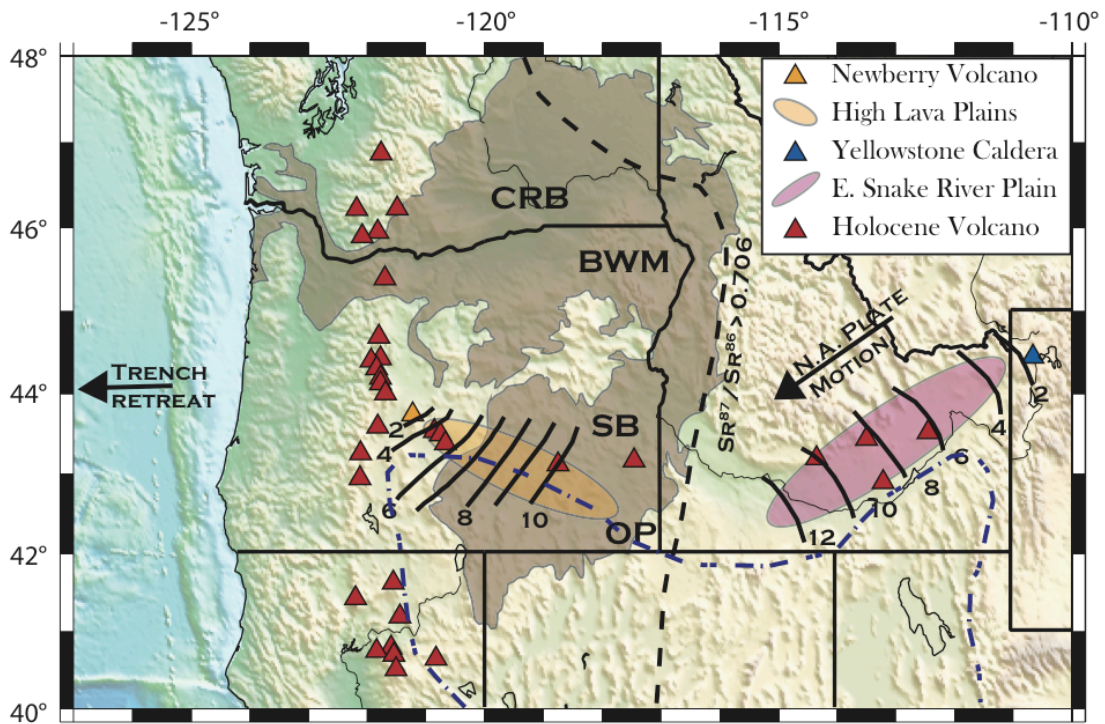


Figure 2.1. Geologic map of eastern Oregon and the surrounding region. Black contours indicate the age progression (in Ma) of silicic volcanism along both the High Lava Plains (Jordan et al., 2004), shown in yellow, and the Snake River Plain (Christiansen et al., 2002), shown in pink. The black dashed line shows the location of the $^{87}\text{Sr}/^{86}\text{Sr}=0.706$ line, commonly interpreted to mark the boundary between cratonic North America to the east and the accreted arc terranes to the west. The blue dashed line shows the northern limits of Basin and Range extension. The brown highlighted area indicates the region covered by Miocene flood basalts, including the Columbia River basalts (CRB) to the north and the Steens basalts (SB) farther to the south. Red triangles indicate locations of Holocene volcanism. The geographical locations of the Owyhee Plateau (OP) and the Blue and Wallowa mountains (BWM) are also shown, along with Newberry Volcano (orange triangle) and Yellowstone Caldera (blue triangle). The arrow at the Cascadia trench indicates its direction of motion; the trench is retreating at a rate of ~ 30 mm/yr in a Pacific hotspot reference frame (Schellart et al., 2008).

One important discriminant among the many models that have been proposed for the tectonic evolution of eastern Oregon is the geometry of upper mantle flow. Constraints on this mantle flow can be inferred from measurements of elastic anisotropy, which manifests itself in the seismic wavefield in several different ways. In the upper mantle, seismic anisotropy is generally ascribed to the crystallographic or lattice preferred orientation (LPO) of individual mineral crystals (primarily olivine) that are themselves anisotropic (e.g., Karato et al., 2008). When a volume of mantle rock is subjected to strain under dislocation creep conditions, it develops an LPO, and the resulting anisotropy can be measured using seismological techniques. Anisotropy resulting from shape preferred orientation of partial melt lenses (e.g., Zimmerman et al., 1999) may also be important beneath the HLP, particularly given the evidence of high uppermost mantle temperatures in that region (e.g., Warren et al., 2008). The measurement of the splitting or birefringence of seismic shear waves (particularly core-refracted phases such as SKS) represents one of the most direct ways to probe anisotropy in the upper mantle (for overviews, see Silver, 1996; Savage, 1999; Fouch and Rondenay, 2006; Long and Silver, 2009). However, because splitting is a path integrated measurement, anisotropy anywhere along the receiver side of the SKS ray path will contribute to the observed splitting and in practice this means that the depth resolution of splitting measurements is poor. In particular, in continental settings it can be difficult to distinguish between lithospheric anisotropy that developed as a consequence of past deformational processes and anisotropy in the asthenosphere that is associated with active mantle flow. Despite these difficulties, however, splitting measurements when properly interpreted can yield tight constraints on the geometry of mantle flow beneath a seismic

station, and can help to distinguish among different models for past and ongoing tectonic processes.

In this study we present measurements of SKS splitting at 200 broadband stations in eastern Oregon and the surrounding regions (central Oregon, western Idaho, northern Nevada, and southeastern Washington). The goal of this effort is not only to characterize SKS splitting using an extremely dense broadband array, but also to use these measurements and other geophysical observations to distinguish between lithospheric and asthenospheric contributions to anisotropy and to characterize the pattern of active mantle flow beneath eastern Oregon. These inferences can then be placed in the context of the shear wave splitting pattern observed in the western United States (e.g., Zandt and Humphreys, 2008; Fouch and West, in preparation) and used to discriminate among the many models for the recent tectonic evolution of the region. In this paper, we focus on the presentation of the highest-quality measurements from the splitting data set in order to present a first-order picture of shear wave splitting, upper mantle anisotropy, and mantle flow beneath the region.

2. Tectonic, geologic, and geophysical setting

The western United States in general and the region surrounding Eastern Oregon in particular has a rich and complicated tectonic history (for a recent overview, see Humphreys and Coblenz, 2007). Extensive magmatic activity in eastern Oregon has been documented beginning in the Cenozoic, when the so-called “ignimbrite sweep” (e.g., Lipman et al., 1972) resulted in large-volume silicic magmatism over much of western North America between 50 and 20 Ma. Between 17 and 15 Ma, volcanic activity

in the region was dominated by the massive flood basalt eruptions that began in the McDermitt area near the Oregon/Idaho/Nevada border with the Steens basaltic volcanism. Following the Steens event, flood volcanism propagated northward along the western edge of Precambrian North America, culminating in the voluminous outpourings of Columbia River basalts. Since approximately 14–12 Ma, volcanic activity in eastern Oregon has been dominated by major eruptions along the temporally migrating volcanic track of the High Lava Plains that extends from southeastern Oregon northwest to Newberry volcano in the Cascades (Fig. 2.1). In an almost mirror image, the considerably more voluminous Yellowstone-Snake River Plain (YSRP) volcanism followed a contemporaneous migration northeastward from the McDermitt caldera area in northern Nevada to Yellowstone in Montana, producing a prominent volcanic lineament that has been widely interpreted as corresponding to the trace of the Yellowstone hot spot track (e.g., Pierce and Morgan, 1992). For both HLP and YSRP, the volcanism is characterized by bimodal silicic and basaltic eruptions. In the HLP, the silicic volcanism exhibits an age progression from southeast to northwest that has been documented using $^{40}\text{Ar}/^{39}\text{Ar}$ dating (Jordan et al., 2004), but basaltic volcanic activity has been widespread and there are Holocene basalt flows in disparate locations (Fig. 2.1). To the north of the HLP, the Blue and Wallowa mountains are composed of older Mesozoic accreted terranes; the Wallowas in particular underwent significant uplift during and after the Columbia River basalt eruptions (Hales et al., 2005).

A variety of models has been proposed to explain the formation of the High Lava Plains and the tectonic evolution of eastern Oregon. A primary question is whether or not it is necessary to invoke a mantle plume to explain HLP volcanism. Models that invoke a

plume as the origin for both the Columbia River/Steens flood basalts and the HLP/YSRP volcanic trend have been proposed (e.g., Camp and Ross, 2004), but the role of a mantle plume in northwestern US volcanism continues to be hotly debated (e.g., Humphreys et al., 2000; Jordan, 2005; Hooper et al., 2007). Alternative models invoke asthenospheric inflow due to the rollback and steepening of the Cascadia slab (Carlson and Hart, 1987), significant lithospheric extension associated with the extensional Basin and Range to the south (Cross and Pilger, 1978), or backarc spreading processes (e.g., Christiansen and McKee, 1978; Smith, 1992). It remains unclear what role “topography” at the base of the lithosphere may have played in shaping the evolution of the HLP: for example, Jordan et al. (2004) suggested that buoyant plume material may have been guided along the thinning lithosphere to the northwest beneath the HLP, although lithospheric basal topography may play an equally important role in non-plume models as well. It has also been suggested that lithospheric delamination processes may have played a role in the tectonic evolution of eastern Oregon: Hales et al. (2005) proposed a delamination model to explain the location and timing of both the Columbia River basalt eruptions and the significant uplift (~2 km) of the Wallowa mountains. A consensus about which process (or combination of processes) is responsible for the volcanic and tectonic evolution of eastern Oregon has not yet been reached, but a detailed examination of shear wave splitting patterns in the region provides a promising way to discriminate among the many models because these models make substantially different predictions about contemporary flow processes in the upper mantle. For example, a plume model (e.g., Camp and Ross, 2004) would predict mantle flow radiating out from the presumed plume head location in southeastern Oregon, with flow along the strike of the HLP trend, while

a model that invokes slab rollback and steepening (e.g., Carlson and Hart, 1987) would predict mantle flow in the direction of trench migration.

In addition to shear wave splitting, other geophysical observations can be brought to bear in order to discriminate among the different models. For example, new tomographic images of isotropic wave-speed velocities are yielding insight into mantle structure beneath the region. Several tomographic models for the western US have recently been published (e.g., Burdick et al., 2008; Roth et al., 2008; Sigloch et al., 2008) that provide an unprecedented level of detail. In particular, Roth et al. (2008) imaged several striking structural features in the upper mantle beneath the region, including an increased-velocity anomaly that is interpreted to be the Juan de Fuca slab, pronounced reduced-velocity anomalies beneath Newberry volcano, north-central Oregon, and (especially) the YSRP, reduced velocities in the uppermost mantle (~50–125 km depth) beneath the HLP, and increased velocities extending deep into the upper mantle beneath the Blue Mountains. The present-day crustal deformation field can also be used to discriminate among models for the tectonic evolution of eastern Oregon; crustal deformation has been studied in this region using GPS (e.g., McCaffrey et al., 2000, 2007). Block models that have been produced to match the GPS observations indicate that eastern Oregon is currently undergoing rigid rotation about a pole located in northeastern Oregon or Idaho, with very little present-day crustal strain (McCaffrey et al., 2007).

3. Data and methods

Data from three different broadband seismic experiments are used in this study; a station map is shown in Fig. 2.2. First, we utilize data from the Transportable Array (TA) seismic component of USArray, which will eventually cover the entire continental United States with an average station spacing of ~70 km. We present measurements for TA rows E (which covers southern Washington state and northern Idaho) through M (which covers northern California and northern Nevada), and TA columns 05–11 (that is, E05–E11, F05–F11, etc., through M05–M11), for a total of 62 stations. TA stations in this region were generally installed between late 2005 and mid-2006 and demobilized in mid- to late 2008. Second, the High Lava Plains (HLP) seismic experiment consists of an array of 118 broadband instruments, with a maximum of 104 currently operating (as of late 2008). The first stations in the HLP array were installed in early 2006; the bulk of the array was installed in mid-2007. The HLP station configuration consists of two dense lines, one of which stretches from the eastern Owyhee Plateau in southwest Idaho to Bend, Oregon (Fig. 2.2) and follows the spatiotemporal trend in the silicic volcanism (Jordan et al., 2004). The second line is aligned N-S and is designed to probe the transition from (south to north) Basin and Range extension to High Lava Plains volcanism to the accreted terranes of the Blue Mountains. The average station spacing along the dense lines is ~15–20 km and they are surrounded by “clouds” of stations with sparser spatial coverage. The third source of data is the Wallowa Mountains experiment, which began in Fall 2006. This experiment consists of an initial deployment of 20 stations around the Wallowa Mountains; in May 2008 10 instruments were moved to create a 30-station array. The stations extend across the Precambrian continental margin to the east and north of the

Wallowa Mountains and also sample the transition across the old oceanic embayment to the northwest. Together, these three deployments provide extremely dense spatial sampling of eastern Oregon and the surrounding regions.

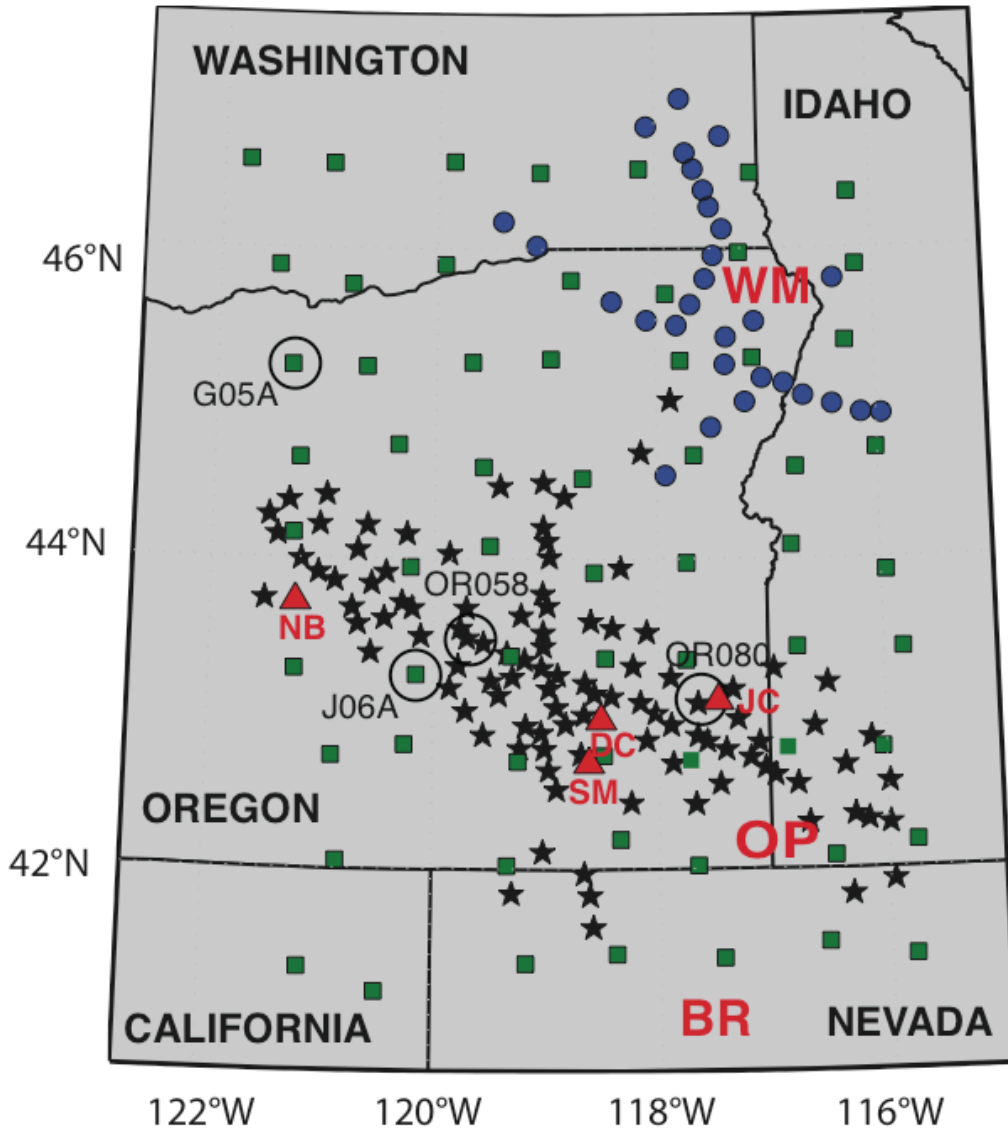


Figure 2.2. Map of stations used in this study, including those from the Transportable Array (TA) (squares), the Wallowa Array (circles), and the High Lava Plains (HLP) array (stars). State names are shown and geographical features are marked for reference: the Basin and Range (BR), the Owyhee Plateau (OP), and the Wallowa Mountains (WM). Newberry Volcano (NB), Diamond Craters (DC), Jordan Craters (JC), Steens Mountain (SM), are all marked with red triangles. Four stations (G05A, J06A, OR058, and OR080) that are referred to by name in the paper are labeled.

The measurements presented here resulted from a data processing effort involving the visual inspection of approximately 35,000 waveforms for data covering the period between January 2006 and October 2008. The splitting measurements were carried out using the SplitLab software package (Wüstefeld et al., 2007). We selected events of magnitude $M_w \geq 5.8$ located at epicentral distances between 88° and 130° for processing. An event map is shown in Fig. 2.3, along with a circular histogram showing the backazimuthal coverage in the dataset. We note that the backazimuthal coverage for SKS phases in eastern Oregon is not ideal and is heavily weighted towards events in the western Pacific Ocean, which precludes a complete analysis of backazimuthal dependence of splitting parameters. We initially applied a bandpass filter to retain energy at periods between 10 and 100s and the horizontal components of the SKS waveform were examined for high signal-to-noise ratio and good waveform clarity. In approximately 20% of cases, the corner periods on the filter were adjusted slightly to optimize signal-to-noise ratio, such that energy at periods between 8 and 12s and 50 and 100s was retained. We then manually windowed around the SKS phase, selecting a window length that covers at least one full period of the signal. For several HLP stations, we experimented with different window lengths and found that varying the window length had a negligible effect on the measurements, particularly for the highest-quality measurements in the dataset.

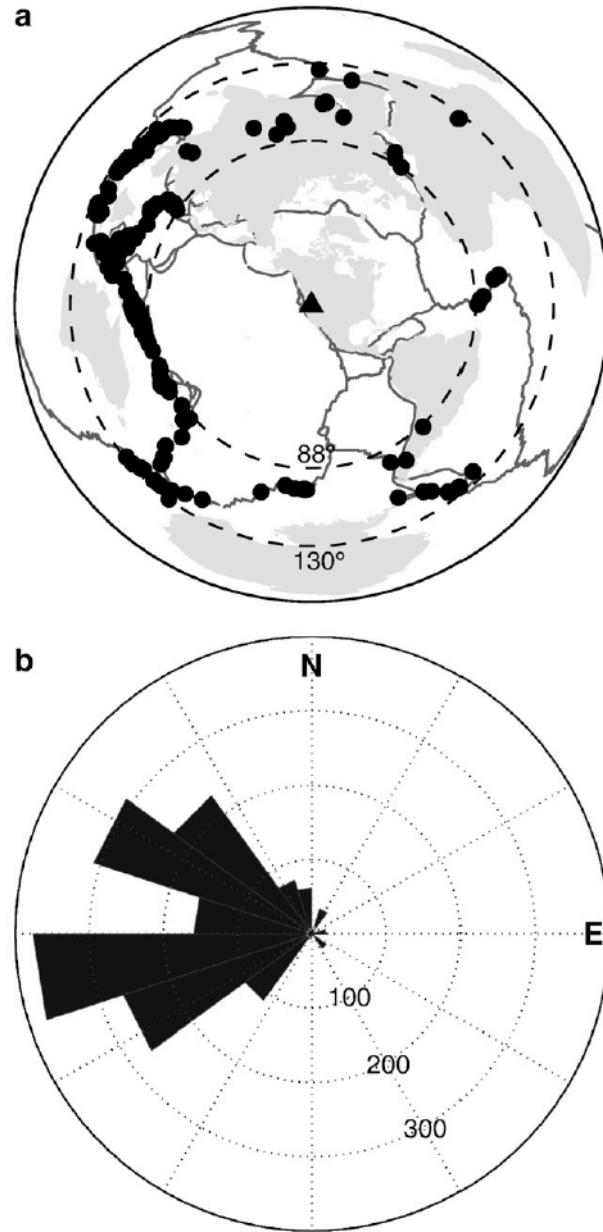


Figure 2.3. Map of earthquake distribution. Figure 2.3a shows a map of large-magnitude seismicity ($M \geq 5.8$) in the 88° – 130° epicentral distance range around a representative station (OR058; see Fig. 2.2) for the period 2006-2008. Figure 2.3b is the circular histogram of event backazimuths for all “good” and “fair” quality measurements (null and non-null) in the data set; the backazimuthal coverage is heavily weighted towards events to the west.

We used both the cross-correlation and the transverse component minimization methods to identify the best-fitting splitting parameters (fast polarization direction ϕ and delay time δt) and only retained those measurements for which the 95% confidence regions using the two methods overlap. It has been shown that the two measurement methods can disagree for noisy data, complex anisotropic structure, or when the incoming polarization azimuth is close to the null direction (e.g., Long and van der Hilst, 2005; Wüstefeld and Bokelmann, 2007). Those few measurements which yielded well-constrained but discrepant splitting parameters from high-quality non-null waveforms using the different methods are not presented here, as the goal of this study is to identify the highest-quality splitting measurements at each station. We are mindful, however, that discrepancies among measurement methods may be due to complex anisotropy beneath the station, discussed further in Section 5. These measurements likely warrant further investigation in a future study. For the vast majority of the measurements in the dataset, however, potential biases introduced by the choice of measurement methods should be minimal, as previous studies have shown that different measurement methods yield similar results when applied to high-quality data in the presence of a single layer of horizontal anisotropy (Long and van der Hilst, 2005).

We identified as “good” those splitting measurements for which the signal-to-noise ratio and waveform clarity were high, the initial particle motion was elliptical, the corrected particle motion was linear or very nearly linear, the cross-correlation and transverse component minimization methods yielded splitting parameter estimates that were consistent within the errors, and the 2σ error spaces for each measurement were nearly elliptically shaped and small, with errors less than $\pm 15^\circ$ in fast direction and ± 0.3 s

in delay time. Measurements with larger error bars (up to $\pm 30^\circ$ in ϕ and ± 1 s in δt) and lower signal-to-noise ratios (down to $\sim 2-3$) were marked as “fair” but were retained as long as the measurement methods agreed. Null measurements were identified by the initial linear particle motion and were also classified as “good” or “fair,” with noisier measurements classified as “fair.” An example of a high-quality splitting measurement is shown in Fig. 2.4.

4. Results

The splitting measurement procedure described above yielded a total of ~ 1950 well-constrained measurements of $(\phi, \delta t)$ at eastern Oregon stations. Of these, ~ 680 were classified as “good” and ~ 1270 as “fair.” In addition to these, ~ 950 high-quality (“good”+“fair”) null measurements were identified. Some individual stations had as many as 10–15 “good” quality measurements, while others had only a few and at several stations the measurement procedure only yielded “fair” quality measurements. In this paper, we focus on presenting the highest-quality measurements at each station; that is, either all “good” measurements or, at stations which have none, all “fair” measurements. A map showing the highest-quality individual splitting measurements at each station is shown in Fig. 2.5a, and a similar plot of all the well-constrained (“good”+“fair”) null measurements is shown in Fig. 2.5b.

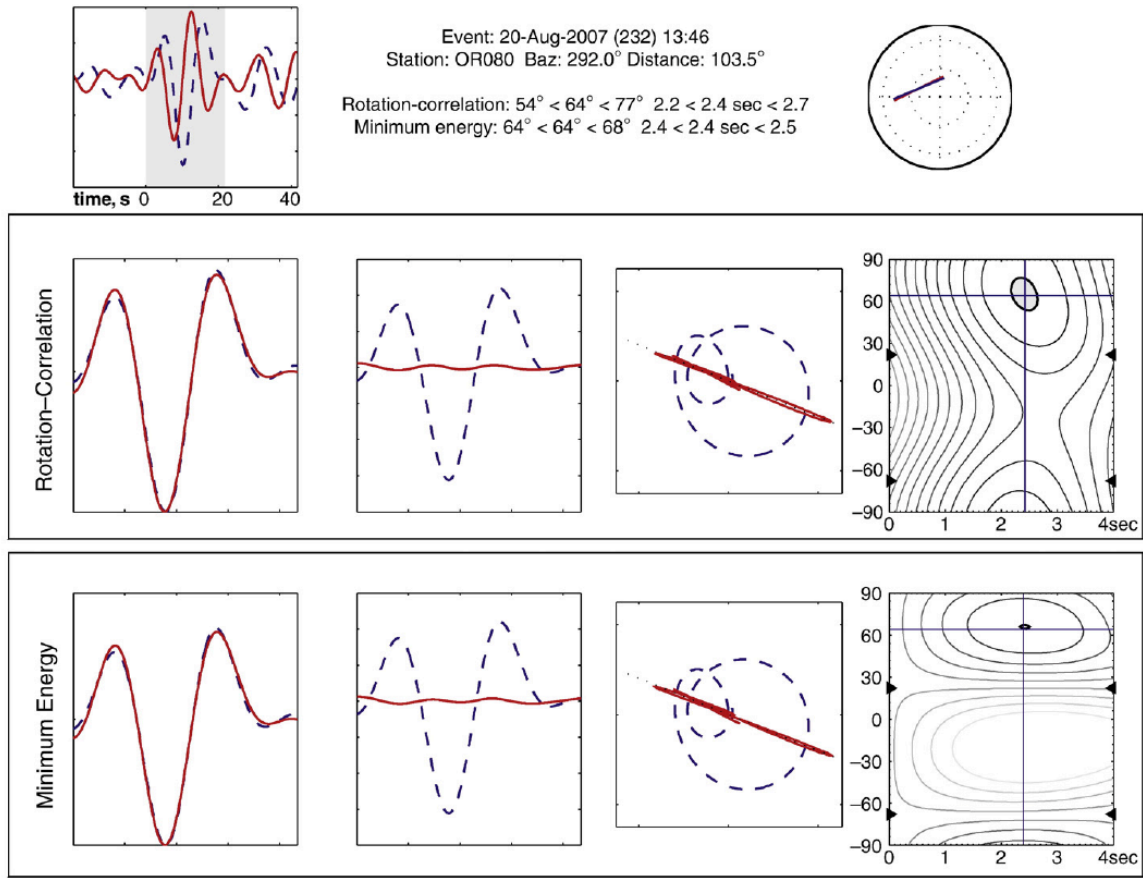


Figure 2.4. An example of a high-quality (“good”) measurement at HLP station OR080 (see Fig. 2.2) obtained using SplitLab (Wüstefeld et al., 2007). Top left panel shows the uncorrected radial (blue dashed) and transverse (solid red) components; the time window used in the analysis is shown in gray. The middle and bottom rows of panels show the diagnostic plots for the rotation-correlation method and the transverse component minimization method, respectively: from left to right, the corrected fast and slow components, the corrected radial and transverse components, the uncorrected (blue dashed) and corrected (solid red) particle motion diagrams, and the error space maps. The gray region in the error space maps represents the 95% confidence ellipse. For the transverse component minimization method, this is calculated by assuming that the transverse component energy is χ^2 -distributed and estimating the number of degrees of freedom from the seismogram; for further details, see Silver and Chan (1991). For the rotation-correlation method, it is calculated using a Fisher transform approach; for further details, see Wüstefeld et al. (2007). Both methods yield well-constrained splitting parameters of $\phi=64^\circ$, $\delta t=2.4$ s, as shown in the plot at the top right.

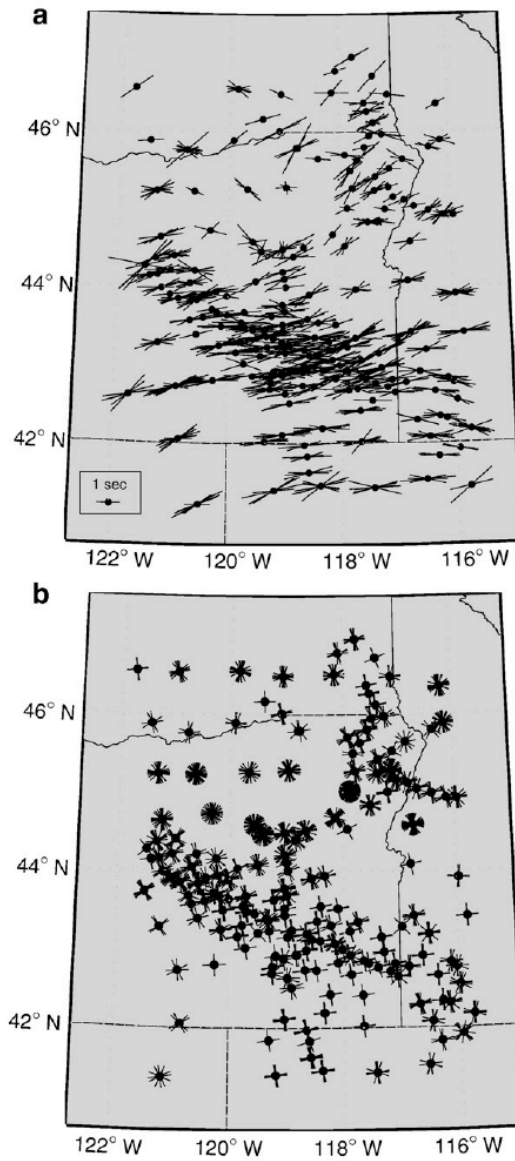


Figure 2.5. Splitting result for all stations. Figure 2.5a is a map of individual splitting measurements in the data set, plotted at the station location. The orientation and length of the bar correspond to the fast direction and delay time, respectively. For clarity, we have shown only the highest-quality measurements at each station; either all “good” measurements or, at stations where no “good” measurements were found, all “fair” measurements. Figure 2.5b shows map of all “good” and “fair” quality null measurements, plotted at the station location as crosses whose bars correspond to the backazimuth of the event and the corresponding potential null direction. Many stations in the northern part of the study area exhibit null directions over a large range of backazimuths, indicating weak and/or complex anisotropy beneath the station.

Overall, splitting patterns beneath the region are fairly simple, with a few areas of localized complexity. At most stations, particularly the stations located in the southern part of the study area, the measured fast directions and delay times cluster closely around average values of $\sim N80^\circ E$ for ϕ and ~ 1.8 s for δt . There is somewhat more variation in the measured splitting parameters at individual stations located farther to the north in the Blue and Wallowa Mountain regions. At many of these stations, there is considerable scatter in the measured ϕ values, the delay times tend to be smaller than at stations to the south, and the backazimuthal spread in null measurements tends to be larger (Fig. 2.5b). Additionally, the waveforms themselves tend to be more complex at stations located in the northern part of the study region. In order to demonstrate this regional difference in splitting pattern complexity, we show in Fig. 2.6 the backazimuthal distribution of measured splitting parameters for a station located in the northern part of the study area (G05A) and a station located in the HLP (J06A). The northern station exhibits significant variations in $(\phi, \delta t)$ with backazimuth and well-constrained nulls were identified over a large swath of backazimuths; such a pattern is consistent with complex anisotropic structure beneath the station (e.g., Silver and Savage, 1994), and the delay times indicate that the anisotropy is weaker than elsewhere in the study area. In contrast, the southern station exhibits very similar splitting over a wide range of backazimuths, and the measured null directions are consistent with the measured fast directions beneath the station. This behavior is characteristic of stations located in the southern part of the study area, where the splitting tends to be large ($\delta t=1.5-2.5$ s) and the splitting patterns are simple and exhibit little spatial variation.

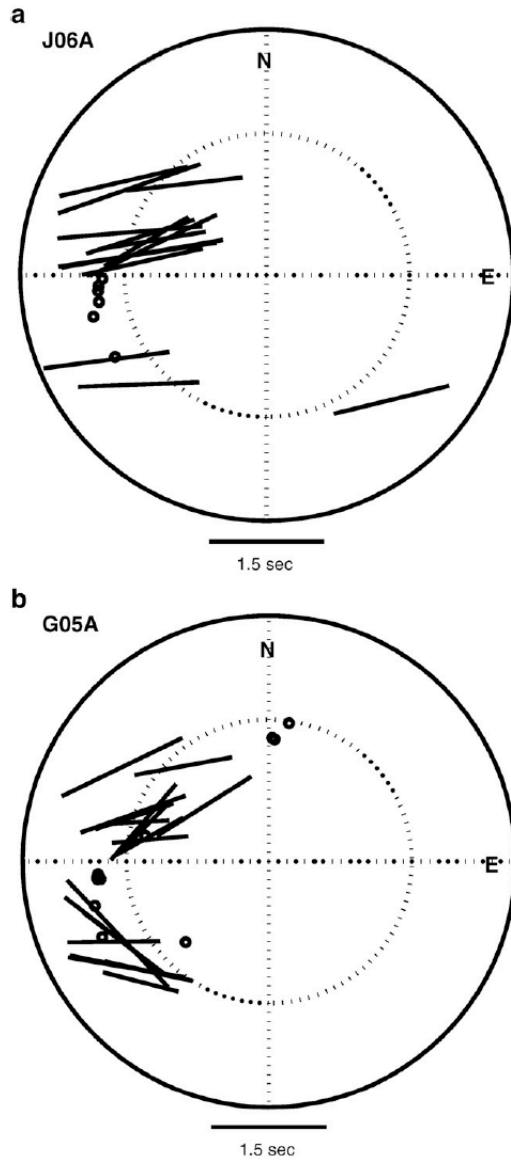


Figure 2.6. Examples of detailed splitting patterns at two stations (J06A and G05A; station locations are shown in Fig. 2.2). Bars representing splitting parameters are plotted as a function of backazimuth and incidence angle (hatched line indicates an incidence angle of 8°). All “good” and “fair” measurements are shown (note that this is a larger subset of the measurements than shown in Fig. 2.5a, where only the “good” quality measurements are shown). Null measurements are plotted as circles. a. Splitting pattern observed at station J06A, located in the HLP. The splitting measurements exhibit very little variation with backazimuth. b. Splitting pattern observed at station G05A, located in the northern part of the study area. At this station the splitting pattern is markedly more complicated and the measured splitting parameters exhibit significant variation with backazimuth.

Fig. 2.7b shows a circular histogram of all fast direction measurements shown in Fig. 2.5a along with a histogram of the corresponding delay times. The circular histogram is overwhelmingly dominated by nearly E-W fast directions and the delay time measurements yield an average δt of ~ 1.8 s, with well-constrained δt values of up to ~ 3 s and a standard deviation of 0.49 s. This average delay time is considerably higher than the global average of ~ 1 s for continental regions (e.g., Silver, 1996), which indicates that the anisotropy beneath eastern Oregon is unusually strong and/or that the anisotropic layer in the upper mantle is unusually thick.

In order to present a clear first-order picture of SKS splitting and mantle flow patterns beneath eastern Oregon, we calculate average splitting parameters (ϕ , δt) for each station in the data set (splitting parameter values can be found in the supplementary data). These single-station average splitting parameter estimates are, in general, more reliable in the southern part of the study region where the splitting patterns are simpler. The map of average splitting parameters for each station is shown in Fig. 2.8, and there are a few regional trends that are evident from this map. First, there are clear trends in the distribution of average delay times, with the smallest average δt values in the Wallowa Mountain region, and slightly larger δt at stations to the north of the Wallowas. Further to the south, delay times tend to be larger ($\delta t > 1.2$ s) and there is a concentration of still larger delay times ($\delta t > 1.7$ s) in the southeastern part of Oregon. The largest delay times ($\delta t > 2.2$ s) delineate a region in the heart of the HLP province (Fig. 2.8). There is also a small group of stations to the north of Newberry volcano that exhibit somewhat larger delay times than the surrounding stations. Spatial variations in the fast directions are more subtle, but there are a few well-defined patterns. In the HLP, most fast directions

strike approximately N80°E, and although there are a few isolated regions that exhibit some complexity in ϕ , the overall pattern is remarkably uniform. In a few regions, including the Owyhee Plateau and stations located in the southwestern part of the study area, there is a slight rotation of the ϕ values; in the Owyhees, the average fast directions strike approximately N100°E, while stations in south-central Oregon and northern California tend to exhibit fast directions closer to ~N60°E. In northeastern Oregon and southeastern Washington, there is a slight rotation to more northeasterly fast directions, although the more complex splitting patterns observed in this region means that the single-station average splitting parameters may be less reliable than in the HLP.

The splitting pattern shown in Fig. 2.8 is consistent with results from previous studies of eastern Oregon splitting (e.g., Xue and Allen, 2006), although the data set described here has much better spatial resolution than previous studies. The pattern in fast directions found in our study region is also generally consistent with the larger-scale splitting pattern observed in the western US (e.g., Zandt and Humphreys, 2008; Fouch and West, in preparation). We emphasize, however, that the High Lava Plains region of Oregon represents the broadest region of particularly high delay times in the western US (which is itself a region of relatively high δt compared to most continental regions). The high δt observed in the HLP contrast with those observed in the eastern Snake River Plain, which average ~1.0–1.5 s. This contrast is notable, as the eastern SRP is also associated with temporally migrating tectonomagmatic activity (with volcanic production that is an order of magnitude more voluminous than in the HLP).

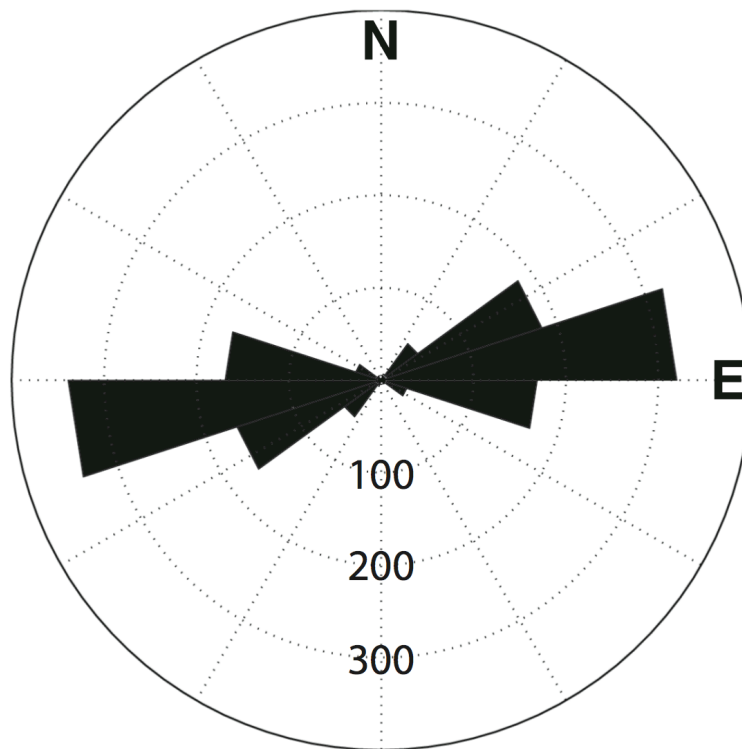
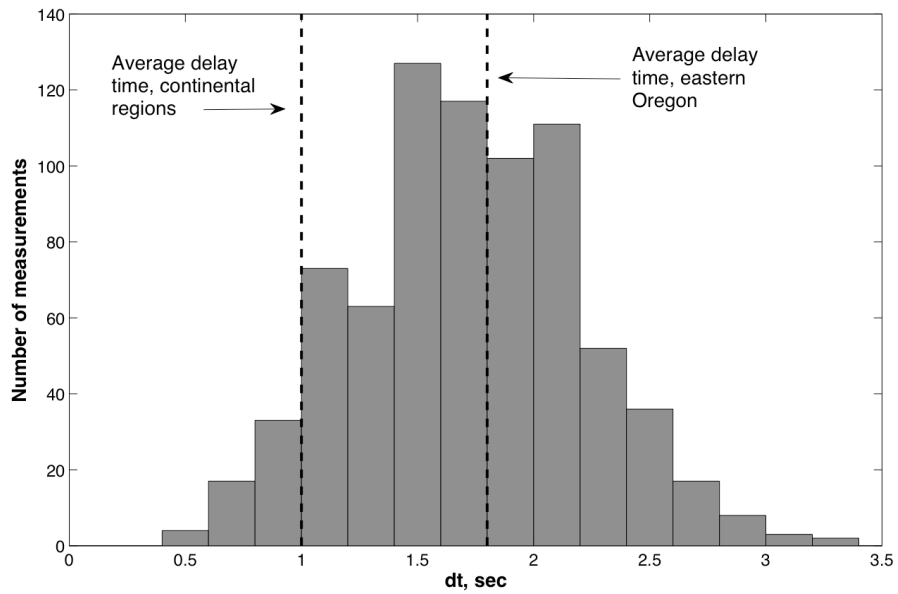


Figure 2.7. Histogram of splitting pattern. Figure 2.7a. is a histogram of measured delay times shown in Fig. 2.5a. Figure 2.7b shows the circular histogram of measured fast directions shown in Fig. 2.5a.

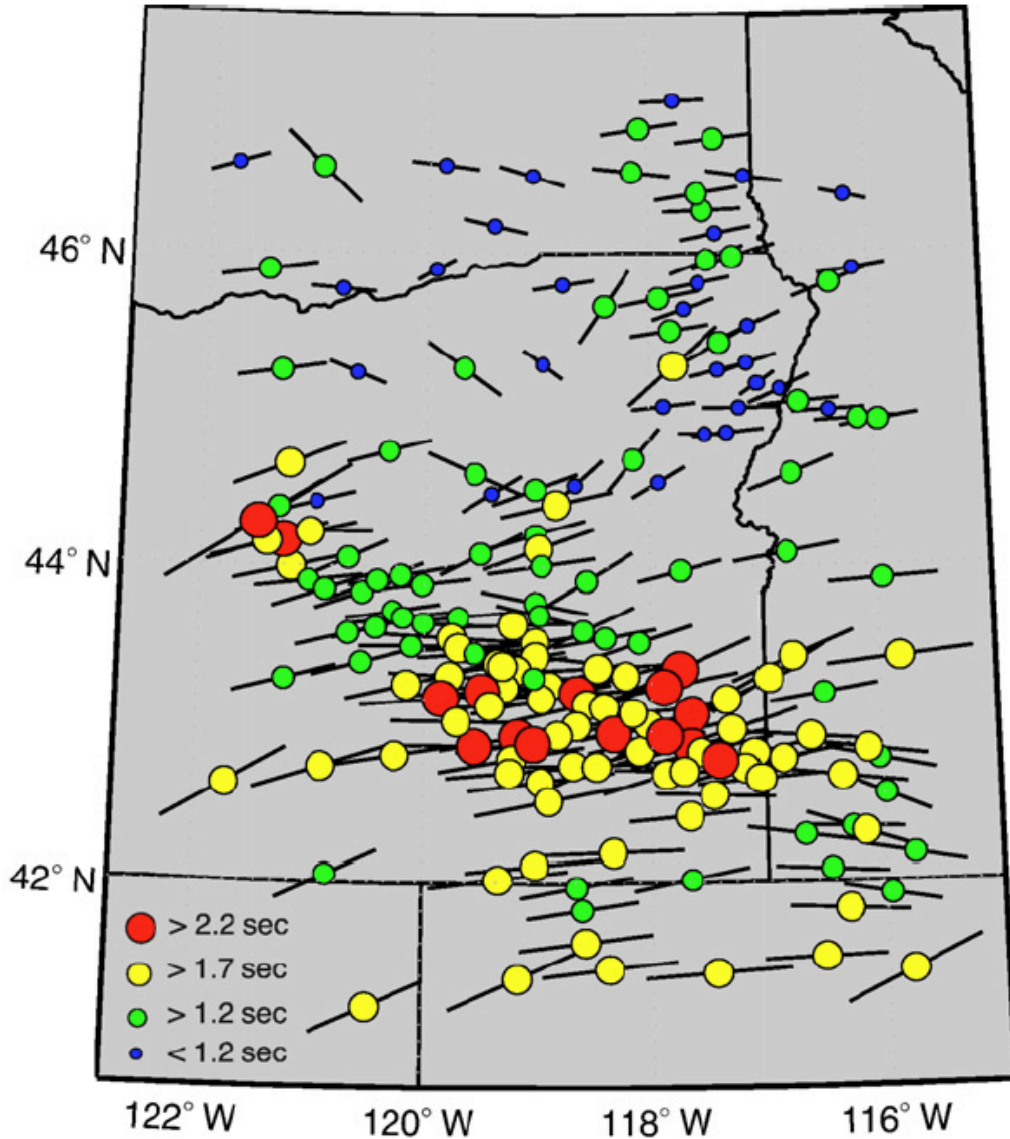


Figure 2.8. Map of average splitting parameters in Eastern Oregon and surrounding regions. Estimates were obtained by a simple average of the highest-quality measurements at each station; nulls were not taken into account in the averaging process. The symbols are color-coded by the magnitude of the delay time, as indicated by the legend at bottom left, but the length of the bar is uniform at all stations.

5. Interpretation

5.1. Distinguishing between lithospheric and asthenospheric anisotropy

A first key question is whether the splitting observed in eastern Oregon reflects anisotropy in the crust, in the mantle lithosphere (reflecting past deformational episodes),

in the asthenosphere (related to present-day mantle flow), or a combination of these factors. Because SKS paths through the upper mantle are nearly vertical, and because shear wave splitting is a path-integrated measurement, the depth resolution of the measurements is poor. However, an argument about the relative contribution from different parts of the crust/mantle system can be made based on the large delay times observed in this study and the likely thickness of the lithosphere in the region. In the HLP, the unusually large delay times argue for a primary contribution from the asthenospheric mantle. The lithosphere beneath the HLP is likely thin; S wave velocities in the uppermost mantle to depths of 50 km or even less are low (~ 4.2 km/s; Li et al., 2007; Warren et al., 2008) and the mantle lithosphere is considerably thinner here (~ 50 – 60 km thick) than in the cratonic region to the east (e.g., Lowry and Smith, 1995). Because the observed delay times are so large, a model in which all of the anisotropy is in the crust and mantle lithosphere would imply an unreasonably large magnitude of anisotropy (roughly 20% anisotropy for a ~ 60 km thick lithosphere) and we can confidently infer that the large delay times and uniform fast directions reflect contemporary flow in the asthenospheric mantle. While a small contribution to the observed splitting from crustal anisotropy is likely, average values for crustal splitting are on the order of perhaps ~ 0.1 – 0.3 s (e.g., Savage, 1999) and thus the large delay times observed here cannot be attributed mainly to crustal anisotropy. Even if we attribute 1s of delay time to anisotropy in the crust and mantle lithosphere, the asthenosphere would have to contribute 1.5–2s of splitting beneath the central HLP, which corresponds to ~ 6 – 8% anisotropy for a 150-km thick asthenosphere. This is within the observed range for mantle-derived xenoliths (e.g., Mainprice and Silver, 1993; Ben Ismail and Mainprice,

1998).

At stations located in the northern part of our study area, most notably in the Blue and Wallowa Mountains, the relative contributions to the observed splitting from the crust, lithosphere, and asthenosphere are less clear-cut. The splitting in this region is often weaker than in the HLP and the lithosphere is likely to be thicker (e.g., Lowry and Smith, 1995; Roth et al., 2008). Splitting patterns at individual stations in this region are often complicated, which implies that the anisotropic structure beneath this region is complex. In particular, the observation of well-constrained null measurements over a wide range of backazimuths (Fig. 2.5b) indicates that the anisotropy in this region is weaker and more complex than beneath the HLP. This, in turn, indicates a likely contribution from several different regions of the crust and/or upper mantle; the complicated SKS waveforms and splitting patterns observed in the Wallowas are plausibly due to multiple layers of anisotropy, considerable lateral heterogeneity, vertical mantle flow (i.e., West et al., 2009), or a combination of these factors. Without more detailed modeling, it is difficult to characterize the relative contributions to the observed splitting from the lithospheric vs. asthenospheric upper mantle, but we can say with confidence that the lithosphere and/or crust likely makes a significant contribution to the splitting signal in this region, in marked contrast to the HLP. Despite the indications of complexity, however, the average fast directions for stations in the Wallowa array tend to be roughly E-W, as in the southern part of the study area.

5.2. Implications for mantle flow

In order to infer the flow direction beneath a seismic station from an observed fast splitting direction, knowledge of the relationship between strain and anisotropy is required. Our understanding of this relationship comes from mineral physics experiments and petrographic analysis of mantle-derived rocks (for recent overviews, see Karato et al. (2008) and Mainprice (2007)). The usual relationship used to interpret shear wave splitting beneath continents is that the fast splitting direction tends to align with the mantle flow direction beneath the station, based on experimental results from olivine aggregates deformed in simple shear that produce so-called A-type olivine fabric. Mineral physics studies have shown that this relationship can be affected by the physical conditions associated with deformation, including temperature, stress, water content, and pressure (e.g., Karato et al., 2008). It is generally thought that the conditions needed to produce B-type olivine fabric – a fabric which is rotated by 90° from the customary expected relationship between strain and anisotropy – are not present in the subcontinental asthenosphere (Karato et al., 2008). While some recent experiments have suggested that B-type fabric can be produced in the laboratory at pressures greater than ~3 GPa (corresponding to a mantle depth of ~100 km; Jung et al., 2009), the applicability of these experiments to mantle conditions remains uncertain (e.g., Long and Silver, 2009), and geodynamical modeling studies that utilize the A-type (or similar) fabric paradigm to explain splitting patterns in the western United States have been quite successful (e.g., Silver and Holt, 2002; Becker et al., 2006). Therefore, we rely on the usual relationship used to interpret anisotropy beneath continents (see also Fouch and Rondenay, 2006) and infer that the fast splitting direction indicates the direction of

(horizontal) mantle flow beneath the station.

The strong, consistent splitting with an E-W fast direction observed at stations in southeastern Oregon, western Idaho, and northern Nevada suggests the presence of a well-organized mantle flow field beneath the region. Because the splitting patterns observed in the HLP are generally simple and exhibit little backazimuthal variation that might indicate multiple anisotropic layers, and because the large delay times argue for a primary contribution from the asthenospheric mantle, their interpretation is much less ambiguous than is typical for shear wave splitting measurements in a continental setting. We argue that the strong E-W splitting observed beneath the HLP can be unambiguously attributed to consistent and well organized flow in the asthenospheric upper mantle in a roughly E-W direction. This E-W direction does not align with either the strike of the HLP volcanic trend or with the direction of absolute plate motion (Fig. 2.1). In the northern part of our study area, it is more difficult to make a blanket statement about the direction of mantle flow, because the relative contributions to the splitting signal from frozen lithospheric anisotropy and active flow in the asthenosphere are more difficult to assess. One possibility is that the mantle flow direction beneath the Blue and Wallowa Mountains is similar to that beneath the HLP, but an additional contribution to splitting from the lithosphere and/or crust results in a complex splitting signal and reduced delay times. Without more detailed multiple-layer modeling of the splitting patterns observed in this region, however, it is not possible to characterize fully the active mantle flow regime.

5.3. *The source of the large delay times*

As the histogram in Fig. 2.7 demonstrates, the average delay times observed in eastern Oregon are considerably higher than the global average for continental regions, and in the heart of the HLP they range up to ~ 3 s, on the high end of the range of delay times observed globally for SKS-type phases (e.g., Fouch and Rondenay, 2006; Long and Silver, 2009). Understanding the source of these unusually large delay times is an important piece in sorting out the puzzle of the origin and evolution of the HLP. Strikingly, the magnitude of the delay times in eastern Oregon and the surrounding regions seem to correlate spatially with isotropic uppermost mantle wavespeeds inferred from body wave tomography (e.g., Roth et al., 2008; West et al., 2009). Specifically, relatively low wavespeeds and relatively high δt values are found beneath the HLP and in the vicinity of Newberry volcano, while relatively high wavespeeds and relatively low δt are found beneath the northern part of the study area, particularly the Blue and Wallowa Mountains (Fig. 2.9).

There are three possible scenarios that would result in unusually high delay times. First, the thickness of the anisotropic layer beneath the HLP might be greater than is usual for continental regions. Because the splitting is inferred to be due to the LPO of olivine in the asthenospheric mantle, it is plausible that the thin lithosphere beneath the HLP is associated with a correspondingly thick asthenosphere. It seems unlikely, however, that any difference in asthenospheric thickness could explain delay times of ~ 2.5 – 3.0 s instead of the typical ~ 1 s. A second possibility is that olivine LPO is particularly strong in the anisotropic layer beneath the HLP, possibly due to differences in upper mantle temperatures or due to local differences in water content. There is,

however, little experimental data on the effect of temperature or other factors such as water content on the strength of LPO. The overall strength of LPO beneath the region may also be stronger than surrounding areas due simply to particularly well-organized and coherent mantle flow.

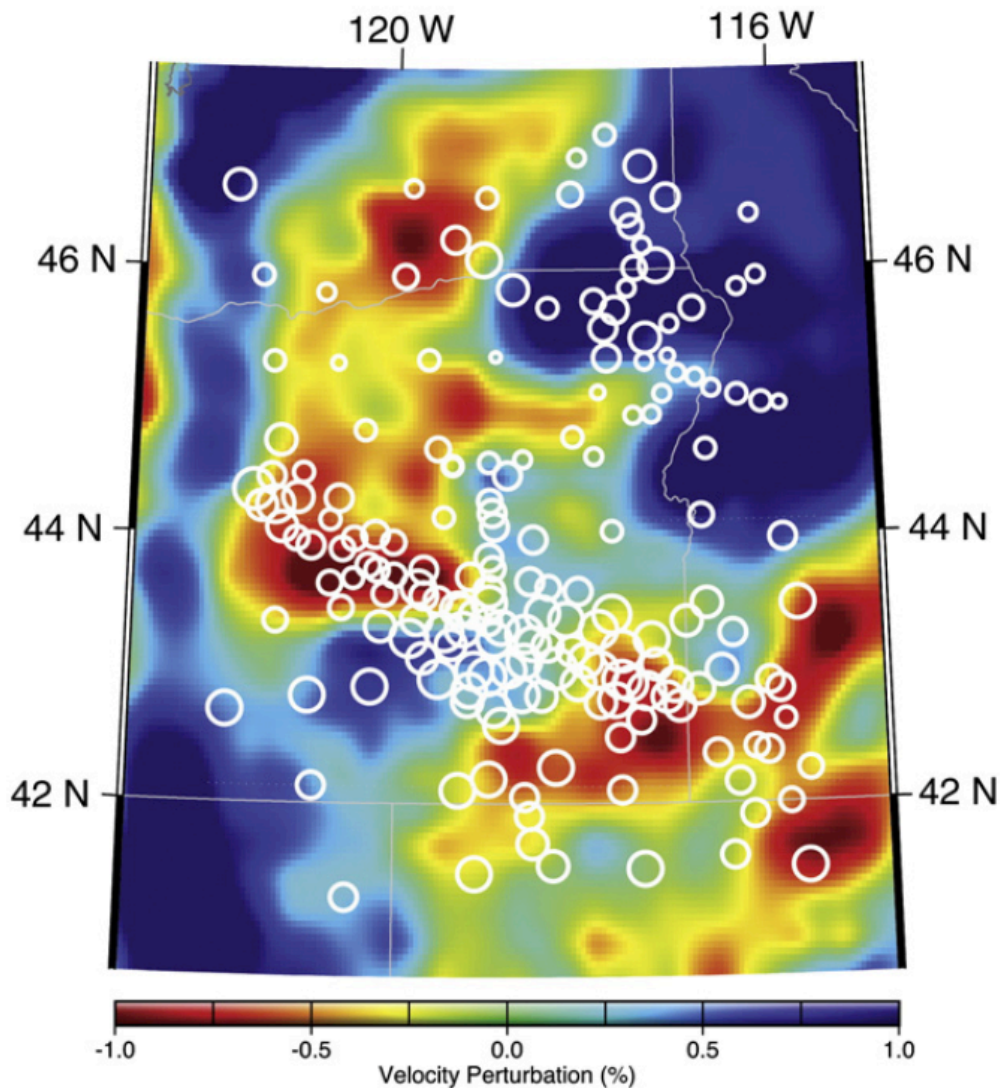


Figure 2.9. A horizontal slice through the three-dimensional P velocity model of West et al. (2009) at a depth of 100 km. The single-station average delay times (see Fig. 2.8) are plotted at the station locations; the size of the circle corresponds to the size of the delay time, with the smallest circles corresponding to delay times <0.6 s and the largest corresponding to delay times >2.2 s. To first order, relatively fast uppermost mantle wavespeeds correlate spatially with relatively low splitting delay times and vice versa. This correlation is not perfect, however, particularly in the central part of the HLP, where splitting delay times are large but P wave velocities are not particularly low.

A third possibility is that there is an additional contribution to the observed splitting from the shape preferred orientation of partial melt in the uppermost mantle, which can result in strong anisotropy (e.g., Zimmerman et al., 1999). There is some indication that the largest delay times in the eastern Oregon data set are spatially correlated with Holocene volcanism; both Jordan Craters and Diamond Craters are located within the swath of particularly high delay times, and δt values at stations just to the north of Newberry are also higher than at surrounding stations (Figs. 2.2 and 2.8). Enhanced delay times due to a contribution from the shape preferred orientation of partial melt might plausibly explain the difference between the HLP and the Wallowa Mountains, as one major difference between these regions is the probable presence or absence of partial melt. It has been shown that a small amount of partial melt (a few percent) can result in significant anisotropy if the melt is aligned in lenses or similar shapes (Vauchez et al., 2000), and a preexisting LPO may also play a role in aligning melt structures (Waff and Faul, 1992); the presence of partial melt may also, in turn, affect the development of olivine LPO (Holtzman et al., 2003). Partial melt has been invoked to explain large delay times observed in New Zealand (Greve et al., 2008; Greve and Savage, 2009), but because the relationships between mantle flow, the alignment of partial melt, and the resulting anisotropy remain poorly understood, it is difficult to quantitatively test the ability of partial melt to explain the eastern Oregon splitting patterns.

The shape preferred orientation of partial melt may play a role in generating the high delay times observed in this study, but there is no compelling evidence as yet that partial melt is ubiquitous in the upper mantle beneath the HLP, which would seem to be

required to explain the widespread high δt values with a shape preferred orientation mechanism. A combination of the three mechanisms discussed here may be required to explain the large delay times observed in the HLP, but given the first-order spatial correlation between relatively slow upper mantle wavespeeds and high delay times, we cannot at present rule out any of the three mechanisms discussed here.

5.4. Explaining lateral variations in delay times in the HLP

The observation of splitting delay times within the HLP province that are both unusually large and that vary spatially over small length scales is one of the most intriguing findings of this study. Because the SKS waves under study have characteristic periods of ~ 10 s, their associated regions of sensitivity (which can be approximated by the first Fresnel zone) will be relatively large at depth (e.g., Long et al., 2008). The observation of small-scale variations in δt therefore suggests that the responsible spatial variations in anisotropy are likely to be relatively shallow, most likely in the uppermost mantle. The combination of unusually large δt and small-scale variations in δt values argues for an anisotropic model in which the geometry of the anisotropy varies little but the strength of the anisotropy exhibits strong lateral variations. In contrast, a model in which the geometry of anisotropy varied dramatically over small length scales would result in relatively small average delay times, as finite-frequency shear wave splitting measurements would tend to average over regions of incoherent anisotropic structure. While the dataset presented here does not uniquely constrain a mechanism for the lateral variations in delay times observed in the HLP, the enhanced delay times in the central HLP must be consistent with a mechanism (perhaps stronger LPO or partial melt) that is

capable of producing lateral variations in the strength of anisotropy without corresponding variations in its geometry.

5.5. Implications for the tectonic evolution of eastern Oregon

As discussed in Section 5.2, the combination of large delay times and uniformly E-W fast directions beneath the HLP places a very strong constraint on the geometry of mantle flow in this region. In turn, this knowledge of the mantle flow patterns in the region places a strong constraint on models for the tectonic evolution of eastern Oregon. By itself, our inference of strong, coherent E-W mantle flow does not uniquely constrain such a model. However, any model proposed for the formation of the HLP and, more generally, for the volcanic history and tectonic evolution of eastern Oregon and the surrounding region must be consistent with the constraints on present-day mantle flow provided by the splitting observations. One possible mechanism for consistent E-W mantle flow beneath the HLP is that it is a consequence of the rollback of the Cascadia slab; the E-W direction is roughly parallel to the direction of present-day trench migration. Further to the north, the complexity in the splitting patterns may indicate a local disturbance to the large-scale E-W flow field near the edge of the North American craton.

We emphasize that models invoking a mantle plume to drive mantle flow in a pattern radiating out from the presumed plume impact location in southeastern Oregon (e.g., Camp and Ross, 2004) do not appear to be consistent with the upper mantle flow field inferred here. The splitting observations are not consistent with any model that requires mantle flow in a northwestern direction along the strike of the spatiotemporal

trend in silicic volcanic activity in the HLP. This interpretation is consistent with the inferences from the tomographic wavespeed models of Roth et al. (2008) and the Rayleigh wave dispersion analysis of Warren et al. (2008) that the presence of a plume beneath the HLP volcanic province is not required by seismic data.

6. Outlook and summary

The splitting data set presented here provides a first-order picture of anisotropy and deformation in the upper mantle beneath eastern Oregon and yields strong constraints on the contemporary flow geometry in the asthenosphere. Work on characterizing the detailed anisotropic structure (and the tectonic processes that generate it) of the crust/mantle lithosphere/asthenosphere system beneath eastern Oregon continues. In particular, an additional year of data from the HLP experiment (Fall 2008–Fall 2009) will shortly be available. This will allow us to characterize splitting patterns at individual stations in greater detail with regard to potential backazimuthal complexity that might indicate complex anisotropy, particularly if splitting measurements from direct teleseismic S phases are included. For stations located farther to the north in the Blue and Wallowa regions, where the splitting patterns are consistent with complex anisotropy beneath the stations and may reflect contributions from both lithospheric and asthenospheric structure, a forward modeling approach that takes into account multiple layers of anisotropy should further constrain anisotropic structure at depth. The measurement of splitting parameters over a range of frequency bands may also shed additional light on complex anisotropy, as splitting has been shown to be frequency dependent in the presence of complex structure (e.g., Marson-Pidgeon and Savage, 1997;

Fouch and Fischer, 1998) and high-frequency measurements may be biased towards near-surface anisotropy (e.g., Saltzer et al., 2000).

The data set presented here, with its excellent spatial resolution, is also a very promising candidate for the application of new methods for shear wave splitting tomography to image anisotropic structure at depth (e.g., Chevrot, 2006; Long et al., 2008). The tomographic inversion of measurements of the splitting intensity, a quantity that is closely related to the splitting parameters (ϕ , δt) measured in this study, can resolve the 2-D or 3-D distribution of anisotropy at depth and, in particular, can place constraints on the depth distribution of anisotropy. Another promising line of inquiry is the integration of the shear wave splitting measurements presented here with a geodynamical modeling framework to help to narrow the class of plausible models for mantle dynamics beneath eastern Oregon. Laboratory models that take into account the kinematics and temporal evolution of the Juan de Fuca slab, the possible effects of a plume, and the effects of lithospheric topography on the resulting mantle flow field have been carried out (e.g., Kincaid et al., 2008) and we are currently comparing splitting predictions from these models to the dataset presented in this paper. Such detailed comparisons will provide strong constraints on the type of models that are consistent with the splitting observations. Finally, we expect to integrate the SKS splitting measurements with other constraints on anisotropy, including measurements of direction-dependent Pn (and possibly Sn) velocities from the active source component of the HLP project and constraints on azimuthal anisotropy from surface wave inversions. In particular, constraints on the magnitude of anisotropy in the uppermost mantle from Pn measurements may in turn constrain a possible contribution to splitting from the shape

preferred orientation of partial melt in the shallowest mantle.

To summarize, the shear wave splitting trends in eastern Oregon are fairly simple and tend to be dominated by approximately E-W fast directions and delay times that range from ~ 0.8 s to ~ 2.7 s. We observe a difference in splitting patterns between stations located in southeastern Oregon and stations located further to the north in northeastern Oregon and southern Washington. At stations located in the Blue and Wallowa Mountain regions, the splitting patterns tend to be complex at individual stations, exhibiting well-constrained null measurements over a wide range of backazimuths and smaller delay times than the rest of the study region. We interpret this as evidence for weaker and/or more complex azimuthal anisotropy, suggesting that SKS splitting in this region reflects contributions from both active mantle flow in the asthenosphere and frozen lithospheric anisotropy. In the HLP, the splitting patterns are simpler than those observed farther to the north; fast directions are predominantly E-W, ranging from $\sim N80^\circ E$ to $\sim N100^\circ W$. Delay times in the HLP are large, with an average value of ~ 1.8 s and maximum values of ~ 2.7 s at individual stations. The observed splitting cannot be primarily due to relict anisotropy in the lithosphere and likely reflects contemporary mantle flow beneath the HLP in a generally E-W direction. The largest delay times observed in the HLP correlate spatially with regions of slow isotropic mantle wavespeeds and with the occurrence of Holocene volcanism. The large HLP delay times could be a consequence of a thicker-than-average anisotropic layer beneath the region, particularly strong LPO, a contribution to anisotropy from the shape preferred orientation of melt, or a combination of these processes. The splitting measurements presented here place a very strong constraint on present-day mantle flow beneath eastern Oregon, particularly beneath the HLP, and any

model for the recent tectonic evolution and volcanic activity of this region must be consistent with the generally E-W mantle flow that is inferred from the SKS splitting measurements.

In this chapter I described the average anisotropy pattern of the upper mantle in eastern Oregon and its surrounding areas using SKS-splitting method. In the following chapter, I will study the crust and uppermost mantle structures of the U.S. Pacific Northwest with fundamental-mode Rayleigh-wave ambient noise tomography.

CHAPTER III
CRUST AND LITHOSPHERE STRUCTURE OF THE NORTHWESTERN
U.S. WITH AMBIENT NOISE TOMOGRAPHY: TERRANE ACCRETION AND
CASCADE ARC DEVELOPMENT

This work was published by *Earth and Planetary Science Letters* in February, 2011. Coauthors Huajian Yao, and Robert van der Hilst assisted in the methodology, and Eugene Humphreys contributed to the interpretations of seismic results, and all aided in the editorial process. I was responsible for the instrument deployment, data collection and processing, performing the ambient noise tomography and was the primary author.

1. Introduction

The Pacific Northwest (PNW) of the United States coalesces a wide range of lithospheres, tectonic conditions and rock ages in a compact area (Fig. 3.1). In recent years the major PNW structures have become much better resolved with the deployment of EarthScope Transportable Array and several regional networks, and with the use of improved seismological methods. Existing body-wave studies image average upper mantle anisotropy (from shear-wave splitting (Fouch et al., 2008; Long et al., 2009)) and velocity structures deeper than ~100 km (teleseismic tomography of Roth et al., 2008; Burdick et al., 2008; and Schmandt and Humphreys, 2010), but do not constrain the structure of the crust and uppermost mantle. The base of the crust and lithosphere have been imaged using receiver functions (Gilbert and Fouch, 2007; Levander et al., 2008; Eagar et al., 2010), and western U.S. crust and upper mantle velocity structures have been

obtained using ambient noise and tomography with EarthScope Transportable Array data (e.g., Yang et al., 2008; Lin et al., 2008; Moschetti et al., 2010).

In our PNW study of the crust and uppermost mantle we employ ambient noise tomography using about 70 more seismometers than Yang et al. (2008) to construct an isotropic 3-D shear-wave velocity model with improved resolution. We then interpret the images in a geological context to understand better the influences of Cenozoic tectonic and magmatic activity into the PNW on the structure and evolution of the lithosphere. A seismic study of this region with close consideration of its geologic history has not been done before. We focus on four major tectonic structures: (1) the boundaries and distribution of the Siletzia terrane (a large fragment of Farallon oceanic lithosphere, Fig. 3.1 (Snively et al., 1968; Simpson and Cox, 1977; Duncan, 1982)); (2) the large sedimentary basins within Siletzia in south-central Washington, now largely covered by Columbia River Flood Basalt (CRB) flows; (3) the relatively young and spatially heterogeneous Cascade volcanic arc; and (4) the source area of the CRB eruptions. We argue that Siletzia, although strongly rifted shortly after accretion (creating the large sedimentary basins), underlies much of Oregon and most of Washington including the pre-accretion forearc, that the Cascades' seismic structure reflects strong variations in advection of magma and heat, and that the CRB event occurred at the margin of accreted Siletzia and has strongly modified the seismic structure in the vicinity of Moho.

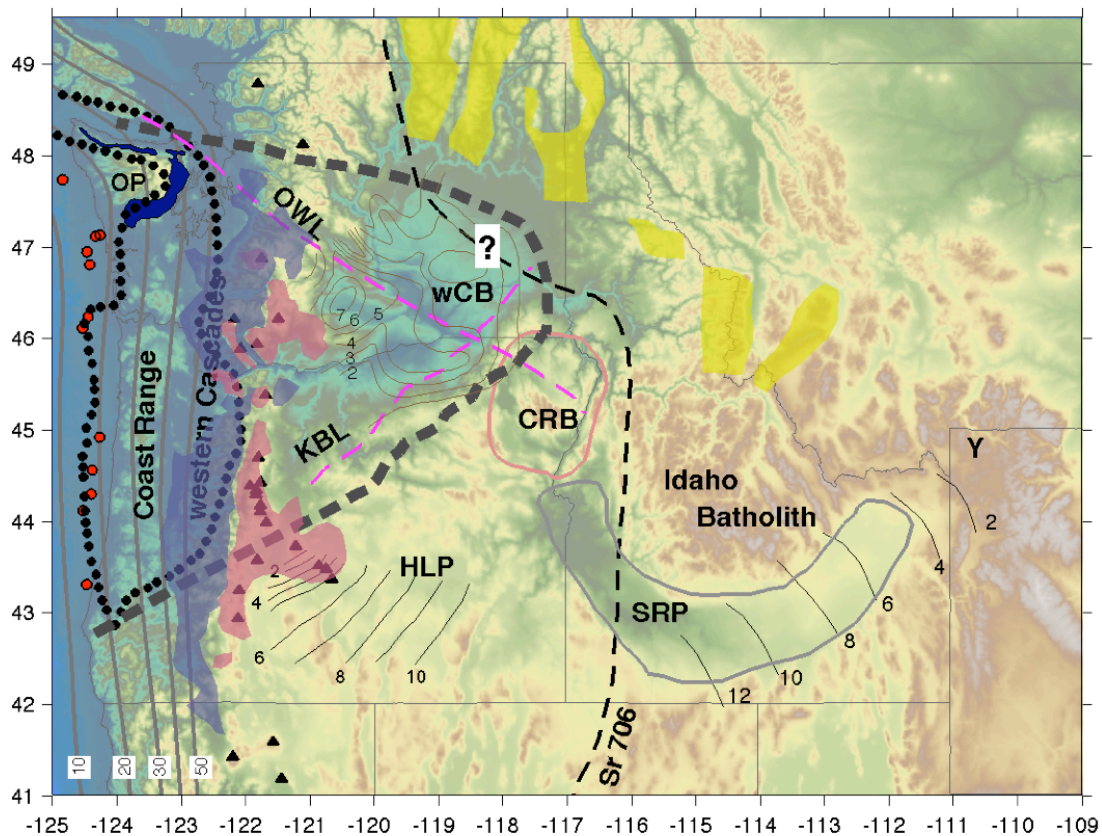


Figure 3.1. Geological structures of the U.S. Pacific Northwest, including: depth contours of the Juan de Fuca plate interface at 10-50 km; outline of Siletzia west of the Cascades (black dotted line) and sampled outcrop of Siletzia (red dots) from Wells et al. (1998); our inferred outline of Siletzia (heavy gray dashes); the Olympic Peninsula (OP, Crescent Basalts in dark blue); the old western Cascades (shaded light-blue) and active High Cascades volcanic arc (shaded light-red) with Quaternary volcanoes (black triangles); the sedimentary Columbia Basin (CB) with isopach contours for Eocene basin thickness, in km (Campbell, 1989); the Klamath-Blue Mountains gravity Lineament (KBL) and Olympic-Wallowa Lineament (OWL); Cenozoic metamorphic core complexes (shaded yellow patches); isotopic $^{87}\text{Sr}/^{86}\text{Sr}$ 0.706 line (dashed black line, uncertain location in eastern Washington) that separates the accretionary terrain to the west and Precambrian North America to the east; Columbia River flood basalt source area (CRB, pink outline); Snake River Plain (SRP, gray outline); time-progressive Newberry and Yellowstone (Y) rhyolite eruptive progression across SRP and High Lava Plains (HLP) (thin black lines, in Ma); and the Cretaceous Idaho Batholith.

2. Geological setting

Pacific Northwest structures include the sharply truncated western margin of Precambrian North America (along the isotopic $^{87}\text{Sr}/^{86}\text{Sr}$ 0.706 line, Fig. 3.1 (e.g., Fleck and Criss, 1985)), onto which Mesozoic island arc and Cenozoic oceanic terranes (Snively et al., 1968; Simpson and Cox, 1977) accreted, the Cascade volcanic arc, the ~16 Ma Columbia River Basalt flows, the extending High Lava Plains (HLP, Fig. 3.1) of the northern Basin and Range, the track of the Yellowstone hotspot (the Snake River Plain, SRP, Fig. 3.1). Most of these structures represent an episode of Cenozoic continental growth involving the intense and nearly pervasive magmatic and tectonic adjustments that followed the ~50 Ma accretion of Siletzia within the Columbia Embayment (roughly between the NE-trending Klamath-Blue Mountains gravity lineament [KBL, Fig. 3.1, Riddihough et al., 1986] and the NW-trending Olympic-Wallowa structural lineament [OWL, Fig. 3.1, Raisz, 1945; Mann and Meyer, 1993]).

Accretion of Siletzia ended a period of Laramide-age flat-slab subduction and consequent magmatic quiescence within what was previously a magmatic arc in Idaho (Idaho Batholith [Fig. 3.1], e.g., Gaschnig et al., 2010) and northeastern Washington (e.g., Burchfiel et al., 1992). With its accretion, subduction jumped to the western margin of Siletzia, thereby establishing the Cascadia subduction zone. Cascade arc magmatism is recognized within the Siletzia lithosphere starting about 45 Ma (Priest, 1990). Over a brief duration during or immediately following accretion, tectonic deformation switched from the compression that typified the Laramide orogeny to extension, as exemplified by metamorphic core-complex extension in northern Washington and Idaho and western Montana (Fig. 3.1, Foster et al., 2007). Magmatism was prolific around the accretionary

boundaries of Siletzia (i.e., the Kamloops, Challis and Clarno volcanism of British Columbia and northern Washington, Idaho, and central Oregon, respectively). This new magmatic and tectonic regime represents the sudden onset of the Cordilleran ignimbrite flareup and post-Laramide extension that propagated away from this area to involve, eventually, the entire western U.S., and which is thought to be a consequence of flat-slab removal from basal North America (Coney and Reynolds, 1977; Coney and Harms, 1984; Humphreys, 1995; Schmandt and Humphreys, 2011).

The Cascade magmatic arc has been created by oblique subduction of the Juan de Fuca plate beneath North America. It is segmented in character along strike. In Oregon, the High Cascades have experienced arc-normal extension to create a discontinuous axial graben (Hughes and Taylor, 1986; Priest, 1990; Sherrod and Smith, 1990). Within this graben eruptive rates (Schmidt et al., 2008) and heat flow (Blackwell et al., 1990a, b) are high, and vents are numerous.

With intra-arc extension of the southern Cascades and Siletzia rotation about an Euler pole near the SE corner of Washington (Wells and Simpson, 2001; McCaffrey et al., 2007), the forearc has rotated clockwise at a rate of $\sim 1^\circ/\text{Ma}$ (Wells, 1990). This has transposed the older western Cascades of Oregon to its current position ~ 100 km west of the High Cascades. Cascade magmatic eruption rate and heat flow diminish rapidly to the north, corresponding with the decreasing intra-arc extension rate (Blackwell et al., 1990a, b). In Washington, the axis of the active High Cascades partly overlies the older western Cascades (Fig. 3.1) as well as uplifted pre-Tertiary basement. Along the entire length of the Cascades, heat flow is low in the older western Cascades (Blackwell et al., 1990b). The distribution of subducted sediment is irregular along the Cascade forearc Coast

Ranges, but a large mass comprises the Olympic Mountains, where sediment accumulation has uplifted the overlying basaltic crust (Crescent formation, Fig. 3.1), which has been lost to erosion (Brandon et al., 1998).

A third major magmatic event, following the ignimbrite flareup and the formation of the Cascade arc, began with the ~16 Ma Steens-Columbia River Basalt eruptions (e.g., Hooper et al., 2002; Camp et al., 2003). Earth's most recent flood basalt event, erupting over 200,000 km³ of basaltic andesite and basalt that covered much of eastern Oregon and southern Washington east of the Cascades, this event is the initial Yellowstone hotspot magmatism within North America. The fissure eruptions were concentrated along a ~N-S trend in easternmost Oregon that parallels the western margin of Precambrian North America. The Columbia River Basalt eruptions occurred within a narrow swath of Mesozoic and Paleozoic terranes that lie adjacent to Precambrian North America; the basement of the Steens source area is unknown. The Columbia River Basalt eruptions are the largest and most northerly of these flood basalt eruptions, occurring at the northwestern end of what would become the Snake River Plain. Whether they have a mantle plume origin (Brandon and Goles, 1988; Camp and Ross, 2004) or are related to back-arc hydration and extension (Carlson and Hart, 1987), the magmatic activity can be expected to have modified the lower crust. Geochemical evidence places one or more large magma chambers in the lower crust (Carlson, 1984; Wolff et al., 2008), and the ~2 km of uplift focused on the Wallowa pluton during and shortly after the Columbia River Basalt eruptions indicates the loss of its dense plutonic roots at about this time (Hales et al., 2005). The Wallowa uplift lies at the center of an oscillating circular pattern of uplift and downwarp ~200-km in diameter (pink outline in Fig. 3.1), suggesting lithospheric

modification on this scale. The circular uplift pattern and the short duration of eruptions from this area suggest significant and simply-structured changes in the crust or mantle lithosphere created by a combination of Columbia River Basalt magmatism involving lower crustal magma chambers and a (probably related) lower-crustal delamination event.

3. Data and methods

Fig. 3.2 shows the station distribution used in this study of the Pacific Northwest, color coded by array and comprising a total of about 280 broadband stations. These include stations from EarthScope Transportable Array, the Wallowa array, 30 stations of the High Lava Plains array, and seven permanent stations. We deployed the Wallowa flexible array of 20 broadband three-component seismometers that were borrowed from PASSCAL (Program for Array Seismic Studies of the Continental Lithosphere) in the fall of 2006 and operated the stations for two years in parts of southeastern Washington, northeastern Oregon and western Idaho. In the summer of 2008, 10 of these stations were moved to new locations to extend the array and recorded data for one additional year. The average station spacing is ~10 km for the Wallowa array along 5 short lines, ~30 km for selected High Lava Plains stations used in this study, and ~75 km for Transportable Array stations. The station coverage and deployment time overlap of these three networks from 2006-2009 make it possible to create a dense array and study the shallow structures in detail with ambient noise method. The seismic data are archived at and retrieved from the IRIS Data Management Center and re-sampled to 20 points/second.

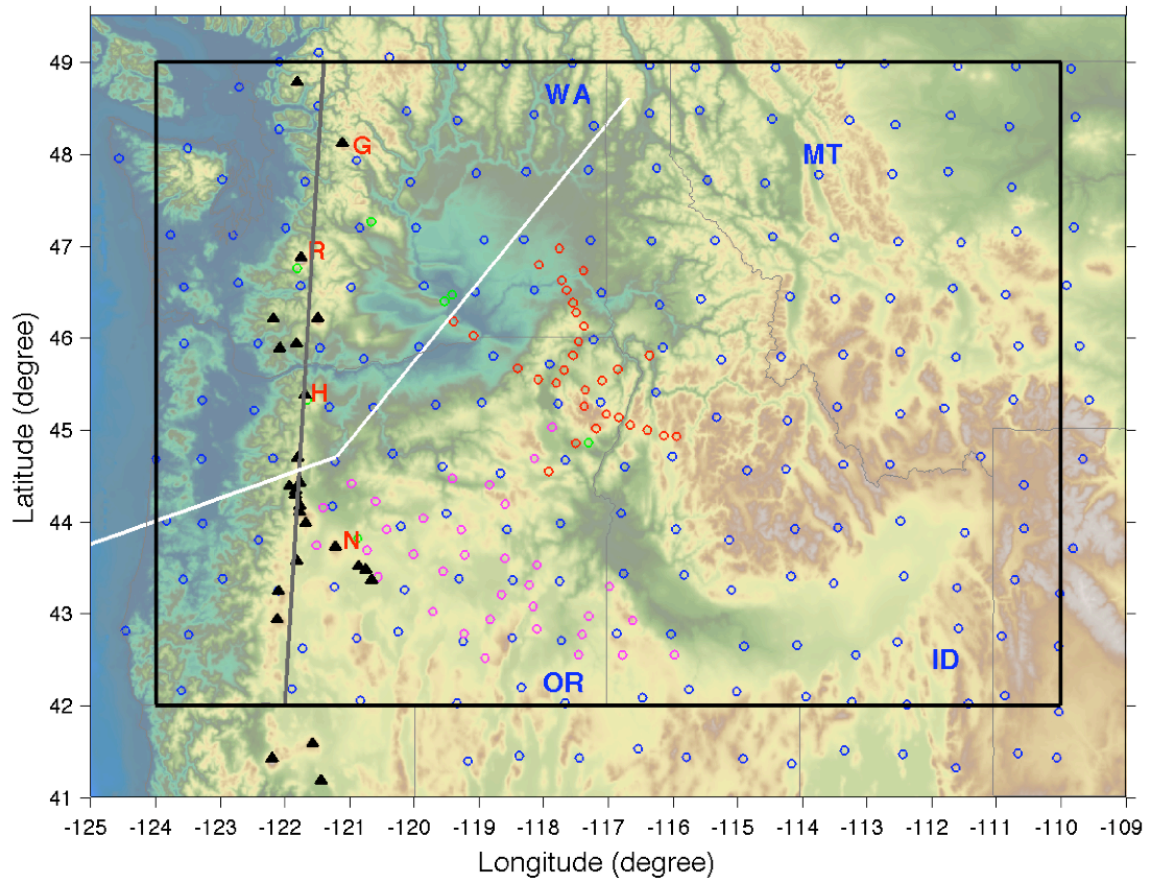


Figure. 3.2. The station distribution used in this study: blue circles, Earthscope USArray Transportable Array; Red circles, Wallowa flexible array; Magenta circles, 30 stations of High Lava Plains array; Green circles, 7 permanent stations. The gray line is the profile location shown in Fig. 3.7 and the white line is the profile of the cartoon in Fig. 3.8. The black rectangle is the imaging area shown in Figs. 3.4-3.6. Quaternary volcanoes (black triangles) are shown as in Fig. 3.1, with volcanoes as: G, Glacier Peak; R, Mt. Rainier; H, Mt. Hood; N, Newberry.

In recent years the ambient noise method has been applied to measure the short and intermediate period dispersion of phase or group velocity for Rayleigh and Love surface waves (e.g., Campillo and Paul, 2003; Shapiro and Campillo, 2004; Yao et al., 2006; Bensen et al., 2007; Yang et al., 2008; Lin et al., 2008; Moschetti et al., 2010; and now, many others). Here we consider fundamental-mode Rayleigh waves recovered from ambient noise cross-correlation and estimate the phase velocity from periods 6-40

seconds to study the crust and uppermost mantle structures of the Pacific Northwest using the methods of Yao et al. (2006, 2008). The recovered Rayleigh-wave empirical Green functions from noise cross-correlations of continuously recorded waveforms on the vertical component between two stations are used to calculate frequency-dependent inter-station phase velocities; to satisfy the far-field approximation of surface wave propagation, we require that the inter-station distance is at least twice the wavelength. For each station pair, the cross-correlations of data from three years are stacked in order to increase the signal-to-noise ratio. The three years of data resulted in $\sim 35,000$ inter-station ray paths with a good path coverage in the study area, and the farthest distance between two stations exceeds 1000 km. Using a node spacing of $0.25^\circ \times 0.25^\circ$, the inter-station phase velocity dispersion curves are inverted for 2-D isotropic phase velocity maps at periods of 6-40 seconds. For this inversion we used the continuous regionalization method of Montagner (1986) and we choose the spatial correlation length (which controls model smoothness) as the maximum between 50 km and one-third of the wavelength for each period.

The phase velocity maps were inverted using the Neighborhood Algorithm of Sambridge (1999a, b), see Yao et al. (2008) for details, to construct a 3-D isotropic shear-wave velocity model of the crust and uppermost mantle. For our initial and reference shear-wave velocity models we use the western United States tomography model of Yang et al. (2008), which is based on ambient noise tomography and two-plane wave earthquake Rayleigh wave modeling and resolves structure to 200 km depth, and the North America upper mantle velocity model TNA of Grand and Helmberger (1984) deeper than 200 km. For Moho depth we use the initial value estimated from our receiver

function study, which uses the same stations that are used in our ambient noise study. Moho depth is found to vary from 22 to 55 km in the study area.

For each map node the Neighborhood Algorithm searches for the ensemble of the best-fitting 1-D models. Each 1-D model is represented by Moho depth and the velocity in five layers: the crust has three layers of thickness ratio 0.25:0.35:0.40 (from the upper to the lower crust), and there are two layers beneath the Moho, of thickness 40 km and 70 km, representing the uppermost mantle and deeper upper mantle, respectively. The shear-wave velocity is allowed to vary ± 0.5 km/s in the crust and ± 0.4 km/s in the uppermost mantle with respect to the reference model of each grid point. For the deepest layer, the range for shear-wave velocity perturbation is restricted to ± 0.25 km/s since our dispersion data (up to 40 seconds) have little sensitivity to structure in that depth range. The V_p/V_s ratio is fixed at 1.76 in the crust and 1.80 in the mantle. The crustal density is calculated from empirical relationships due to Brocher (2005) and for the upper mantle layers we use a perturbation relationship given by Masters et al. (2000). Moho depth is allowed to vary by ± 6 km during inversion. Using this approach, the most serious problem is the tradeoff between Moho depth and model velocities for layers near the Moho. For instance, if Moho was erroneously located too deep, lower crust and uppermost mantle velocities would be assigned velocities that were, respectively, too fast and too slow.

At each map node we first perform Neighborhood Algorithm search for these 6 parameters to identify regions of global minimum in the model space. In the second step we perform statistical analysis of the generated models to obtain the posterior mean model and the associated standard error of each model parameter (Sambridge, 1999b). Except grid points near the model margins, the Neighborhood Algorithm usually finds

models that fall within given uncertainties (see example in Fig. 3.3). To check the reliability of the velocity model given by the Neighborhood Algorithm we perform forward calculations of dispersion from the obtained model and compare against the observed phase velocity for each grid point. The predicted phase velocities agree well with the observed phase velocities (Fig. 3.3).

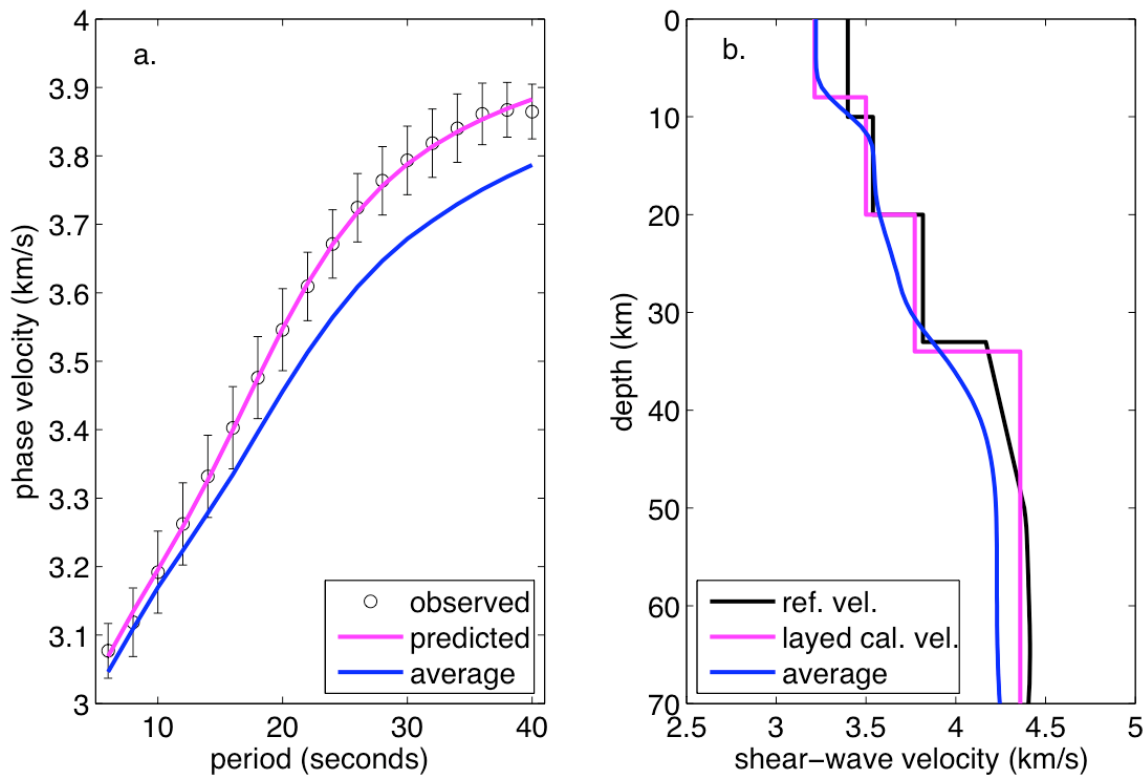


Figure. 3.3. Inversion result at one grid point (longitude: -117.5, latitude: 46.5). (a) Comparison of the observed (black circles with uncertainty bars) and predicted (magenta line) phase velocities estimated from the inverted shear-wave velocity (magenta line in (b)). The blue line is the average phase velocity in the studied area; (b) 1-D shear wave velocity from the surface to 70 km depth. The black line is the reference velocity model from Yang et al. (2008) at this location. The magenta line is the posterior mean layered shear-wave velocity model from the Neighborhood Algorithm. The blue line is the average 1-D shear-wave model in the studied area.

4. Results

Our isotropic Rayleigh-wave phase velocity and shear-wave tomography results are similar to those produced with the use of only EarthScope Transportable Array data (Yang et al., 2008; Lin et al., 2008), though inclusion of the many ray paths recorded by the Wallowa and High Lava Plains flexible arrays has resulted in higher resolution of the Cascades, Siletzia and the greater source region of the Columbia River Basalts (Figs. 3.4-3.6). Average phase velocities from periods 6-40 seconds are ~ 3.05 - 3.78 km/s, corresponding to shear-wave velocities of 3.25-4.30 km/s from the surface to 70 km depth (Fig. 3.3). The average Moho depth in the study area from our receiver function estimate, at 36 km, is ~ 4 km deeper than that of Yang et al. (2008), resulting in significant differences in shear-wave velocity models near the Moho. Fig. 3.4 shows our phase-velocity perturbation maps and Fig. 3.5 shows the shear-wave velocity anomaly model averaged in the upper, middle, and lower crust and uppermost mantle. Considering the variations in Moho depth in the area studied, the shear-wave velocity structure at depth between 25-45 km (Fig. 3.6) is a combination of lower crust and uppermost mantle structures in different regions. Generally, we resolve small-scale structures (~ 50 km) at shallow depths and uniform large-scale structures (~ 100 km) at lower crustal and upper mantle depths.

In a regional sense, most of Oregon except the western Cascades and northernmost part is slow in the upper crust and upper mantle, with a more complex but generally fast lower crust. This depth-alternating velocity structure is more pronounced in Idaho. In southern Idaho, velocities are slow, fast, slow for the upper crust, mid- to lower crust, and upper mantle (respectively), whereas in northern Idaho and western Montana

the respective velocities are fast, slow, fast. Eastern Washington and northernmost central Oregon east of the Cascades are seismically fast at all depths, with a prominent exception of the very slow western Columbia Basin upper crust. The average crustal velocity in the 15-30 km (and especially 25-30 km) depth range is remarkably similar to surface elevation throughout the studied area, with low velocities corresponding to high elevations.

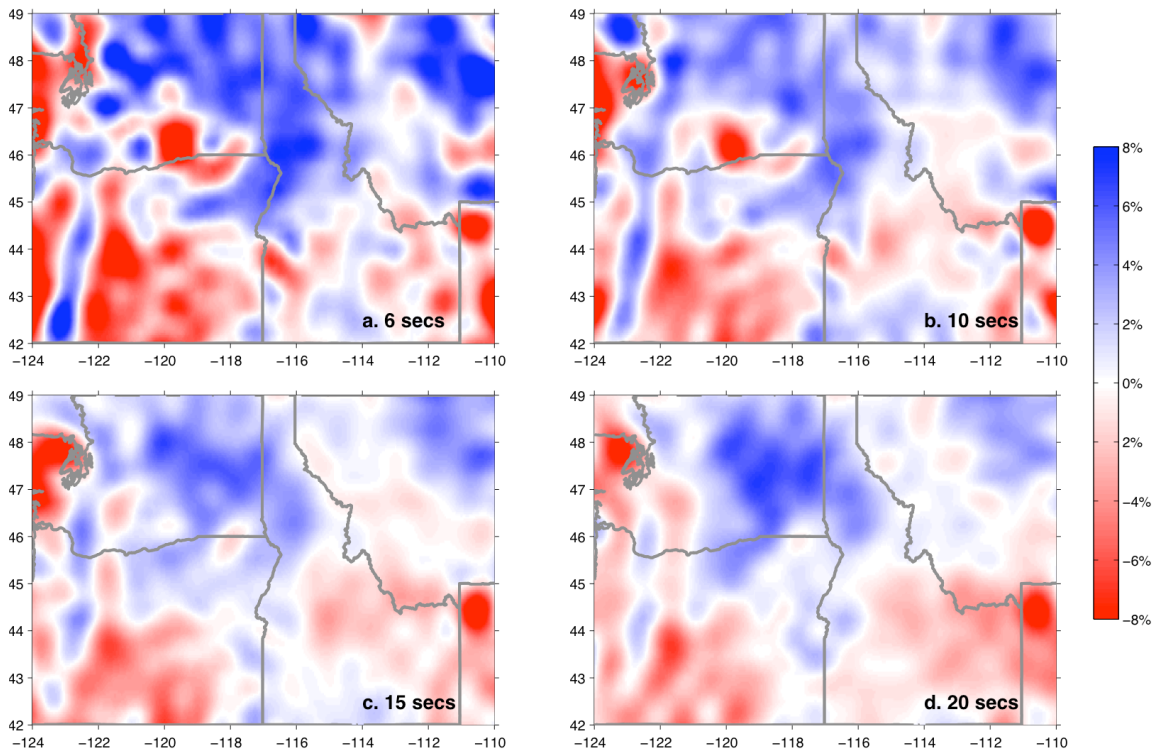


Figure. 3.4. Fundamental-mode Rayleigh-wave phase velocity perturbation maps at periods indicated in a range of $\pm 8\%$ velocity perturbation relative to the average in the studied area. Figs. 3.4-3.6 share the same color scale.

The Cascades are highly structured from the upper crust through to the upper mantle (Fig. 3.7). Uppermost crustal velocities in northeastern Washington display a series of north-trending low- and high-velocity stripes (Fig. 3.5a). These structures could be related to the similarly oriented metamorphic core complexes that experienced

significant extension ~50 Ma across much this area and extending to near the Idaho-Montana border (yellow patches in Fig. 3.1, Foster et al., 2007). Below, we focus on four major structures. In chronological order of creation, these are the Siletzia terrane, the western Columbia Basin, the Cascade Mountain range, and the Columbia River Basalt source area.

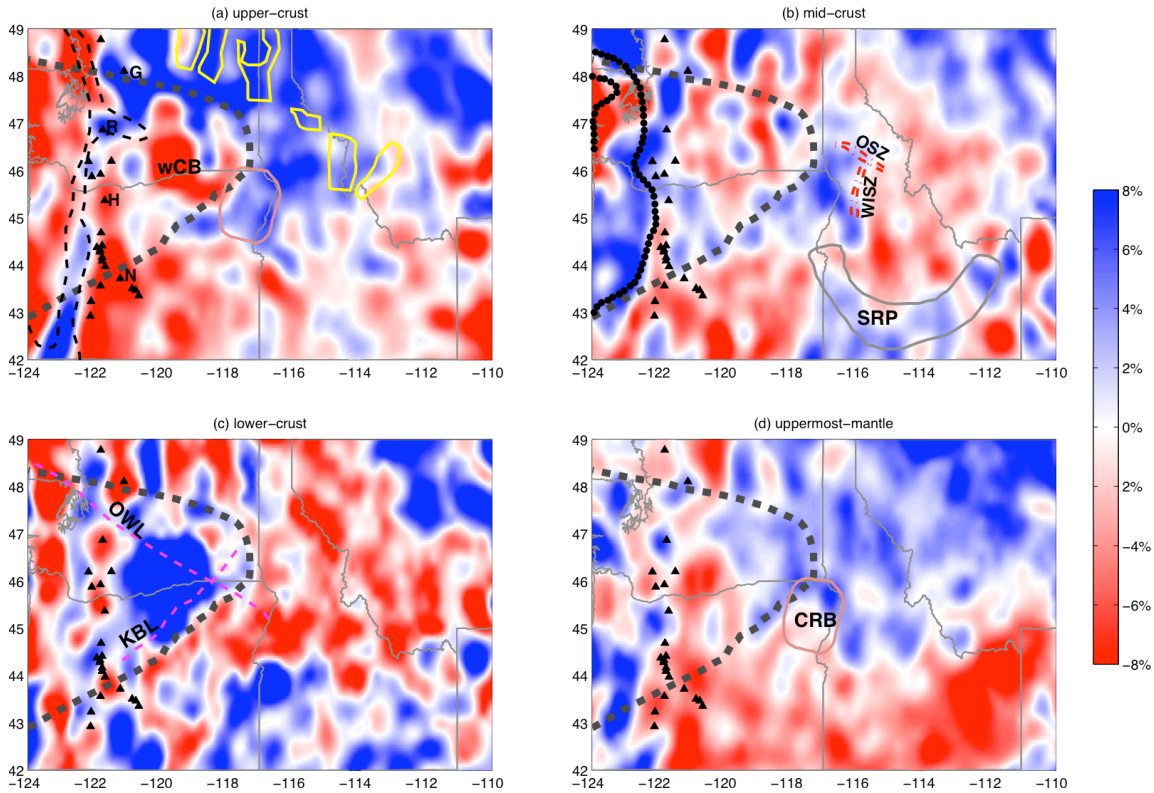


Figure 3.5. Shear-wave velocity variation (in percent) with respect to the average model in the study area of the upper crust, middle crust, lower crust and uppermost mantle, respectively. Layer thicknesses vary to conform to Moho depth. In the crust, the thickness of each layer (from upper- to lower-crust) is laterally variable while the thickness of the uppermost mantle is set to be 40 km. The thick dashed gray line in (a-d) shows our inferred distribution of Siletzia. In (a), the black dashed line shows 40 and 50 mW/m² heat flow contours (Blackwell et al., 1990b). Yellow lines outline the Cenozoic metamorphic core complexes. In (a) and (d), the source area of Columbia River flood basalt is marked (CRB, pink outline). In (b), outline of western Siletzia indicated by magnetic anomalies (black dots, Wells et al., 1998) is marked, and western Idaho shear zone (WISZ, N-trending red dot-dashed lines) and Orofino shear zone (OSZ, NW-trending red dot-dashed lines) are shown. In (c), the Klamath-Blue Mountains gravity Lineament (KBL) and Olympic-Wallowa Lineament (OWL) are shown. See Fig. 3.1 for other structures and abbreviations.

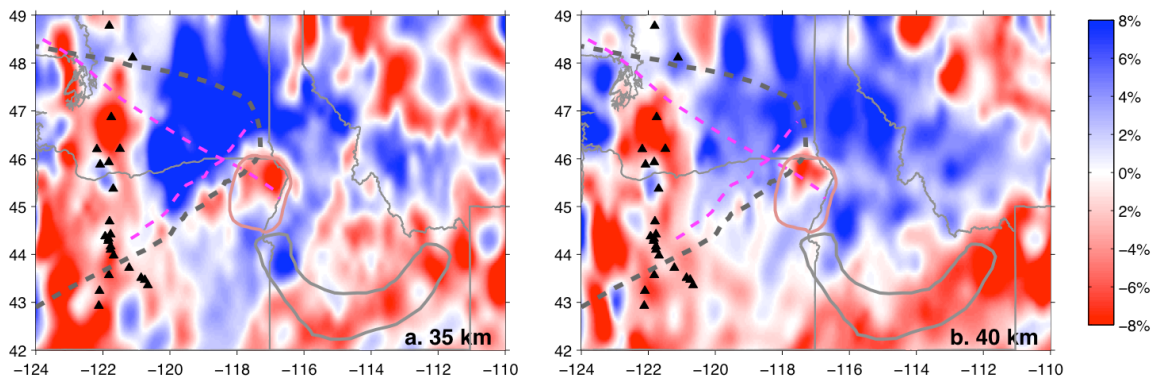


Figure. 3.6. Imaged shear-wave velocity anomaly model at depths 35 km and 40 km. See structures in Figs. 3.1 and 3.5.

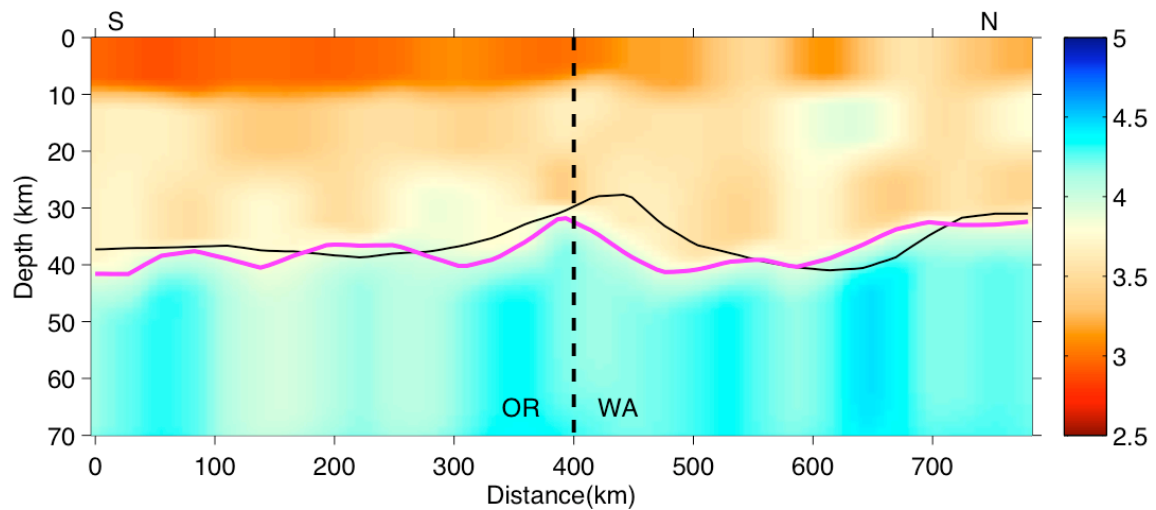


Figure. 3.7. Vertical cross section along the Cascade volcanic arc, showing the absolute shear-wave velocity (km/s) with depth. Fig. 3.2 shows profile location. Black line is the Moho interface from Yang et al. (2008), and the Magenta line is from this study. The vertical dashed line marks the state boundary between Oregon and Washington.

4.1. Siletzia terrane

The boundaries and distribution of the oceanic Siletzia terrane are well defined west of the Cascades using geologic outcrop and a strong and distinctive magnetic pattern (outlined on Figs. 3.1 and 3.5b, Wells et al., 1998), and in this area Siletzia coincides with the area of distinctive high seismic velocity imaged in the middle crust (Fig. 3.5b). This is consistent with the interpretation of the Siletzia terrane as accreted oceanic lithosphere (Trehu et al., 1994; Schmidt et al., 2008). An exceptional area in and around the Olympic Peninsula is seismically slow at and above 30 km depth. This low-velocity volume (as discussed by Calkins et al., 2009) is consistent with the crust being composed of off-scraped and underthrust subducted sediments (Brandon et al., 1998). The area of this low-velocity crust extends west to near the Washington coastline, roughly paralleling the subducting Juan de Fuca slab (Fig. 3.5), but it does not extend south into Oregon, where Siletzia is imaged to increase to ~35 km in thickness (Trehu et al., 1994). At greater depths, seismic velocities are fast, consistent with the presence of the subducting Juan de Fuca slab beneath the area.

The distribution and structure of Siletzia east of the Cascades is based on indirect evidence and speculation. The strong gravity gradient across the Klamath-Blue Mountains lineament in north-central Oregon suggests an abrupt transition from the accreted Siletzia and older North America to the south. A strong and sharp seismic contrast across the Klamath-Blue Mountains lineament in north-central Oregon is in the lower crust (Fig. 3.5), supporting the view that this lineament represents a suture between Siletzia and North America. The NE boundary of Siletzia is not exposed. The lower crust in south-central Washington and north-central Oregon is seismically very fast, whereas

the upper crust is very slow and surrounded by high velocities. The area of slowest upper crust and fastest lower crust occupies the region that experienced major rifting, which is the subject of the following subsection. Adjacent to the very fast lower crust to the east and north, the lower crust and uppermost mantle is moderately fast.

4.2. Western Columbia Basin

The western Columbia Basin in south-central Washington and northernmost central Oregon is underlain by set of deep Eocene sedimentary basins (Campbell, 1989) that now are largely covered by several kilometers of Columbia River Basalt flows (Reidel et al., 1989), which themselves are overlain by a thin Quaternary and Pliocene sedimentary layer. The average velocity of the upper crust beneath the western Columbia Basin is very slow (Fig. 3.5), consistent with preexisting views of deep sedimentary basins there (Campbell, 1989; Evans, 1994). The lower crust beneath these basins is very fast, with a velocity comparable to the upper mantle (Fig. 3.5). The area of very high velocity extends north farther than does the area of very low velocity upper crust, extending beneath the area of northern Washington core complexes and locally reaching the Canadian border in the lower crust and the uppermost mantle (Fig. 3.5).

4.3. Cascade mountain range

The seismic structure and the magmatic and tectonic character of the Cascade volcanic arc vary strongly along strike. Seismic velocities in Oregon are slow at all depths from the upper crust to upper mantle beneath the active High Cascades volcanoes and Newberry volcano in the adjacent back-arc (Figs. 3.5 and 3.7). In contrast, seismic

velocities beneath the Washington Cascades appear spotty with volcano-centered velocity anomaly pattern, and velocities tend to be fast, slow, fast for the upper crust, lower crust and upper mantle, respectively. Mt. Rainier (near 47°N) and Glacier Park (near 48°N) show this pattern especially well. The area south of Mt. Rainier and north of Mt. Hood is transitional in character between the northern Washington Cascades and the Oregon Cascades. The upper mantle beneath the active Cascades tends to be slow to the depth of our resolution at 50 km, with local high-velocity volumes occupying the upper mantle beneath the northern Washington Cascades.

A well-imaged trend of high seismic velocity is present in the upper and middle crust of the old western Oregon Cascades (Fig. 3.5). This trend extends north at 10-30 km depth with an axis near but west of the Washington Cascades. The shape of the high-velocity forearc mid-crust parallels the Cascadia subduction zone, even where the slab bends around the Olympic Peninsula (Fig. 3.5b).

4.4. Columbia River Basalt source area

The Columbia River Basalt eruptive source area, in the NE corner of Oregon (Fig. 3.1), is seismically fast in the upper-to-middle crust and slow in the lower crust. Velocities are 3-5% fast at and above 20 km. The distribution of high velocities in the upper crust corresponds well with the area of Mesozoic accreted arc terranes. In the mid-crust we find a seismic contrast at the eastern margin of the Columbia River Basalt source area along west of the western Idaho shear zone, at the Precambrian margin of North America (Fig. 3.5b). The high velocities correlate with and may well be consequence of the Cretaceous-accreted oceanic Blue Mountains terrane, although

velocities are fastest within the circular area shown in Fig. 3.1, especially at 20 km depth. At near-Moho depths (30-40 km, Fig. 3.6) beneath this circular area we image a pronounced low velocity volume (3-6% slow) that, with increasing depth, becomes slower, smaller, more northerly, and more completely surrounded by high velocity rock. This is very pronounced at 35 km depth (Fig. 3.6), giving the appearance of a lithospheric hole beneath the main area of CRB eruptions.

5. Discussion

Continental growth is typically associated with magmatic silica enrichment processes within a volcanic arc, either within a continent or an oceanic island arc that is later accreted. Accretion of the Siletzia fragment of Farallon ocean lithosphere is related to the termination of amagmatic flat-slab subduction, initiation of the ignimbrite flareup and continental extension. The combination of these processes added area to North America and modified both North America and the accreted lithosphere itself, thereby growing and evolving a large portion of continent in ways not often considered. We use several observations relevant to the Cenozoic evolution and physical state of the Pacific Northwest to propose in the following sections that Siletzia lithosphere currently underlies much of Washington and Oregon, and suggest that the occurrence of extension around and within Siletzia was enabled by the change from compressive Laramide subduction to extension associated with rollback of the newly-established Cascadia subduction zone. Accretion of Siletzia is also thought to be responsible for the magmatic flareup that occurred around its margins as the flat-subducting Farallon lithosphere fell away (Schmandt and Humphreys, 2011) and initiated flat-slab removal that propagated

away from the PNW across most of the western U.S. An illustrative cartoon (Fig. 3.8) is used to display the major structures discussed in the following sections.

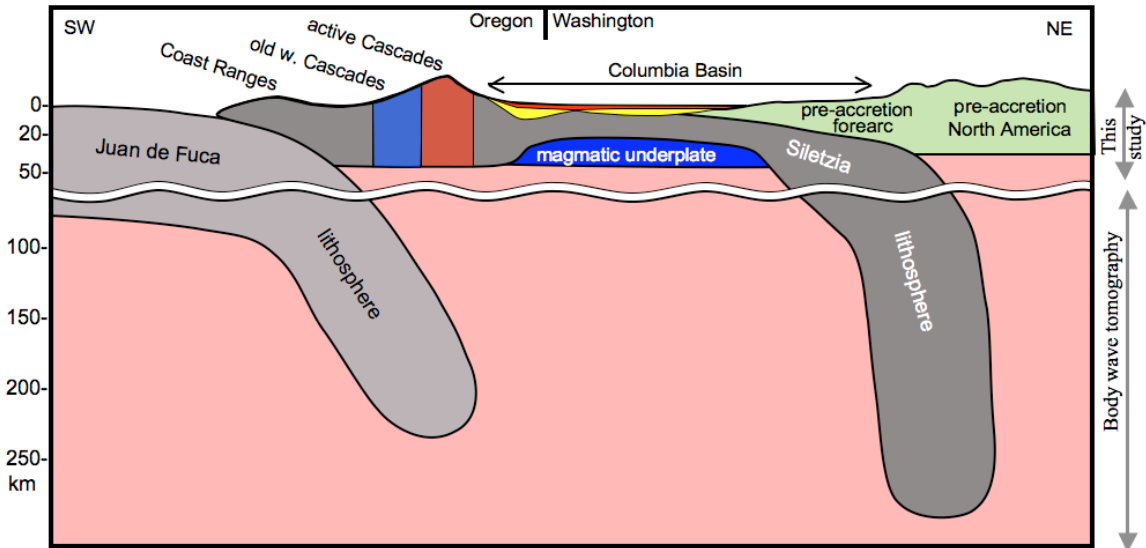


Figure. 3.8. Cartoon cross section illustrating the major structures inferred from our ambient-noise tomography, emphasizing the inferred distribution of Siletzia (dark gray). Cross section location shown in Fig. 3.2. Structure deeper than 70 km is from body-wave tomography (Schmandt and Humphreys, 2011). Seismic velocity is fast beneath the Oregon western Cascades and slow beneath the Oregon High Cascades. The dark blue patch is the underplated crust (seismically fast) overlaid by deep Eocene sedimentary basins (dotted yellow area, seismically slow) which are largely covered by Columbia River Flood Basalts (CRB) in south-central Washington. Siletzia lithosphere thrusts under the pre-accretion forearc.

5.1. Distribution of Siletzia lithosphere within North America

Geologic outcrop delineates well the northern and southern sutures west of the Cascades, and the NE-trending Klamath-Blue Mountains gravity lineament appears to be the southern boundary of Siletzia (Riddihough et al., 1986). The interpretation of this lineament as a suture is reinforced by the strong seismic contrast imaged across this boundary (Fig. 3.5) and by its along-strike extension to the mapped suture west of the Cascades (Fig. 3.1, Wells et al., 1998). In detail, the high-velocity lower crust and upper

mantle extend 30-40 km SE of the Klamath-Blue Mountains lineament (Fig. 3.5), beneath the northern Blue Mountains, suggesting that the upper crustal and lower crustal suture are offset from one another. This suggests that Siletzia occupies a strip of lower crust and upper mantle just southeast of the inferred upper crustal suture (i.e., the Klamath-Blue Mountains lineament) and that with Siletzia accretion the flat-subducting slab to the south tore away from Siletzia. The area exposed to asthenosphere experienced the Clarno magmatism ~54 Ma (Retallack et al., 2000), ending a period of magmatic quiescence.

The major outstanding questions about Siletzia are the nature and distribution of Siletzia along its NE side. We hypothesize that Siletzia lithosphere underlies the area outlined with the gray dashed line in Fig. 3.1 (and Fig. 3.5), and that the NE margin of Siletzia underlies the pre-accretion forearc of its subduction zone. The reasons leading us to infer this extensive distribution of Siletzia lithosphere beneath much of the area east of the Cascades are: (1) Prior to Siletzia accretion Siletzia subducted beneath a forearc located between an early Cretaceous volcanic arc (trending from north-Washington Cascades to central Idaho, e.g., Gaschnig et al., 2010) and the vicinity of the Olympic-Wallowa lineament (e.g., Christiansen and Yeats, 1992; Burchfiel et al., 1992). Subduction beneath this area continued amagmatically until the time of Siletzia accretion (Giorgis et al., 2005; Geherls et al., 2009), and there is an absence of magmatic or tectonic evidence for post-accretion removal of this lithosphere. (2) The lower crust just inside of the gray dashed line in Fig. 3.1 (and Fig. 3.5c) is seismically fast compared to nearby North America lithosphere, as expected for oceanic lithosphere. The upper mantle also is fast there and farther east, beneath northern Idaho (Fig. 3.5d, and at 60-125 km depth from Schmandt and Humphreys, 2010), which may represent the eastward

continuation of Siletzia lithosphere at greater depth. (The very fast lower crust in south-central Washington and north-central Oregon is attributed in the following sub-section to post-accretion rifting of Siletzia lithosphere.) (3) The area of fast lower crust and upper mantle spans the gap between central Washington and the seismically-inferred deeper distribution of subducted Siletzia lithosphere thought to be preserved and hanging vertically across most of the upper mantle beneath an arcuate trend extending from the north-Washington Cascades to south to central Idaho (Schmandt and Humphreys, 2011). And (4) all of eastern Washington south of the core complexes lies at low elevation (Fig. 3.1) and acts as a rigid block (Magill et al., 1982; McCaffrey et al., 2000) as it rotated clockwise at a rate of $\sim 1^\circ/\text{Ma}$ since accretion (Wells et al., 1984; Wells and Simpson, 2001), accompanied by Basin and Range extension within the High Lava Plains to its south, and N-S contraction along its northern side across the Yakima fold-and-thrust belt (within the forearc rocks beneath which Siletzia subducted). The nearly rigid behavior and low elevation of Siletzia, both of which are anomalous in the western U.S., are attributed to its strong oceanic rheology and high density. This behavior is expected for oceanic lithosphere that has been incorporated into a continental setting, similar to that of the Black Sea (Zonenshain and Pichon, 1986), southern Caspian Sea (Brunet et al., 2003) and western Great Valley (Godfrey et al., 1997).

5.2. Rifting origin of the western Columbia Basin

The extension that followed Siletzia accretion included both the Pacific Northwest core complexes within the mountainous areas in northern Washington and the Rocky Mountains of Idaho and Montana (yellow outlines, Fig. 3.1), and the area now occupied

by the western Columbia Basin (wCB in Fig. 3.1), where extension created major sedimentary basins at low elevation (e.g., Evans, 1994) that later were covered by the Columbia River Basalt flows. Western Columbia Basin extension occurred within what we presume to be Siletzia lithosphere and overlying forearc rocks, and the timing of extension appears to be simultaneous with core-complex extension to the north, based on the contemporaneous age of bimodal volcanism.

The very slow upper crust beneath the western Columbia Basin is consistent with preexisting views of deep sedimentary basins there (Campbell, 1989; Evans, 1994). However, the sediment thickness distribution estimated from scant outcrop and well data (Campbell, 1989) remains poorly defined, and the inferred depocenter is offset ~50 km west from a prominent Bouguer gravity high and Columbia River Basalt thickness maximum, both of which are centered on the area of very low seismic velocity. We suspect that the actual thickness of sediment is greatest where the upper crustal velocity is lowest, and therefore exceeding the ~7 km found by drilling. Considering that mid-crustal velocities are not seismically anomalous in this region (Fig. 3.5b), the deepest sedimentary basins probably do not extend much below ~10-15 km depth. Away from the region of slowest upper crustal velocities, the pattern of low velocity follows well the sediment isopach map of Campbell (1989), especially on the south and east sides of the basins.

The very fast lower crust underlies the entire area of Eocene sedimentary deposition (Fig. 3.5). This structure previously was imaged beneath the Pasco Basin by Catchings and Mooney (1988), who attributed the high-velocity lower crust to mafic underplate emplaced during the Eocene extension. Our images broaden the area of

inferred extension and underplating. The occurrence of Eocene metamorphic core-complex extension across elevated areas of northern Washington contrasts with the simultaneous extension of the low-lying Siletzia lithosphere, presumably reflecting compositional and density differences between the continental and oceanic lithospheres.

A switch from strong contraction during the Laramide orogeny to strong and pervasive extension occurred quickly near the time of Siletzia accretion in the Pacific Northwest (Van der Pluijm et al., 2006; Foster et al., 2007). Flat-slab subduction probably occurred prior to accretion, based on the absence of arc magmatism and the strength and inboard setting of the contraction (e.g., Feeley, 1993). With Siletzia accretion and the initiation of Cascadia subduction, the rapid onset of extension could be driven by gravitational collapse of the thickened crust (e.g., Jones et al., 1998) and enhanced by an active rollback of the newly-subducted Farallon lithosphere at Cascadia (e.g., Gurnis, 1992).

5.3. Cascades

Variations in temperature and composition relate to crustal seismic velocity in simple ways. In northern Washington, the velocity of the active Cascades upper and middle crust is fast (Fig. 3.5) where volcanic production rate (Schmidt et al., 2008) is low and heat flow is ≤ 40 mW/m² (Blackwell et al., 1990a, b). In contrast, Oregon Cascades volcanic production rate is very high, heat flow typically ≥ 80 mW/m² (Blackwell et al., 1990a, b) and crustal seismic velocities are very low. This set of observations suggest that magmatic intrusion of the upper crust increases seismic velocity (for Washington), but that the thermal effects of heat advection counteract this and become dominant when

magmatism is strong (for Oregon). The one feature that characterizes the entire active Cascades volcanic arc is seismically slow lower crust, which could reflect the near- to super-solidus conditions there.

The older western Cascades define a zone ~100 km wide that strikes NNE across Oregon and into southern Washington, where they trend beneath the active Cascades (Fig. 3.1). Magmatism in the western Cascades was last active about 17 Ma, and the heat flow is low (generally ≤ 40 mW/m²). The western Cascades middle crust shows a strong correlation between the area of high velocities and the distribution of Siletzia (Fig. 3.5b, Wells et al., 1998), which we attribute to the basaltic composition of Siletzia and the overlying western Cascades, along with the low temperatures.

5.4. Columbia River Basalt source area

Several major structures align with the circular pattern of uplift and downwarp (pink outline in Figs. 3.1 and 3.5) that were created during and after Columbia River Basalt eruptions (Hales et al., 2005) from this area. Considering that the magmatic volume of the CRB eruptions was very large and that the magma equilibrated at depths above ~30 km (Ramos et al., 2005), it is reasonable to infer that a large magma chamber resided within the crust beneath the topographically disturbed area and that the mantle lithosphere was lost. The seismic structure at 35-40 km (Fig. 3.6) images such a hole in the mantle lithosphere. Because the CRB eruptions were the first in this region since Cretaceous, we suggest that it was Siletzia lithosphere remained beneath NE Oregon until it was displaced by the CRB event.

Directly beneath the location of the topographically disturbed circular area and

the anomalously low-velocity rock at 35-40 km depth, teleseismic body-wave tomography (Schmandt and Humphreys, 2011) images a hole within a patch of high-velocity mantle at 60-90 km depth, indicating that this hole extends yet deeper. At greater depth, a strongly anomalous (up to 3% P-wave velocity perturbation) high-velocity upper mantle anomaly is imaged at depths of ~125-300 km. The location of the high-velocity body beneath the apparent lithospheric hole provides a plausible accounting for the missing lithosphere. If these interpretations are correct, then the source area for the CRB event has a series of elements that are generally well aligned vertically extending from the surface to ~300 km depth, including: the main CRB dikes exposed at the surface, the mid- to lower-crustal magma chamber that fed these dikes, a patch of missing mantle lithosphere (presumably Siletzia), and the detached lithosphere. Although not understood, we note that these structures are near the Precambrian margin of North America ($^{87}\text{Sr}/^{86}\text{Sr}$ 0.706 line in Fig. 3.1), the presumed southern crustal suture of Siletzia (KBL in Fig. 3.5c) and the slab-like high-velocity body extending vertically across the upper mantle beneath Idaho (argued to be subducted Siletzia lithosphere by Schmandt and Humphreys, 2011).

6. Conclusions

Accretion of the Siletzia terrane to North America ~50 Ma abandoned a piece of oceanic lithosphere within what now is continent. Seismically imaged crust and upper mantle structure (Figs. 3.5, 3.6 and 3.8), when considered with the geologic record of magmatism and tectonism, supports a view that this high-velocity lithosphere remains beneath the pre-accretion forearc (the seismically-fast lower crust in Fig. 3.5c), was torn at its southern margin (the NE-trending sharp velocity gradient in Figs. 3.5c and 3.6a),

and was strongly extended and magmatically underplated during or shortly after accretion (Fig. 3.8, very slow upper crust and very fast lower crust in Fig. 3.5). This oceanic lithosphere remains dense and strong compared to the elevated and deforming western U.S. Cordilleran in which it is embedded, although the construction of the Cascade arc and the addition of magmatic underplate and sediment fill within deep extensional basins is converting this lithosphere into continent. Thus, North America has grown through the addition and modification of oceanic lithosphere.

The accretion of Siletzia terminated flat-slab subduction beneath North America and initiated normal-dip subduction at Cascadia. This led to a sudden termination of Laramide amagmatic compression and initiation of the magmatically intense ignimbrite flareup and post-orogenic extensional collapse across the Pacific Northwest. This switch in magmatic and tectonic regime then propagated south from the site of the lithospheric tear across the western U.S., probably representing the progressive removal of the flat slab from the base of North America. Later, at ~16 Ma, the Columbia River Basalt flows appear to have created and erupted through a lithospheric hole near the torn edge of Siletzia (Fig. 3.6).

In this chapter I constructed a 3D velocity structure of the crustal and uppermost mantle of the U.S. Pacific Northwest with ambient noise tomography, with focus in particular on the accreted Siletzia oceanic lithosphere and the development of the Cascade arc. In the following chapter, I will describe the time-dependent slip distributions of slow slip events on the Cascadia subduction zone in the last decade.

CHAPTER IV
SOURCE PARAMETERS AND TIME-DEPENDENT SLIP
DISTRIBUTIONS OF SLOW SLIP EVENTS ON THE CASCADIA
SUBDUCTION ZONE FROM 1998-2008

This work was published in volume 115, *Journal of Geophysical Research*, 2010, and coauthored with David Schmidt who was the first author. I was the second author and was responsible for data processing, inverting for the slip distributions, and interpreting the inversion results and aided in the editorial process.

1. Introduction

The plate interface of subduction zones is characterized by an updip portion that is kinematically locked and a downdip half that is freely sliding, as is inferred from surface observations of strain accumulation on the overriding plate. Some subduction zones also exhibit an unlocked zone in the top few kilometers nearest the trench. Strain energy is accumulated over centuries and released during megathrust earthquakes on the locked segment of the plate interface. On the downdip portion, higher temperatures allow for steady slip or ductile flow between the subducting plate and the underside of the overriding plate (Tichelaar and Ruff, 1993).

The discovery of slip transients inferred from GPS (Hirose et al., 1999; Dragert et al., 2001; Miller et al., 2002) and the accompanying nonvolcanic tremor (Obara, 2002; Rogers and Dragert, 2003) provide insight into how strain is accumulated and released at the boundary of the kinematically locked updip and freely sliding downdip portions of

the plate interface. On the Cascadia subduction zone, previous studies have found that slow slip maps between the 25 and 40 km depth contours if the transient surface displacements are modeled as fault slip on the plate interface (McGuire and Segall, 2003; Szeliga et al., 2004; Melbourne et al., 2005; Szeliga et al. 2008; Wang et al., 2008). This depth is near the lower part of the traditionally defined transition zone. Slow slip events are thought to represent slip instabilities at the transition between velocity weakening and velocity strengthening portions of the plate (Shibazaki and Iio, 2003; Liu and Rice, 2005). Given the observed nonvolcanic tremor and the abundance of water from metamorphic dehydration reactions, fluids are thought to play an important role in facilitating slow slip at these depths by reducing the effective stress (Kodaira et al., 2004). Similar transient processes have been documented on most subduction zones around the world, although the source parameters, such as slip amplitude and event duration, vary depending on the region (Schwartz and Rokosky, 2007).

Slow slip events on the Cascadia subduction zone (Fig. 4.1) occur over a period of several weeks where station displacements show a westward drift of 2–5 mm oriented in the direction opposite to plate convergence. Both the station displacement and tremor migration show a spatially and temporally correlated pattern suggestive of along-strike propagation (Dragert et al., 2001). Recurrence intervals of slow slip events are on the order of months which is short compared to the several hundred year recurrence interval for megathrust earthquakes on Cascadia. The short recurrence interval allows for multiple events to be observed and compared to better understand how the kinematics vary in time and space.

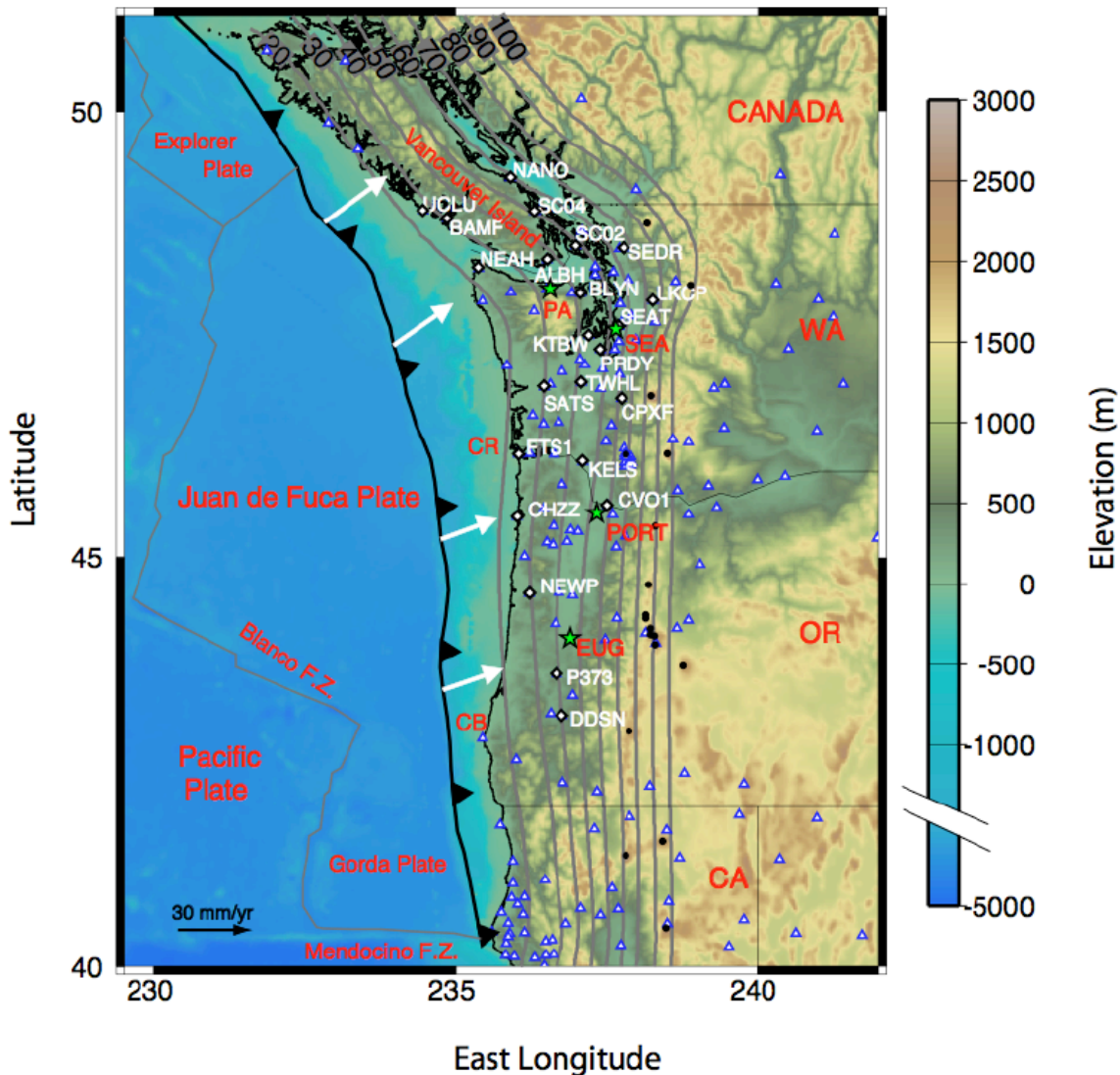


Figure 4.1. A map of the Cascadia subduction zone indicating the depth contours of the plate interface (gray lines) and Holocene volcanoes (black dots). All continuous GPS stations (diamonds and triangles) active within the time period from 1998–2008 and used in our analysis are shown. Those GPS stations where the time series are explicitly plotted in Fig. 4.2 are indicated by an open diamond (white station names). White arrows indicate the convergence of the Juan de Fuca plate relative to North America in the north and the Oregon forearc to the south. Cities (green stars) and other geographic locations are abbreviated as follows: EUG, Eugene; PORT, Portland; SEA, Seattle; PA, Port Angeles; CR, Columbia River; CB, Cape Blanco.

The mapping of slow slip events along the subduction zone provides insight on the spatial and temporal pattern of strain release. First-order questions include how source parameters vary along strike and what percentage of the plate convergence is released by large slow slip episodes at various locations. Additionally, the updip and downdip limits of slow slip can be correlated with other geophysical data, such as porosity, temperature, and structure, in an effort to better understand the underlying processes that facilitate aseismic slip. Slow slip and tremor also constrain the lower edge of the seismogenic zone, a variable that is useful for seismic hazard studies, and event histories are an input into studies that explore the time-dependent loading of stress on the seismogenic zone (Mazzotti and Adams, 2004).

In an effort to address some of the above issues, several previous studies have performed slip inversions using the GPS time series in Cascadia (McGuire and Segall, 2003; Szeliga et al., 2004; Melbourne et al., 2005; Szeliga et al., 2008; Wang et al., 2008; McCaffrey, 2009). While some of these studies performed static inversions, McGuire and Segall (2003), Melbourne et al. (2005), and McCaffrey (2009) explored the time-dependent slip history of individual events. Szeliga et al. (2008) was the first to provide a systematic inversion of multiple events.

The objective of this study is to chronicle the time-dependent evolution of slip on the plate interface for 16 conspicuous slow slip transients on the Cascadia subduction zone from 1998 to 2008. We resolve the kinematic slip history for all of the major slow slip episodes that occurred in the decade using a time-dependent analysis tool that addresses the intrinsic noise sources of the GPS time series. We examine patterns in the slip propagation direction, slip amplitude, subevent sequencing, and dislocation risetime

of events. Our results reveal a complex sequencing of slow slip events, and suggest that the strain release and other source parameters are variable along strike.

2. GPS data

We process GPS data collected at continuous stations in the Pacific Northwest from January 1998 to August 2008. Several geodetic networks span the study area, including the Pacific Northwest Geodetic Array, the Western Canada Deformation Array, and the Plate Boundary Observatory (PBO) (Miller et al., 2001; Dragert et al., 1995). Daily positions are determined using the GAMIT/GLOBK processing package (Herring et al., 2006, versions 10.32–10.34). ITRF2005 is used to stabilize station positions within a global reference frame (Altamimi et al., 2007). Loosely constrained daily solutions are processed in subnets in order to expedite the analysis in GAMIT. Subnets are recombined and time series are constructed in GLOBK using a local reference frame of 30 stations. Eight of the local stations (DRAO, DUBO, PRDS, YELL, CHWK, WILL, WHIT, and HOLB) are also defined in ITRF2005. Given that we are only concerned with transient surface displacements, all three-component time series are detrended to remove the long-term interseismic signal associated with the convergence of the Juan de Fuca and North American plates (Fig. 4.2).

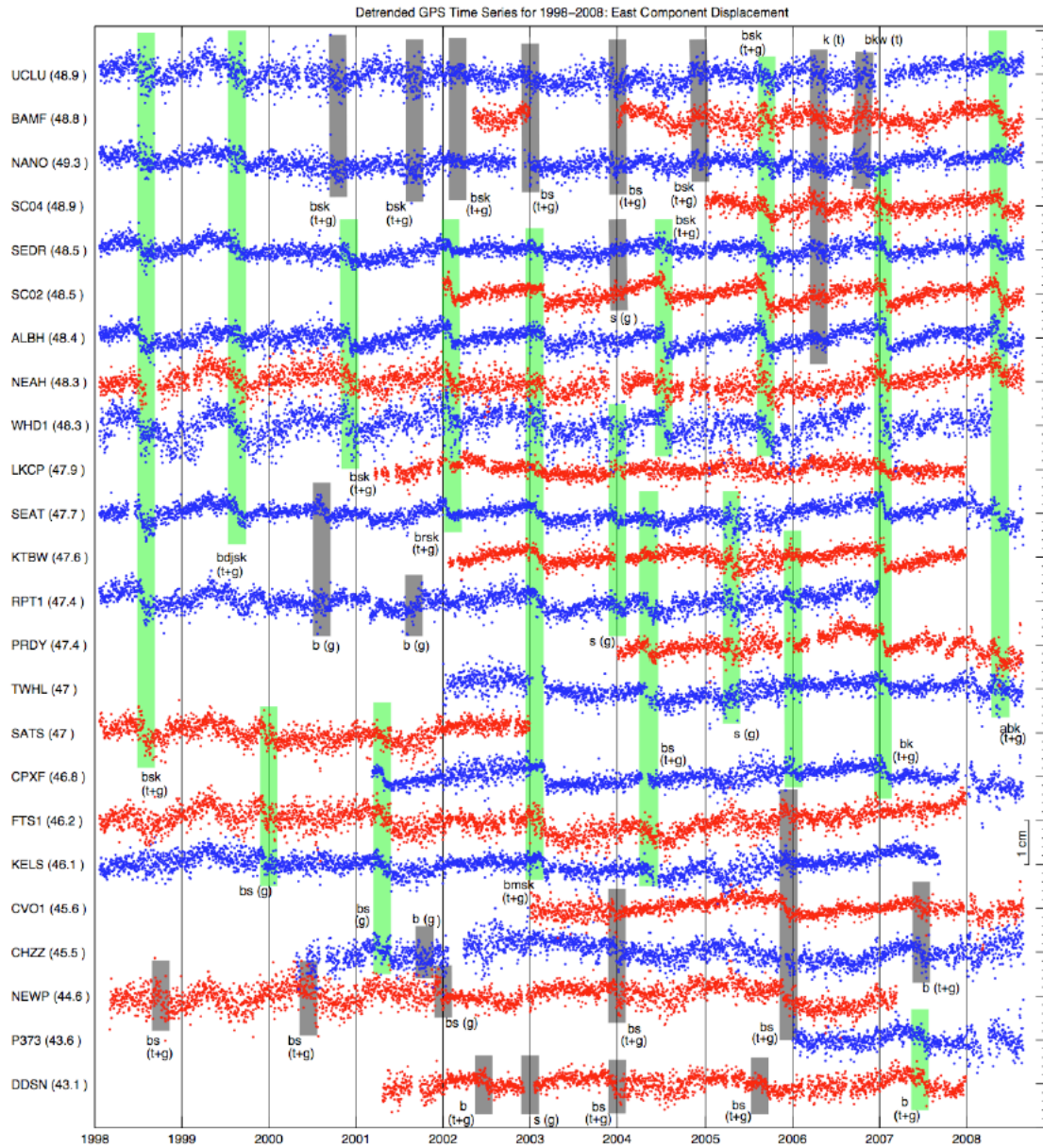


Figure 4.2. Detrended GPS time series from 1998 to 2008 for selected GPS stations from north (top) to south (bottom) along the Cascadia subduction zone. Only the east displacement component is shown. The name and latitude of each station is shown to the left of each time series. The green vertical bars mark the 16 largest slow slip events with offsets observed on three or more stations and slip distributions that are well resolved by our analysis. The gray bars indicate slow slip and tremor events that do not have sufficient station coverage for formal inversions but are detected by GPS (g) or show evidence of prolonged tremor at nearby seismic stations (t). Letters next to each bar indicate previous documentation of a given event: d, Dragert et al. (2001); j, McGuire and Segall (2003); m, Melbourne et al. (2005); r, Royle et al. (2006); b, Brudzinski and Allen (2007); k, Kao et al. (2007); a, Wech and Creager (2007); s, Szeliga et al. (2008); w, Wang et al. (2008).

Some GPS stations are dominated by a seasonal signal in their time series that is caused by seasonal mass changes, atmospheric and groundwater loading, as well as artifacts imposed by the reference frame and processing errors (Dong et al., 2002). Typically, this seasonal signal appears as an asymmetric sawtooth function unique to each station (Fig. 4.3). This seasonal signal is removed for a subset of stations by estimating the temporal signature. For a particular station and component, the GPS time series for the entire period is divided into individual years, detrended, and stacked into one calendar year. The normalized function is assumed to be a yearlong basis function of the seasonal deformation unique to each station. This basis function is scaled to the time series for each year and removed from the original data. It is possible that some small artifacts are introduced into the time series with this procedure. However, the total seasonal fluctuation is greatly reduced and final results are improved when resolving the transient slip on the plate interface. Stations that have undergone this seasonal correction include DWH1, SEAT, SEAW, TRND, FTS1, JRO1, KELS, TPW2, and YBHB.

3. Time-dependent inversions

Slow slip transients are estimated using the Extended Network Inversion Filter (Segall and Matthews, 1997; McGuire and Segall, 2003). This methodology, based on an extended Kalman filter, has been successfully used to estimate slip transients on the San Andreas fault (Murray and Segall, 2005), slow slip in Cascadia (McGuire and Segall, 2003), and slow earthquakes in Japan (Miyazaki et al., 2003). The filter is based on the premise that tectonic deformation is spatially correlated between adjacent stations, whereas benchmark motions are uncorrelated. This information is used to filter out the

uncorrelated trends and random noise, and estimate the fault slip that best models the temporally and spatially correlated surface deformation. A formal discussion of how the filter is formulated can be found in the work of McGuire and Segall (2003).

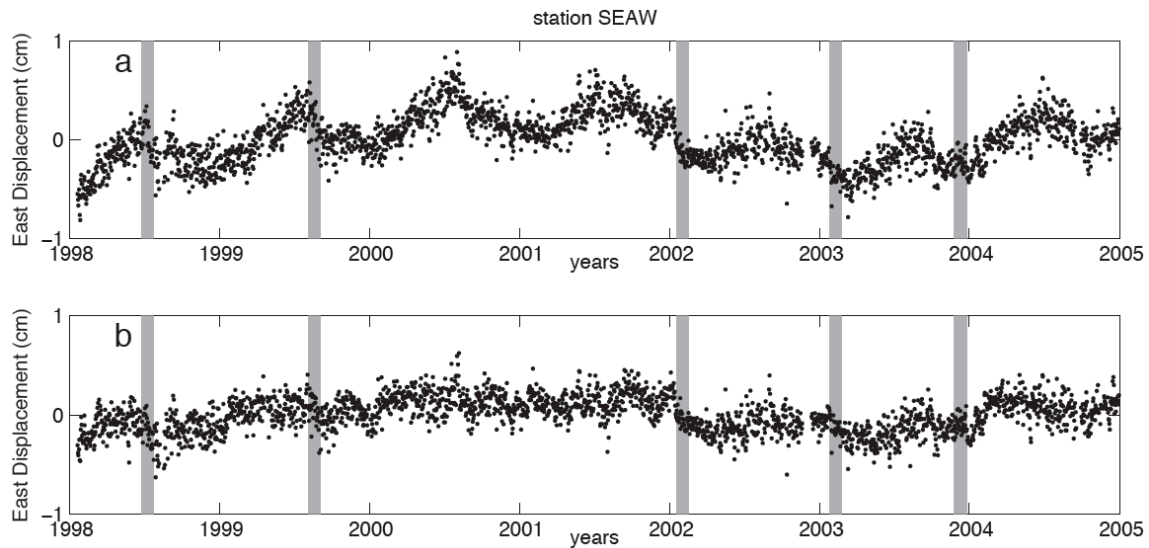


Figure 4.3. Seasonal trends that complicate the identification of transient tectonic offsets are removed from a subset of GPS time series. Figure 4.3a is the original east component for station SEAW. Figure 4.3b shows the corrected time series where the seasonal trend has been estimated and removed on individual components (see text for an explanation). Slow slip events are indicated by vertical gray bars.

For each epoch, the filter estimates the slip and slip rate on each fault element, and the benchmark motion for each three-component GPS time series. A set of hyperparameters scale the white noise uncertainty (σ) and the benchmark motion (τ) of the data time series. The degree of temporal smoothing, spatial smoothing, and positivity of the transient slip rate function on the plate interface are controlled by the hyperparameters α , ρ , and γ , respectively. The hyperparameters are also estimated directly by the filter, and are included in the state vector using a natural logarithmic parameterization in order to enforce their positivity. The hyperparameters are given a large initial variance so that the filter is free to refine the final value through a procedure

discussed by McGuire and Segall (2003, section 3.2). Final hyperparameter values for spatial smoothing are assessed by plotting the tradeoff between the data misfit and the roughness of the slip distribution. Though network reference frame terms can also be estimated by the filter (Miyazaki et al., 2003), they are ignored in our analysis because of a tradeoff between slip on the plate interface and east-west stretching of the network.

The three-dimensional plate interface is specified using the model of McCrory et al. (2004). The fault surface is discretized into triangular fault elements with an average side length of 25 km. Updip fault elements nearest the trench are ignored since they lay offshore and are poorly constrained by the onshore geodetic network. The fault model used in this analysis includes the portion of the plate interface within the 20–50 km depth range. The Green's functions are calculated using Poly3D, a boundary element code that accommodates triangular dislocations in an elastic half-space (Thomas, 1993).

The Juan de Fuca and North American plates converge at an oblique angle to the strike of the subduction zone in Oregon and Washington (Miller et al., 2001). However, northward translation of the Oregon forearc offsets much of this oblique convergence along the central and southern portion of the subduction zone (Wells and Simpson, 2001). Therefore, convergence along the plate interface is predominately dip-slip. A similar scenario is observed beneath Vancouver Island where the strike of the subduction zone rotates counterclockwise, nearly perpendicular to the local convergence direction. Additionally, the transient displacements in the GPS time series are predominately observed in the east component for stations south of Seattle. Therefore, we assume that transient slip on the plate interface is limited to the reverse component of each triangular fault element. The one region where this assumption may be suspect is beneath northern

Washington where tremor polarization is locally subparallel to the downdip direction of the plate interface (Wech and Creager, 2007). However, we find no significant differences in the final slip distribution for inversions where the rake is fixed to the convergence direction suggesting that any bias is small.

4. Inversion results

In this work, we focus on the major slow slip events that have occurred on the Cascadia subduction zone. The GPS time series are compared to the event record of Brudzinski and Allen (2007), who look for correlated offsets in GPS time series and evidence of tremor activity in seismic data. Szeliga et al. (2008) performed a similar detection exercise with the GPS time series using a wavelet transform. Using these existing catalogs as well as other sources, we identify events with clear evidence of transient displacement at three or more stations. Once a consistent signal is observed by multiple stations, several months of the three-component GPS time series are extracted and analyzed using the filter. Although we do not find evidence for longer-duration transients in the GPS time series, it is possible such transients exist in the data but are difficult to resolve because they have a low signal-to-noise ratio or are otherwise masked by transient signals of nontectonic origin (i.e., groundwater pumping). Similarly, it is likely that numerous smaller events occur that do not produce enough surface displacement to be observed by GPS (e.g., Wang et al., 2008).

There has been a significant change in the number of GPS stations in the Pacific Northwest over the period of this study. The number of stations overlapping the fault model from 1998 to 2008 has increased by at least a factor of four. Much of this

expansion is related to the development of the regional geodetic networks and the installation of PBO. As a consequence of this expansion, the resolution of transient slip varies greatly in time. The augmentation of GPS stations on Vancouver Island helps to improve resolution in 2004. Fault plane resolution greatly improves in Washington beginning in 2005 with the densification of GPS benchmarks in Puget Sound (47.5°N latitude). In Oregon, resolution is poor prior to 2007 from inadequate station coverage. Therefore, we focus our analysis on events that occur north of Portland (>45.5°N) because the GPS stations are too widely distributed in the south for proper inversions. Likewise, we also limit our analysis to regions south of 49.5°N on Vancouver Island.

In the following sections, the results for each slow slip event are described along with the caveats for interpreting the slip distribution. A number of geographic markers, such as Portland or Vancouver Island, are used when describing the location of slip on the plate interface. These locations are indicated in Fig. 4.1 for reference. The final slip distribution for each event is displayed in Fig. 4.4.

4.1. July 1998 event

The July 1998 event occurred on the segment of the subduction zone between Seattle and Vancouver Island (47.6°N to 48.7°N). The main slip patch was centered beneath Port Angeles (48.1°N), where slip first nucleated just south of the GPS station ALBH. Slip propagation was generally from north to south. Displacement at stations SATS and RPT1, both at the southern end of Puget Sound (47.8°N), were underestimated by the filter suggesting that slip may be greater than what was resolved on the southern

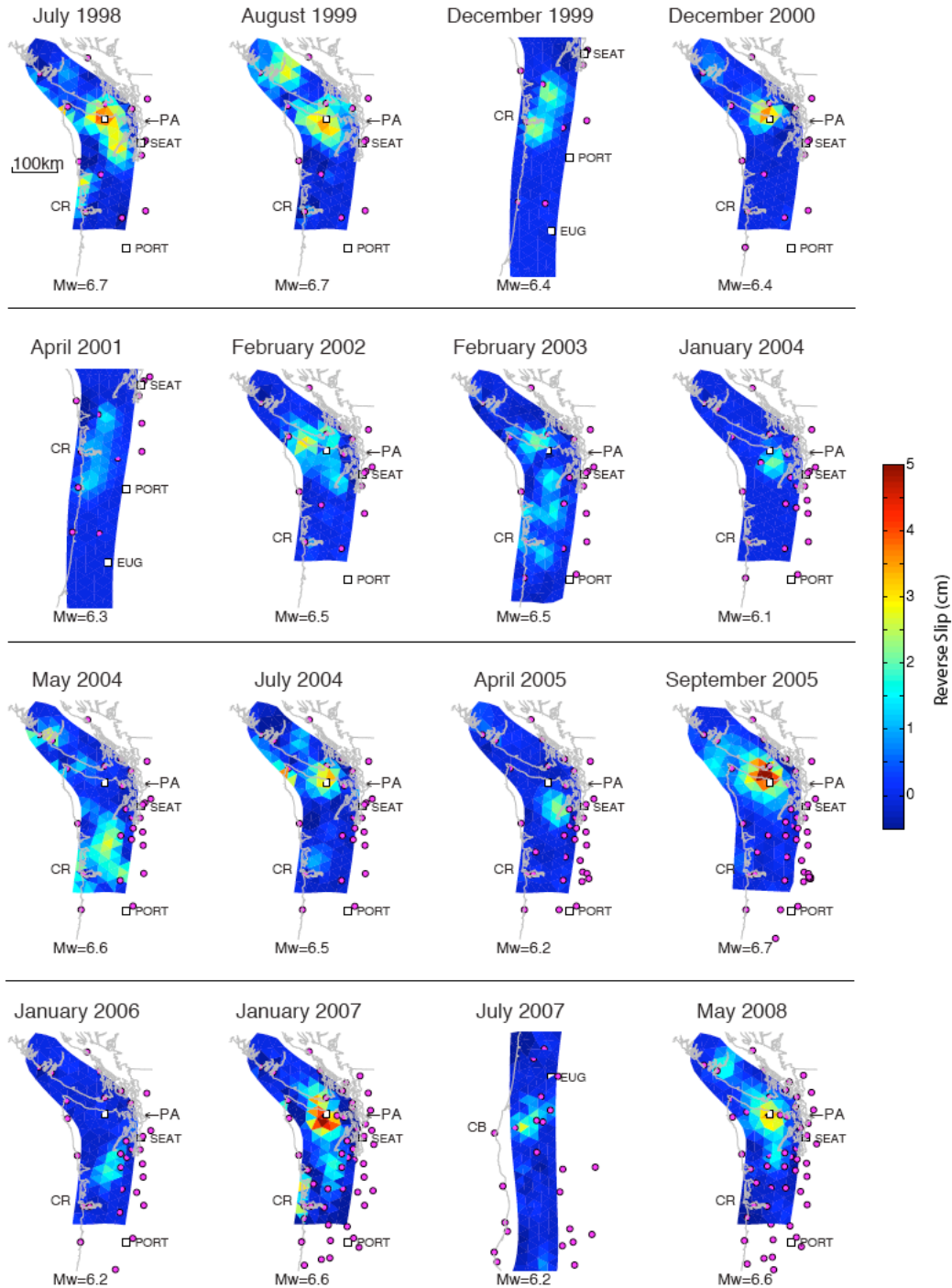


Figure 4.4. The estimated slip distribution for 16 slow slip events from 1998 to 2008. The west and east edges of the fault model correspond to the 20 and 50 km depth contours, respectively, of the plate interface. The GPS network (magenta dots) changes in time as stations are added to the network. The estimated moment magnitude is indicated at the bottom of each slip distribution. The coastline (gray line) and cities (open squares) are included for geographic reference. Abbreviations are identical to Fig. 4.1.

end of the slip distribution. The time series for station PABH introduced both a positive and negative slip artifact along the upper edge of the fault model.

4.2. August 1999 event

The main slip patch for the August 1999 event was centered beneath Port Angeles and was shifted slightly updip compared to other slip events. Nearly a month after slip first initiated, a second slip patch was estimated on the northern end of the fault model. Resolution of slip on the subduction zone beneath Vancouver Island was limited because there are only two stations (NANO and UCLU) which were separated by ~150 km. Slip was detected by the filter and agreed well with the east displacement time series of UCLU.

4.3. December 1999 event

In December of 1999, a transient slip event was estimated in the vicinity of Portland near the mouth of the Columbia River (46.2°N). Four stations observed transient displacement. However, the resolution of slip was poor because stations are widely spaced. Regardless, the filter resolved two patches of slip, each centered beneath stations SATS and FTS1. These slip patches were likely connected, but the wide spacing between stations was problematic. Attempts to connect the slip patches by increasing spatial smoothing were unsuccessful.

4.4. December 2000 event

The filter estimated a compact slip event beneath Port Angeles in December of 2000. This event may have extended farther to the south, but the lack of a GPS station immediately south of Port Angeles limited resolution. The lack of a transient signal at station SEAT suggested that the slip event did not extend south of Seattle. A low-amplitude slip patch beneath station UCLU on central Vancouver Island appears to be an artifact introduced by the vertical component of the GPS time series.

4.5. April 2001 event

Transient displacement at 4+ stations in northern Oregon and southern Washington indicated a slow slip event in April of 2001. The wide spacing of stations limited the resolution of slip on the central section of the plate interface. As a result, slip tended to localize beneath individual GPS stations. However, the filter resolved a broad, southward propagating slip event extending nearly 200 km along strike. Station CPXF was poorly fit by the filter, suggesting the slip amplitude may be higher to the north than what was estimated.

4.6. February 2002 event

A slip event was estimated in early February of 2002 in the vicinity of Port Angeles. The event nucleated at the latitude of Seattle and propagated to the north over a 2+ week period. The spatial extent of slip agreed well with observations of tremor beneath southern Vancouver Island, although peak slip was located slightly to the west of the tremor epicenters (Royle et al., 2006). Station BLYN strongly impacted the final slip

distribution. Depending on how this station was adjusted for a documented instrument adjustment, the slip patch shifted to the east closer to station ALBH. The fit to station PABH was also problematic because of a very gradual slope in the east time series, which we detrended to avoid large slip amplitudes along the updip edge. Station KTBW was ignored in our analysis because it had a paucity of good data during this time period. However, the filter result was insensitive to whether this station was included in the analysis.

4.7. February 2003 event

The February 2003 event exhibited a complex slip evolution featuring a bilateral rupture and a distinct pause in activity halfway through the event, consistent with the findings of Melbourne et al. (2005). The epicenter was located at the latitude of Seattle in late January where a small slip patch was estimated near the southern end of Puget Sound (47.8°N). After a pause in activity for nearly a month, slip then propagated to the north and south in late February. The northernmost slip patch was centered beneath Port Angeles (48.1°N) while a southern segment extended between Seattle and Portland (47.6°N to 45.5°N). We attributed the patchiness of the slip distribution to the fault resolution because slip tended to be a maximum in the low-resolution regions between stations. Therefore the slip was likely more continuous than visualized. However, the pause between subevents suggests that there were distinct rupture patches along strike. The peak slip amplitude of ~ 2 cm for this sequence was lower than for other inferred events. This sequence was one of the most extensive slip events resolved on the Cascadia subduction zone, extending nearly 300 km along strike.

4.8. January 2004 event

The January 2004 event centered near Port Angeles was one of the smallest and shortest slip events estimated by the filter. The small slip amplitude of 1.5 cm and compact spatial extent resulted in the smallest moment magnitude of all of the 16 slip events discussed here. Despite the event's small magnitude and noisy time series, the filter did a good job of modeling the GPS time series for 4+ stations that showed a coherent transient displacement.

4.9. May 2004 event

Rupturing the segment between Seattle and Portland, the May 2004 event was quite prominent on several GPS time series. Later in the same month, the filter estimated a second slip patch beneath southern Vancouver Island as evidenced by small transient displacements observed at stations UCLU, NANO, NEAH, and ALBH. Because of the distance between stations, this event may be larger beneath Vancouver Island than was estimated by the filter. Nearly 2 weeks separated the onset of slip on the northern and southern segments, with no slip detected in the middle portion of the fault model.

4.10. July 2004 event

In July of 2004, a slip event ruptured the middle portion of the fault model (48.1°N), filling a gap in the May 2004 event sequence. The July event nucleated beneath Port Angeles and propagated northward beneath Vancouver island. Slip may actually extend farther to the south from Port Angeles given that station SEAT was

underpredicted. The station NEAH imposed slip along the updip edge of the fault model. However, it was unclear what aspect of the time series required this response.

4.11. April 2005 event

A localized slip patch was resolved at the latitude of Seattle in April of 2005. The event likely extended farther south than was estimated by the filter as evidenced by transient offsets at stations KELS and JRO1. However, increased noise in these time series appeared to confuse the filter, resulting in a poor fit. It is interesting to note that the estimated slip filled in a small gap between the slip events in May and July of 2004. The filter also estimated a small slip patch beneath central Vancouver Island. The signal is not clearly evident in the time series except for a subtle offset at station BAMF. However, slip is corroborated by observations of tremor that occurred on the central and northern segments of Vancouver Island, and also near Port Angeles in May (Kao et al., 2007). No tremor was observed on the southern part of Vancouver Island suggesting that the two patches are distinct and slip was not continuous along strike.

4.12. September 2005 event

This event began beneath Port Angeles and propagated bilaterally in September of 2005. Several stations observed transient surface displacements as much as 5–7 mm. The estimated slip distribution was spatially broad and had a maximum slip amplitude of 5.6 cm. The slip distribution correlated well with the along-strike occurrence of tremor (Wech and Creager, 2007). Slip propagated southward from the epicenter before propagating to the north beneath Vancouver Island, an observation supported by the

timing of tremor. Initially, the filter placed slip along the updip (western) edge of the fault model. Therefore, we used an expanded fault model for this event that extended from a depth of 10 km to 50 km. All of the stations on Vancouver Island were systematically removed one-by-one to determine if an individual time series forced the slip updip. However, it appears that no individual station biased the result. We suspect that observed subsidence at stations BAMF and NEAH was responsible for forcing slip updip.

4.13. December 2005 through January 2006 event sequence

Beginning in October of 2005, a characteristic offset was observed at stations YBHB and DDSN at the California-Oregon border (42°N). However, station coverage was insufficient to resolve the slip distribution using the filter. Beginning in December, transient surface displacements were evident at GPS stations in northern Oregon with a clear south-to-north progression. By early January of 2006, stations between Portland and Seattle exhibited transient motion and data were well modeled by the filter. Because of the significant spacing between stations on the central part of the subduction zone, it was difficult to determine whether the October through January episode was a continuous slip event or a series of discrete events that initiated in sequence. If the slip patches are continuous, it would constitute one of the longest slow slip events extending 600 km along strike.

4.14. January 2007 event

The January 2007 event extended all the way from southern Washington (46.8°N) to the southern part of Vancouver Island. The event nucleated near Seattle and propagated bilaterally with the largest slip amplitudes found beneath Port Angeles. The estimated slip distribution was remarkably similar to the July 1998 event. Inferred slip at the outlet of the Columbia River was discounted at this location because of significant variability in the time series of nearby stations.

4.15. July 2007 event

All of the previous slip events discussed in this section occur north of Portland because of poor station coverage to the south. Recently installed PBO stations allowed for slip inversions on the southern half of the subduction zone beginning in 2007. An event was resolved at the latitude of Cape Blanco (42.8°N) in early July of 2007, and transient displacements were evident at 4+ adjacent stations. The filter estimated a 2.5 cm slip event that is widely distributed along the downdip direction. Peak slip and rupture initiation were mapped to the 30 km depth contour. This slow slip event may have extended farther to the north or south along the plate interface. However, station coverage is not uniform in this region and slip could easily be missed.

4.16. May 2008 event

The May 2008 event initiated beneath Port Angeles and propagated bilaterally. The slip event extended from the latitude of Seattle up to central Vancouver Island. Slip

appeared to propagate to the south before advancing to the north, similar to what was observed for the September 2005 event.

4.17. Other poorly resolved events

There was evidence of other small transient events within the GPS time series that were only recorded on a limited number of stations or the station density was too low to perform an inversion for slip on the interface. SEAW and SEAT both recorded a small transient in August of 2000. The filter estimated a very localized slip event with an amplitude of 5 cm located just to the west of these two stations. There was no evidence of a slip transient at any other stations, including the nearby station RPT1. In June of 2005, an event was detected on the central portion of the subduction zone. Transient displacement was observed at several stations in western Oregon, including DDSN, CABL, NEWP, and P376. Unfortunately, the stations were sparsely distributed and the filter mapped slip only to those fault elements directly below each station. Where slip was resolved, it consistently nucleated around the 30 km depth contour on the plate interface. In June of 2007, a possible event was visible at the mouth of the Columbia River and the filter estimated a 2 cm slip amplitude. It is unclear from the time series whether this was a real event or a nontectonic transient. Several stations for this event exhibited a correlated sinusoidal signal with a period of 1 month that was unmodeled by the filter.

5. Discussion

Our catalogue of 16 slow slip events allows us to compare repeated episodes and identify characteristic patterns in aseismic strain release in Cascadia. Several noteworthy patterns emerge when the slip distributions are compared. The centroid locations for 9 out of the 16 events are centered beneath Port Angeles, indicating that this is the most frequent patch to rupture. The along-strike propagation direction does not appear to be systematic between Portland and Seattle as both northward and southward propagation is observed. However, subsidiary slip beneath the southern half of Vancouver Island often follows slip events beneath Port Angeles, suggesting a tendency for northward propagation on this segment of the subduction zone for large events.

The slip history and source characteristics from 10 years of slow slip events is synthesized in order to assess long-term spatial trends. For the subsequent analysis, we only consider those triangular fault elements with cumulative slip greater than 5 mm for any given slip event. Fault slip below this threshold is considered to be within the noise. The cumulative strain release from slow slip events is calculated by adding up all of the slip distributions in Fig. 4.4 for events north of Portland. The cumulative slip reveals that the strain release is not uniform along strike (Fig. 4.5a). The greatest amount of total slip is centered beneath Port Angeles. The high total slip at Port Angeles is due to the fact that this fault patch ruptures more frequently and the slip amplitude per event is larger than nearby segments of the fault.

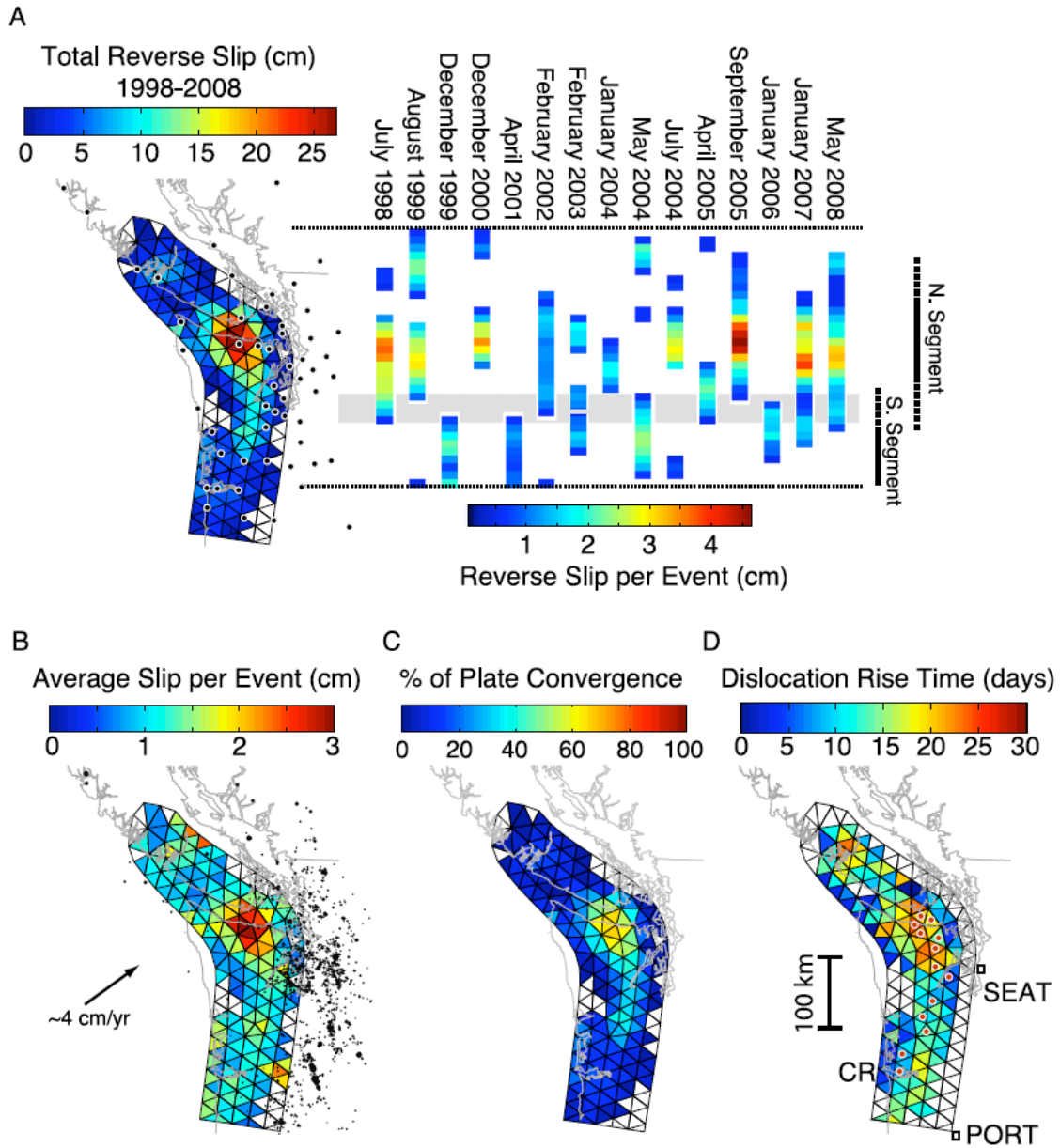


Figure 4.5. Cumulative slip pattern. Figure 4.5a shows the total reverse slip that is calculated by summing the 15 distributions for slow slip events north of Portland. Black dots indicate the location of GPS stations in January of 2007. North-south profiles of the slip distributions along the 35 km depth contour are also plotted to the right. Figure 4.5b shows the average slip per event calculated by taking the total slip and dividing it by the number of events per fault element. Black dots indicate crustal seismicity. The arrow indicates the Juan de Fuca-North American convergence direction. Figure 4.5c shows the percentage of plate convergence released by slow slip events from 1998 to 2008. Figure 4.5d indicates that slip accumulates on each fault element during an average risetime. Red dots mark the epicenters for individual slow slip events.

Fault resolution may bias the inferred along-strike variation in strain release, especially beneath Vancouver Island where there is a reduction in fault resolution due to fewer GPS stations. Station density is more consistent to the south of Port Angeles and we feel that the dropoff in cumulative slip to the south is a more robust feature. A focusing of slip at Port Angeles is also consistent with the observation that the time series of stations near this location (such as ALBH and SC02) have larger and more distinct transient offsets compared to stations to the south (Fig. 4.2). When total slip is normalized by the number of events inferred on a given fault patch, the average slip per event is quite uniform along strike except at Port Angeles where the average slip is nearly twice the value elsewhere (Fig. 4.5b). In regions where the cumulative slip from slow slip is less than at Port Angeles, a couple of scenarios could occur. This slip deficit could be made up by a larger number of smaller slow slip events that are not well resolved by GPS. Alternatively, strain release could occur in a long-duration slip event yet to be detected or strain could be accumulating for future release.

The downdip extent of slip is constrained within the 30–45 km depth contours. Szeliga et al. (2008) have suggested that slip is centered farther updip beneath Oregon than is found in Washington. Slip events resolved in northwest Oregon appear to be shifted updip (December 1999, April 2001, July 2007), but low resolution and greater spatial smoothing make interpretation difficult. Possible evidence of an updip progression may be found in the location of event epicenters (Fig. 4.5c). Fault elements where slow slip first initiates are close to the 30 km depth contour near the Columbia River while near Port Angeles epicenters hover between the 35–40 km depth contours.

5.1. Event statistics

We compile statistics on the rupture kinematics of aseismic slip using our catalogue of 16 slow slip events. All events have a similar moment magnitude (6.1–6.7). Smaller events would produce surface displacements of less than 1 mm, and would be difficult to detect given the intrinsic noise in the GPS time series. Average stress drop for each of the events ranges from 0.01–0.10 MPa, which is nearly 2 orders of magnitude lower than for traditional earthquakes (Fig. 4.6a). Low stress drops are consistent with low effective normal stresses caused by elevated pore pressure. Several studies have argued for the triggering of slow slip by small stress perturbations from climatic loading, a mechanism that would require a low effective stress (Shen et al., 2005; Lowry, 2006). Similarly, recent studies have found that tremor is sensitive to stress changes induced by tidal loading and passing shear waves (i.e., Rubinstein et al., 2008).

The average dislocation risetime is 14 days with a maximum of about 30 days. The estimated slip is temporally and spatially smoothed by the filter, and the predicted time series are often less impulsive than the observed GPS time series. Therefore, the inferred average risetime of 14 days is likely overestimated. Most GPS time series show transient displacement lasting 6–15 days. The risetime tends to be longer beneath Port Angeles (Fig. 4.5c) where average slip per event is also higher. This suggests a proportionality between risetime and slip such that slip rate is relatively constant during rupture.

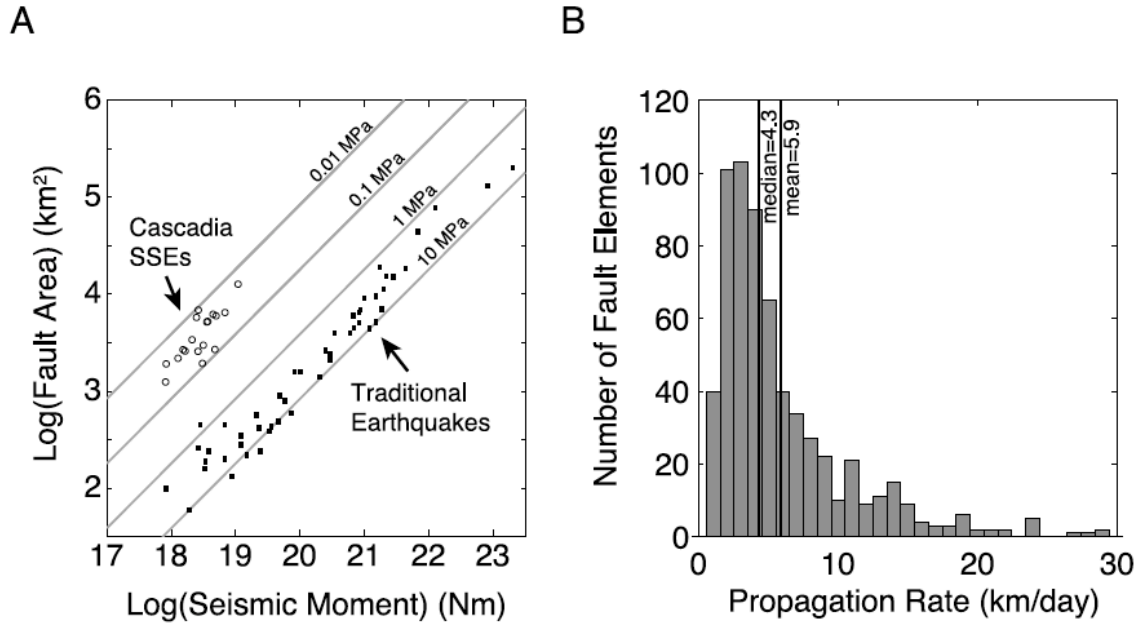


Figure 4.6. Plot of source parameters. Figure 4.6a shows the relationship between fault area and seismic moment for slow slip events in Cascadia (open circles) and traditional earthquakes (squares) (Kanamori and Anderson, 1975). Diagonal lines show contours of constant static stress drop for a circular crack. The average stress drop for slow slip events is 2 orders of magnitude less than traditional earthquakes. Figure 4.6b is the distribution of propagation rates for slow slip inferred from the time-dependent slip distributions.

The propagation rate is determined directly from the time-dependent slip distributions. The initiation of slip on a fault element is defined when the estimated slip exceeds 5 mm. The timing of slip initiation is compared among adjacent fault elements to measure the relative delay time. Finally, a plane is fit to the relative delay times for a group of fault elements and the gradient is used to determine the direction and rate of slip propagation. The average propagation rate for slip initiation is 5.9 km/day, although some fault elements show a rate as high as 17 km/day (Fig. 4.6b).

We do see a general trend where events with larger rupture length have a larger average slip amplitude. For example, the slip distributions for January 2004, December

2000, and September 2005 show a systematic trend where the along-strike rupture length scales with amplitude. Such a relationship is found for standard earthquakes and predicts a nearly constant stress drop that is independent of event magnitude (Kanamori and Anderson, 1975). However, the varying fault resolution along strike and the occurrence of subevents where rupture jumps or pauses, complicate a statistical analysis. Further refinement of the slip distributions is required to fully assess the relationship between these variables. Rupture lengths of contiguous slip patches range from 30 to 300 km along strike, with an average length of 115 km. The maximum slip for a slip patch ranges from 1.2 to 5.6 cm, and the mean is 2.5 cm.

The recurrence interval between events is calculated for triangular fault elements that fall along the 35 km depth contour. An event is noted if cumulative slip exceeds 5 mm on that fault element. A 14 ± 3 month recurrence interval for events with $M_w > 6$ is found near Port Angeles, increasing to 16 ± 8 months south of Seattle. Several investigators have noted the remarkably regular recurrence interval near Port Angeles (Miller et al., 2002; Rogers and Dragert, 2003). It appears that recurrence of large events ($>M_w 6$) is less regular at other locations along strike. Brudzinski and Allen (2007) assessed the recurrence interval of slow slip and tremor episodes along the entire Cascadia subduction zone using both seismic observations of tremor as well as GPS transients. Our estimate of recurrence interval serves as an upper bound given that we likely miss smaller slip events where tremor is detected. Our results are generally consistent with that found by Brudzinski and Allen (2007) and Szeliga et al. (2008) between Port Angeles and Portland suggesting that we image most of the events at these latitudes.

5.2. Implications for slow slip processes

The patch of high cumulative slip centered beneath Port Angeles indicates that the conditions that drive slow slip events are not uniform along strike given that the strain release is nearly twice the value observed elsewhere along the subduction zone. This patch exhibits the greatest slip per event and has the most regular recurrence interval (high periodicity). The location of this patch bears a striking correlation to a first-order feature in the geometry of the plate interface. The subduction zone exhibits an along-strike bend in northern Washington. Additionally, the dip of the plate interface is shallower ($\sim 7^\circ$) compared to the dip in central Oregon ($\sim 15^\circ$) and Vancouver Island ($\sim 20^\circ$). This suggests that the geometry of the subducting plate may play an important role in controlling the behavior of slow slip events.

One possible mechanism for enhancing slow slip events at the bend is through a nonuniform loading rate that increases strain release relative to adjacent segments. Enhanced loading at Port Angeles is supported by the clustering of crustal seismicity around the bend (Weaver and Shedlock, 1996). Additionally, observed and predicted strain rates indicate maximum compressional stresses are located around the bend as well as near the southern end of the subduction zone (Wang et al., 2001). Both the numerical modeling of Wang et al. (2001) and the seismicity of Weaver and Shedlock (1996) are supportive of focused convergence related to the geometry of the subducting plate.

The characteristic nature of the slip patch beneath Port Angeles is similar to characteristic repeating earthquakes on the San Andreas fault (Nadeau and Johnson, 1998). Both exhibit a regular recurrence interval, although repeating earthquakes rupture

a significantly smaller area and slide at seismic velocities. Repeating earthquakes can be modeled as a strong asperity at the border between coupled and uncoupled regions and is preferentially loaded by nearby aseismic slip (Sammis and Rice, 2001). Slow slip events occur in a similar setting at the base of the seismogenic zone. A higher tectonic loading rate results in more frequent events and/or larger events. Thus, the focusing of tectonic loading at the bend of the Cascadia subduction zone provides one possible explanation for why this segment exhibits a high slip amplitude and a low recurrence interval.

The slip distributions shown in Fig. 4.4 exhibit rupture patterns indicative of along-strike segmentation. Segments are proposed based on the along-strike extent of slow slip episodes and the sequencing of subevents. The Port Angeles segment, exemplified by the September 2005 event, typically ruptures bilaterally with greater advancement to the north. A second segment is proposed between the Columbia River and the southern end of Puget Sound (47.8°N) (i.e., December 1999, April 2001, May 2004, and January 2006) (Fig. 4.5a). The space between these two segments is filled in by smaller individual events (April 2005) or by propagation from the north or south. This segmentation model is also evident in the sequence of subevents observed for the February 2003 event. The event sequence initiated with a small patch near Seattle. After a monthlong pause in activity, the north and south segments ruptured independently.

The boundaries between the north and south segments in Washington may reflect structural barriers or abrupt changes in fault properties that inhibit along-strike propagation. The transition between segments is somewhat diffuse given the overlapping slip distributions. However, several important structural features are located to the south of Seattle. Intraslab seismicity suggests a tear in the downgoing slab near the southern

end of Puget Sound (McCroory et al., 2004). Such a feature would disrupt the geometry of the plate interface and introduce structural boundaries. The coast range in Oregon and southwestern Washington is underlain by the Siletzia terrain, a rigid mafic block that controls the local heat flow budget (Wells and Simpson, 2001). The northern terminus of Siletzia is found in southwestern Washington. A change in tectonic environment is evident within this zone as the Oregon forearc migrates northward into northwestern Washington causing north-south transpression. Therefore, the thermal and tectonic environment exhibits an along-strike change at the boundary between slow slip segments. These structural and tectonic controls could influence the along-strike behavior of slow slip by introducing geometrical complexities or by varying the thermal conditions, pore fluid pressure, fault constitutive parameters, or state of stress.

6. Conclusions

Slow slip events along the Cascadia subduction zone represent the short-term accumulation and release of strain energy at the downdip edge of the seismogenic zone. We document the 16 largest events in the time period from 1998 to 2008. Station coverage limits our analysis to those events north of Portland for all but one event located to the south. Newly installed PBO stations in Oregon will help to image slow slip on the southern half of the subduction zone in the future.

Time-dependent inversions of the GPS time series reveal the kinematic slip history of these slow slip events. We identify characteristic segments, and discuss tectonic and structural features that correlate with segment boundaries. The greatest cumulative slip over a 10 year period is centered beneath Port Angeles, and this patch

also features the most regular recurrence interval. This slip patch correlates with a distinct geometrical feature of the plate interface where there is an along-strike bend in the subducting plate. This may suggest that the plate geometry controls the characteristics of slow slip through along-strike changes in the tectonic loading rate.

We use our catalogue of slow slip events along the Cascadia subduction zone to characterize source parameters. The typical slow slip event has an along-strike rupture length of 115 km and propagates at a rate of 5.9 km/day. We do not find a systematic direction for propagation, except possibly for northward propagation from Port Angeles. An average slip patch has a maximum slip of 2.5 cm resulting in a stress drop of ~ 0.05 MPa. While the slow slip phenomenon has been modeled as frictional slip instabilities, the mechanisms that produce slow slip, and the connection between slow slip and nonvolcanic tremor remains enigmatic. Source parameters and event statistics inferred from our inversion results can be used to test proposed models of the underlying processes.

In this chapter I described the characteristics of slip histories of the 16 major slow slip events on the Cascadia subduction zone. In the following chapter, I will explore the general scaling laws of slow slip phenomena worldwide as well as the implication for its physical mechanism.

CHAPTER V
SCALING RELATIONSHIPS OF SOURCE PARAMETERS FOR SLOW
SLIP PHENOMENA

This work has been submitted for review, and is co-authored with David Schmidt and Ray Weldon. All coauthors aided in the editorial process. I was responsible for the data collection and processing and was the primary author.

1. Introduction

A source parameter scaling law is an empirical relationship between source parameters (e.g., fault dimensions, seismic energy, and stress drop) that is not explicitly predicted by theory. The empirical scaling relationships of earthquake source parameters provide important insights and constraints on the dynamics of earthquake rupture. The scaling of source parameters have established several widely accepted characteristics of the faulting process, such as the independence of static stress drop on earthquake size (Kanamori and Anderson, 1975), and the propagation of rupture in a pulse-like manner (Heaton, 1990) with a nearly constant rupture velocity (Geller, 1976).

Slow slip events (SSE) detected on subduction zones (e.g., Dragert et al., 2001; Obara, 2002; Wallace and Beavan, 2006; Ohta et al., 2006; Kostoglodov et al., 2003; Brown et al., 2005). SSEs occur downdip of the transition zone between the locked seismogenic zone and the free-slipping zone on the plate interface, and fluids are thought to be critical for its occurrence (e.g., Obara, 2002; Rogers and Dragert, 2003). Since its discovery, more of these events have been detected, including short- and long-term slow

slip events, non-volcanic tremor, and low-frequency earthquakes. Generally, slow slip has a longer duration from days to years compared to the source time function of tremor sequences which can be as short as seconds. Slow earthquakes have also been reported in other tectonic environments such as the San Andreas fault (Linde et al., 1996) and Hawaii (Segall et al., 2006). Here, we use SSE as a general term, including all of the above transient events.

A general scaling law for seismic moment M_o and event duration T for SSEs was proposed by *Ide et al.* (2007) where $M_o \sim T$, which is different than the $M_o \sim T^3$ (Houston, 2001) relationship observed for earthquakes. In this paper, our major goal is to study the logarithmic scaling relationships between several sets of source parameters and define the general trends applicable to most SSEs. These relationships should help to better constrain the rupture dynamics of this phenomenon, while also providing basic constraints for numerical models.

2. Slow slip data set

We compile source parameters of worldwide SSEs that are inferred directly from the slip distributions for the Cascadia subduction zone of Schmidt and Gao (2010) and reported in the literature for other subduction zones (e.g., Hirose et al., 1999; Kostoglodov et al., 2003; Hirose and Obara, 2005, 2010; Brown et al., 2005; Ito and Obara, 2006; Wallace and Beavan, 2006; Ohta et al., 2006; Sekine et al., 2010; and many others). Source parameters include seismic moment M_o , static stress drop $\Delta\sigma$, average fault slip \bar{D} , average rupture velocity \bar{V}_{rupt} , fault dimension (rupture area A , along-strike fault length L and downdip width W), event duration T and dislocation rise time τ .

Additionally, we include documented aseismic slip on the San Andreas fault (Linde et al., 1996) and Hawaii (Segall et al., 2006; Montgomery-Brown et al., 2009). Source parameters published for earthquakes are collected and used as a comparison to SSEs (e.g., Kanamori and Anderson, 1975; Geller, 1976; Heaton, 1990; Hanks and Bakun, 2002, 2008; and many others).

3. Empirical scaling laws of SSEs

3.1. Fault length versus width

The aspect ratio of earthquakes is empirically found to be constant, $L \sim 2W$, on average (Kanamori and Anderson, 1975; Geller, 1976). This relationship has been used historically to convert between width, length, and area of fault surfaces, especially in cases where direct observations of fault dimensions are limited. The data for both SSEs and earthquakes fall within a range of aspect ratios from 1 to 4 (Fig. 5.1). For the Cascadia events, the trend is nearly flat such that the fault width is roughly constant whereas the length extends out to ~ 4 times the width for the largest events. This reflects the fact that the largest events are constrained within the downdip direction, but are free to propagate along strike. Nevertheless, the aspect ratio of about 2 best describes the entire catalog of SSEs over a broad range of fault lengths. We use this scaling to derive the theoretical relationship of seismic moment versus fault area, as discussed in the next section.

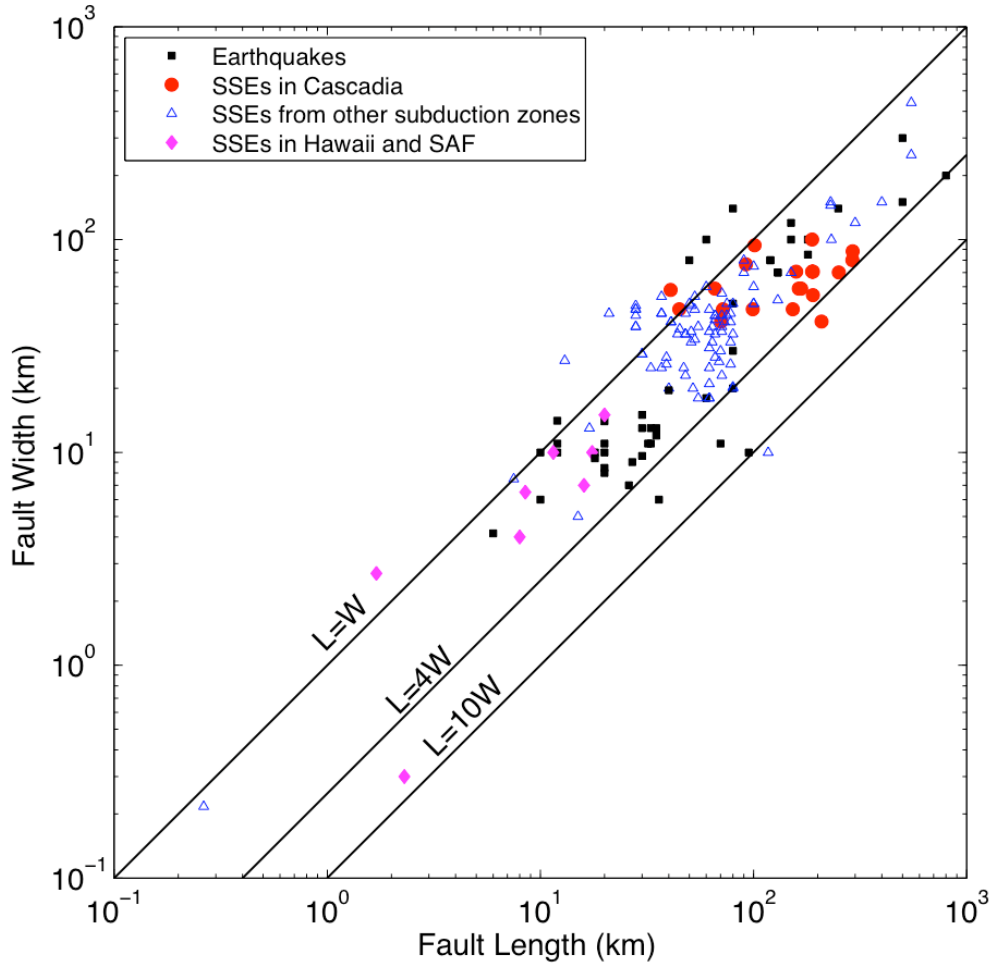


Figure 5.1. The relationship of along-strike fault length L versus downdip fault width W , for slow slip events (SSEs) in Cascadia (red dots), on other subduction zones (blue triangles), on Hawaii's south rift zone and on the San Andreas fault (magenta diamonds). Data for earthquakes are marked as black squares. Black lines denote contours of constant aspect ratio. On average, the along-strike fault length is two times the downdip width for both slow slip events and earthquakes.

3.2. Seismic moment versus fault area

The relationship of seismic moment M_o and fault area A was explored for earthquakes (Kanamori and Anderson, 1975) in which $\text{Log}M_o$ scales with $(3/2)\text{Log}A$. By combining the assumption of constant aspect ratio and the theoretical description of the stress drop on a crack, the following relationship was derived by Kanamori and Anderson (1975),

$$\text{Log}M_o=(3/2)\text{Log}A+\text{Log}\Delta\sigma+\text{Log}C, \quad (1)$$

where C is a non-dimensional factor for the fault shape. When plotted on a graph for moment and area (Fig. 2 in ref. 1), the data were found to follow contours of constant stress drop within the range of 1-10 MPa, and this result established the constant stress drop model for large earthquakes.

Using data available for SSEs, we plot the log-log relationship of seismic moment to rupture area, which is found to be parallel to that of earthquakes (Fig. 5.2). This implies that the static stress drop for SSEs is also independent of event size and rupture area. The stress drop of SSEs is within a range of 0.01-1.0 MPa, generally 1-2 orders of magnitude smaller than earthquakes. One possible explanation would be that the effective stress is very low on the fault. Seismic observations on subduction zones where SSEs occur suggest that the pore fluid pressure is near-lithostatic (Shelly et al., 2006b; Audet et al., 2009), resulting in a very low effective normal stress. The low estimate of the effective normal stress limits the level of shear stress on the fault, which might be on the order of tens of kilopascals (e.g., Rubinstein et al., 2007; Nadeau and Guilhem, 2009). Thus, the stress drop during an event would be limited to a fraction of the shear stress.

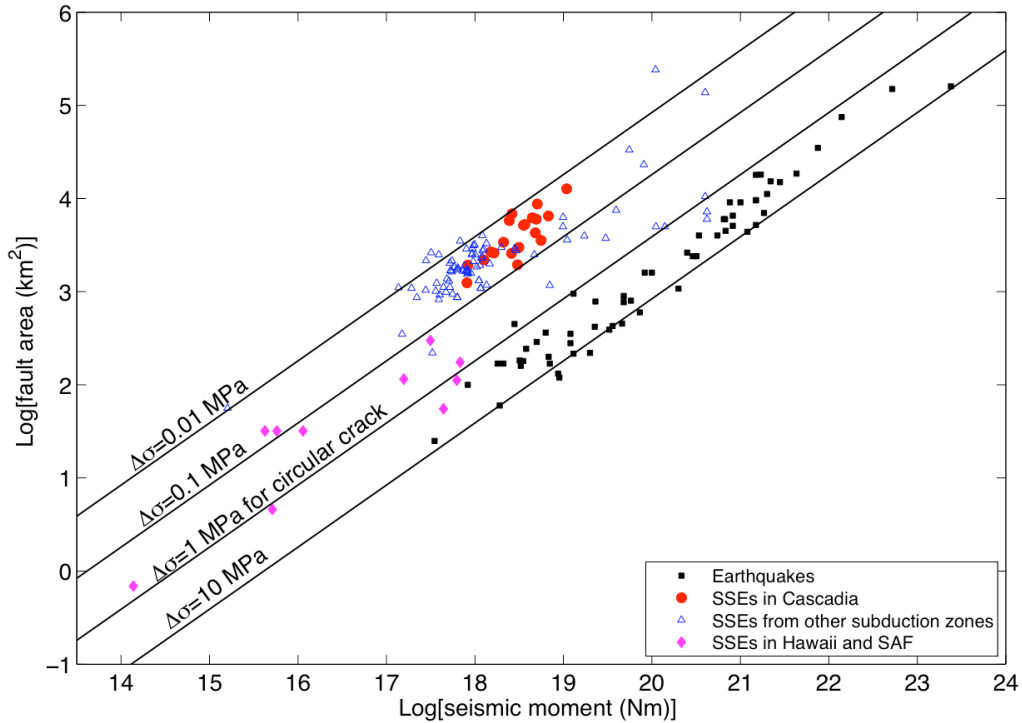


Figure 5.2. The logarithmic relationship of seismic moment M_o versus fault area A . Black lines mark constant static stress drop $\Delta\sigma$ calculated for a circular fault crack. Aseismic slip from Hawaii and the San Andreas fault (SAF) are also included (magenta diamonds). The black squares are earthquakes mainly from ref. 1. The static stress drop of slow slip events (SSEs) is nearly constant (0.01-1.0 MPa), 1-2 orders of magnitude lower than earthquakes (1-10 MPa).

Within the groups of SSEs, events on the San Andreas fault and Hawaii appear to have a higher stress drop (~ 0.1 -1.0 MPa) than those on subduction zones (Fig. 5.2). The subduction setting provides ample sources of fluid that may result in or allow for relatively high pore pressure when compared to the transform setting of the San Andreas and hotspot environment of Hawaii. Abundant fluids may facilitate low effective stress and conditionally-stable behavior on subduction zones. The lack of tremor associated with shallow aseismic slip in Hawaii and the San Andreas fault may indicate that pore pressures are not as high in these regions as on those subduction zones where non-volcanic tremor and SSEs are co-located (Rogers and Dragert, 2003; Obara et al., 2004).

In addition to their different tectonic environments, the depths at which the events occur are strikingly different, which may be a factor. Events on the San Andreas (Linde et al., 1996) and in Hawaii (Montgomery-Brown et al., 2009) occur at depths less than 10 km while those on subduction zones occur at depths greater than 30 km. The lower temperature and pressure at these shallow depths allows for aseismic fault slip on velocity-strengthening fault zones without the need for high pore fluid pressures (Marone et al., 1991).

3.3. Seismic moment versus event duration

Ide et al. (2007) defined a linear scaling relationship of seismic moment versus event duration for slow earthquakes as $\text{Log}M_o \sim \text{Log}T$. To explain this, two models were proposed: the constant stress drop model and the constant slip model. Our present study strongly supports the constant stress drop model (Fig. 5.2). We reassess this logarithmic scaling relationship by adding data of more recent SSEs (Fig. 5.3). By comparing the scaling relationships of slow slip events in Cascadia with those from other subduction zones, the source parameters for Cascadia SSEs are more consistent and well-constrained. Part of the reason is that these SSEs are from the same subduction zone and are determined with a consistent methodology. Source parameters inferred from the literature are estimated with a variety of inversion methodologies by different groups, making the data more scattered. This argues for the need to develop a consistent catalog of SSEs for numerical simulations and theoretical models to be tested against.

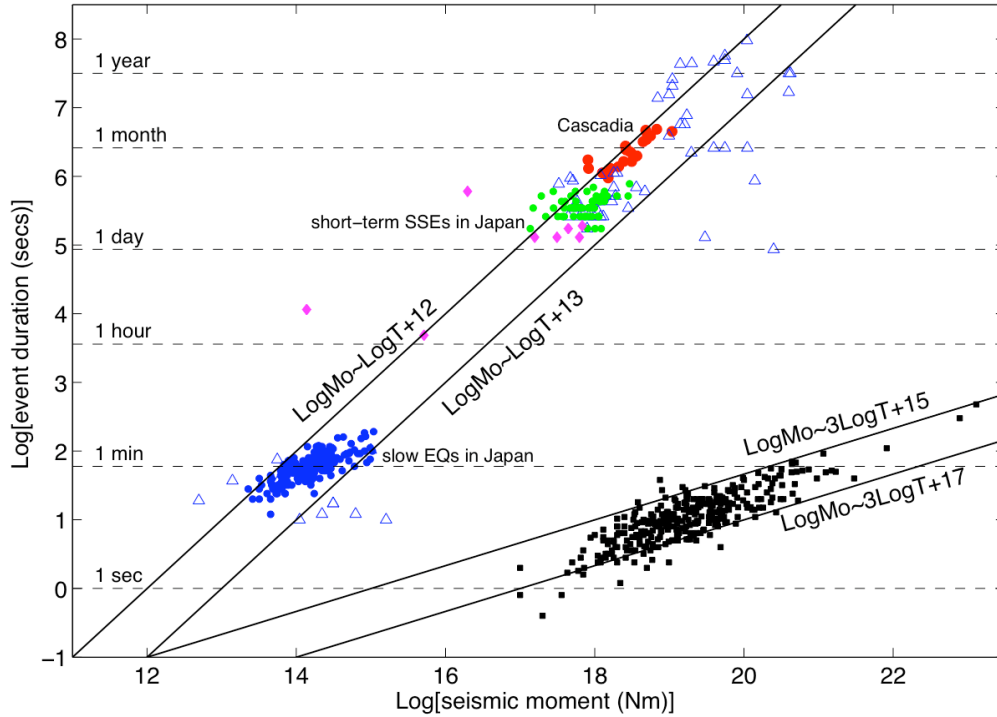


Figure 5.3. The relationship of seismic moment M_o with event duration T for slow slip events (SSEs) in comparison with earthquakes. The horizontal dashed lines indicate contours of constant event duration. The Cascadia SSEs (red dots), a slow earthquake (EQ) sequence (blue dots), and short-term SSEs (green dots) all fall within the $\text{Log}M_o \sim \text{Log}T$ trend. Other markers are the same as Figs. 5.1 and 5.2. Data for earthquakes (black squares) are from <http://www.geo.lsa.umich.edu/SeismoObs/STF.html>.

3.4. Average rupture velocity versus seismic moment

By assuming $\text{Log}M_o \sim n \text{Log}T$ (where n is the exponent) and constant static stress drop, one can show the following general relationship,

$$-(3-n)/(3n) * \text{Log}M_o = \text{Log}\bar{V}_{rpt} + \text{constant}. \quad (2)$$

Equation (2) indicates that if n is less than 3, \bar{V}_{rpt} decreases with the seismic moment, whereas if n is equal to 3, \bar{V}_{rpt} is independent of event size. For earthquakes, as shown by the empirical relation of seismic moment and event duration (Fig. 5.3), n is found to be

~ 3 , supporting the independence of rupture velocity on seismic moment. For SSEs, n is approximately 1 as proposed (Ide et al., 2007), predicting a decrease in rupture velocity with an increase in event size.

Based on the kinematic inversions of coseismic events from strong motion records, the rupture velocity of earthquakes is nearly constant (Geller, 1976). However, the rupture velocity of SSEs decreases with increasing seismic moment (Fig. 5.4) that follows the relationship $\text{Log } \bar{V}_{rpt} \sim (-0.5 \pm 0.05) \text{Log } M_o$. The data suggest a coefficient of $n = 1.2 \pm 0.1$ for Equation (2) which agrees well with $n = 1$ (Ide et al., 2007). The rupture velocity of slow earthquakes varies from tens of kilometers per day to hundreds of meters per day with the seismic moment ranging from 10^{14} - 10^{21} Nm, while being around kilometers per second for low-frequency tremor (solid blue triangle in Fig. 5.4).

In this study, we calculate the average rupture velocity by dividing the rupture length by the event duration. Determining the rupture velocity from tremor is more problematic. Most studies report the propagation of tremor streaks (Shelly et al., 2007; Obara, 2010), whereas few studies have resolved the rupture velocity of an individual event (Ito and Obara, 2006). Because of the difficulty in estimating the fault dimension and individual event duration from tremor, we focus on short- and long-term slow earthquakes (with durations longer than days, Fig. 5.4). However, the details in the actual propagation processes of SSEs are more complicated than described by the average rupture velocity. For example, propagation reversals to the major trend along strike, updip migration faster than the along-strike propagation, and fast-then-slow rupture pattern along strike have been reported (Shelly et al., 2007; McCausland et al., 2010; Obara, 2010; Houston, 2010).

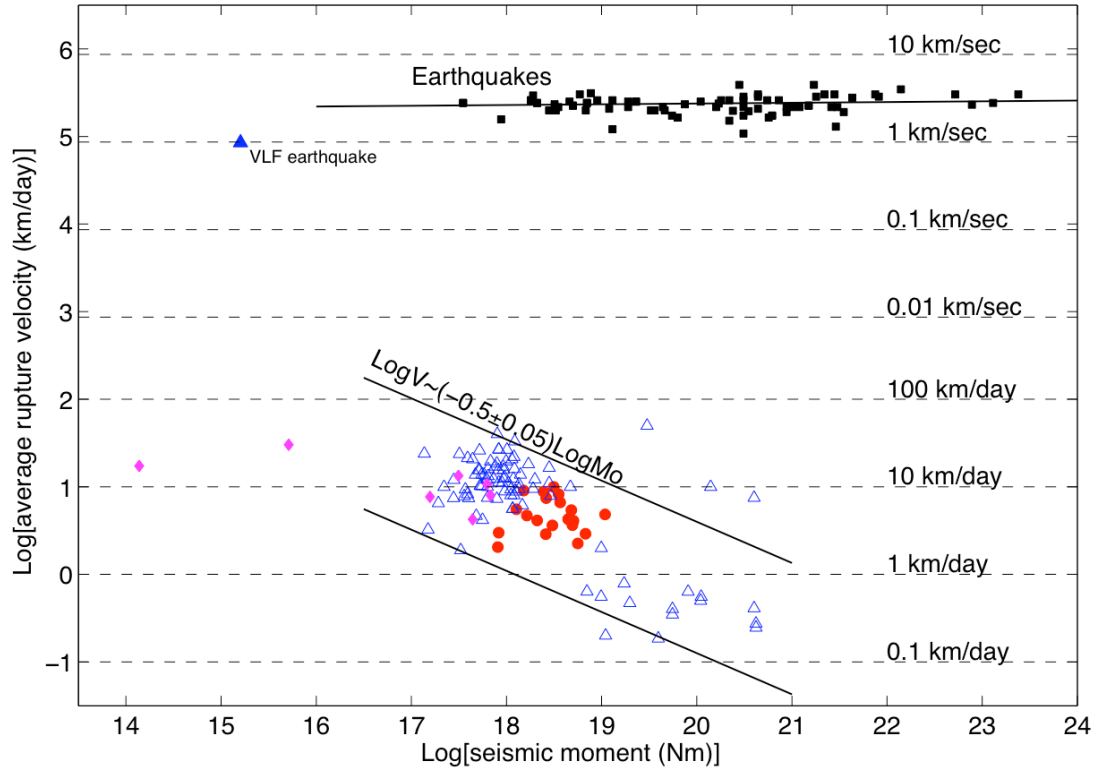


Figure 5.4. The inverse relationship of average rupture velocity with seismic moment for slow slip events. Markers are the same as Fig. 5.1. Earthquakes have a nearly constant rupture velocity whereas slow slip events show a decreasing rupture velocity with increasing seismic moment. Only one very low-frequency earthquake (VLF, solid blue triangle) is available. The solid black lines denote the linear fit for short- and long-term slow earthquakes with durations longer than days (solid red dots and open blue triangles).

Most existing numerical simulations of SSEs (Liu and Rice, 2009; Shibazaki et al., 2010) do not exhibit the inverse dependence of rupture velocity on seismic moment. Thus these models may lack characteristics that produce this behavior. We hypothesize that the dependence of velocity on magnitude could be related to the heterogeneity of fault properties on the SSE generation zone, such as the heterogeneous distribution of the pore fluid pressure, stress state or friction. As the asperity model proposed for earthquakes (e.g., Aki, 1979; Johnson and Nadeau, 2002), the faults that exhibit slow slip and tremor could consist of many small-sized stronger asperities surrounded by weaker regions. The asperity model was previously extended to SSEs as a way to explain the

variety of SSEs observed on subduction zones (Ito et al., 2007). The weaker portions of the subduction interface may arise from increased pore pressure. It is proposed for earthquakes (Day, 1982) that the slip rise time is approximately $W_{eff}/(2\bar{V}_{rupt})$ for a long narrow fault where W_{eff} is the effective width of asperities. If we apply this relationship to non-volcanic tremor using the appropriate rupture velocity and rise time, the effective asperity width is on the order of hundreds-of-meters. Alternatively, slow slip exhibits a longer rise time and slower velocity that translates into an effective asperity size of a few tens-of-kilometers. Thus, tremor may initiate and propagate along small asperities at relatively fast velocities while large-dimension slow slip propagates along the fault surface between the asperities at a slower velocity.

3.5. Rupture duration versus rise time

The dislocation rise time of earthquakes is typically only 10-20% of the event duration based on near-source observations (e.g., Beroza and Spudich, 1988; Heaton, 1990). Two classical models have been proposed to explain the short rise time, the self-healing pulse-like rupture behavior (e.g., Heaton, 1990; Beeler and Tullis, 1996) and rupture propagation through a heterogeneous fault (e.g., Beroza and Mikumo, 1996; Day et al., 1998). The first model assumes that the fault could heal itself shortly after the passage of the rupture front, which allows for the rise time to remain short. The second model, however, attributes the short rise time to the heterogeneous distribution of stress drop.

To compare the rise time to rupture duration for SSEs, we focus on well-constrained events in Cascadia of Schmidt and Gao (2010). Our time-dependent GPS

inversions for slip estimate rise times on the plate interface from 1-2 weeks. However, temporal smoothing in the inversion likely overestimates these values. Therefore, as a proxy, the rise time used here is the average number of days required for the surface displacement to reach 95% of the maximum displacement at each GPS station. As shown in Fig. 5.5, the event duration of SSEs is less than 3 times the rise time whereas earthquakes have ratios significantly greater than 3. Numerical simulations of SSEs show that the fault continues to slip after the passage of the rupture front (e.g., Figure 8 in Liu and Rice, 2009; Figure 8 in Shibasaki et al., 2010; Figure 10 in Liu and Rubin, 2010), consistent with the observation of a small ratio. Our finding suggests that SSEs display less pulse-like behavior than do earthquakes. This may indicate that slow slip faults heal themselves slower after the passage of the rupture front than it does for seismogenic faults. A long rise time for slow slip events might also suggest that the pore fluids do not drain out of the fault zone as quickly, which would otherwise act to strengthen the fault as the fluids drained.

3.6. Recurrence statistics

Recurrence models have been proposed for earthquakes, e.g., the time and slip predictable model (e.g., Shimazaki and Nakata, 1980; Anagnos and Kiremidjian, 1984; Shimazaki, 2002), by assuming constant stressing rate. These models provide a means to estimate the timing or size of future events, assuming that earthquakes conform to one model. For the time predictable model, the recurrence interval to the next event is equal to the static stress drop released by the most recent earthquake divided by the stressing rate, which implies that a larger event requires a longer recovery time until the next one.

For the slip predictable model, the fault slip released for an event is proportional to the shear stress on the fault, which is equal to the time interval since the last event multiplied by the stressing rate. Thus a longer inter-event period produces a larger event. There has been much debate as to whether earthquake sequences display this behavior. We explore the recurrence behavior of SSEs, which do exhibit quasi-periodic behavior at some locations.

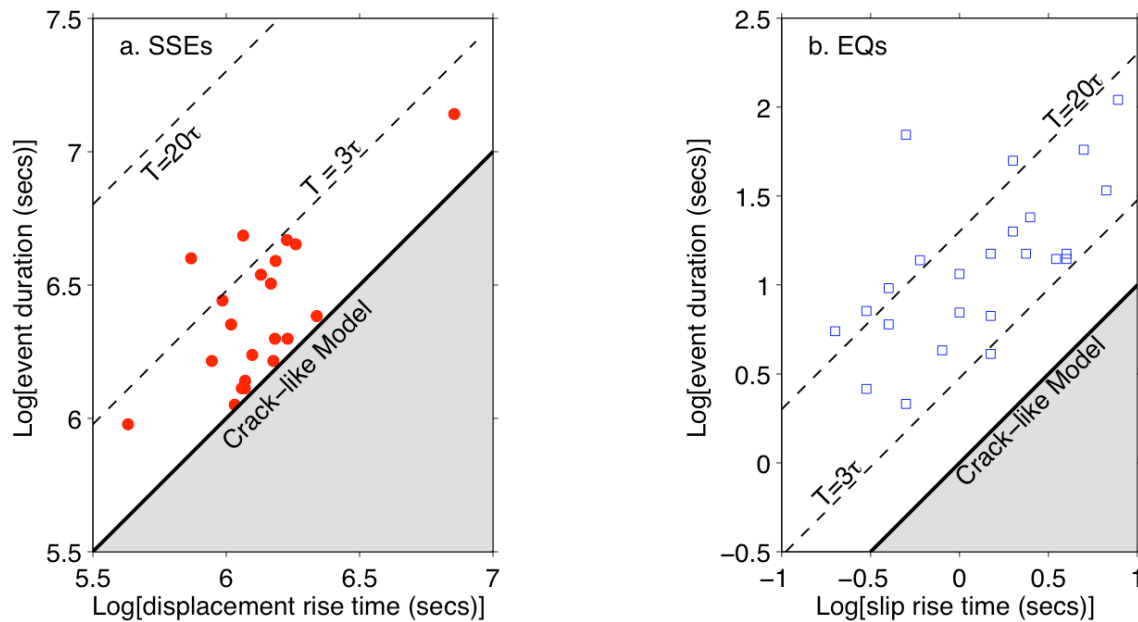


Figure 5.5. The relationship of event duration T versus rise time τ . The solid black line is where rise time is comparable to event duration consistent with a crack-like rupture. The ratio of event duration to rise time is smaller for slow slip events (less than 3) in Figure 5.5a compared to earthquakes (greater than 3) in Figure 5.5b. This indicates that slow slip events are less pulse-like compared to earthquakes.

Time and slip predictable behavior are assessed by plotting the moment magnitude as a function of the recurrence interval for individual SSEs on the Cascadia subduction zone. The short and regular recurrence interval of ~ 14.5 months (Miller et al., 2002) for SSEs near Port Angeles, Washington, makes this area ideal to test the

recurrence behavior. Among the catalog of the Cascadia SSEs (Schmidt and Gao, 2010), 11 are centered around Port Angeles. We calculate the recurrence interval for these events by using the time interval between the starting days of successive transient signals recorded by the GPS station ALBH (latitude: 48.39, longitude: 236.51), which has one of the best records of SSEs in the last decade. The moment and inter-event period are plotted in Fig. 5.6a for the slip predictable case and Fig. 5.6b for the time predictable case. The data are expected to define a clear trend if they conform to a particular recurrence model. We find that the seismic moment is anti-correlated to the pre-event recurrence interval for each event with a R^2 of 0.48, but has a weak positive dependence on the post-event recurrence interval with an R^2 of 0.16. This suggests that SSEs around Port Angeles are moderately anti-slip predictable and weakly time predictable.

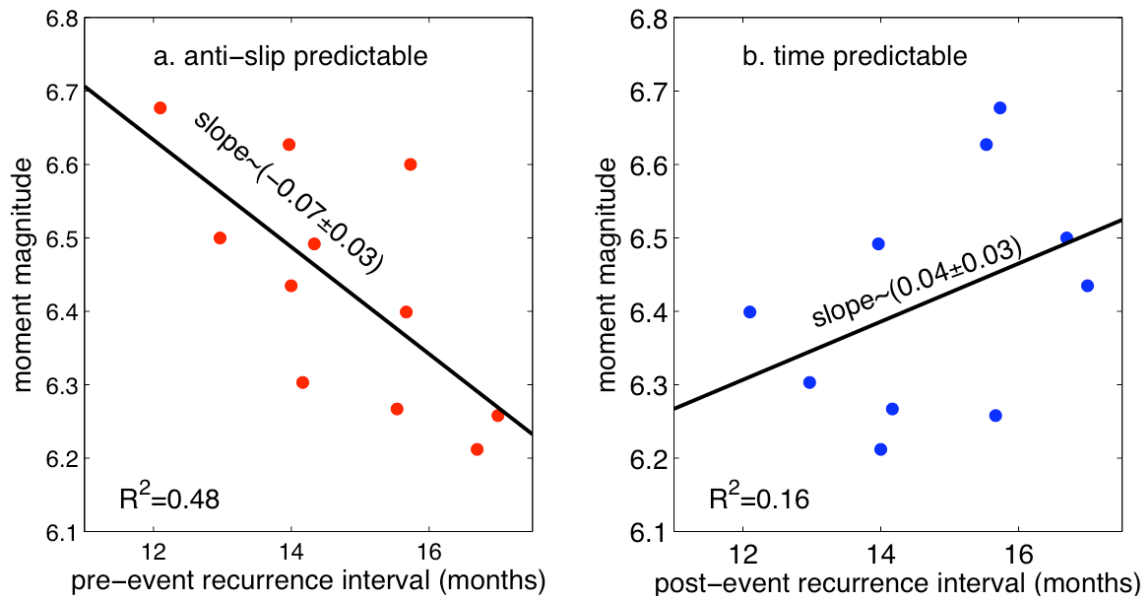


Figure 5.6. Recurrence statistics for slow slip events in northern Cascadia. In Figure 5.6a, the slip predictable model requires that larger events are preceded by longer intervals. However, the data suggests that these parameters are anti-correlated. In Figure 5.6b, the time predictable model expects larger events to be followed by longer intervals. These parameters appear to be weakly positively correlated.

The recurrence statistics presented here for a SSE sequence in northern Cascadia has some implications about the fault healing process on the SSE generation zone. We speculate that longer recurrence intervals may allow greater fault healing over the long term, thereby strengthening the fault and slightly limiting the strain release for the next event causing the anti-slip predictable behavior we see. Anti-slip recurrence behavior has been documented for large event sequences on the San Andreas fault based on paleoseismic data (Weldon et al., 2004). While there are few fault or SSE data sets available to test slip predictable, this suggests that both SSEs and earthquakes may share common recurrence characteristics, at least at some locations. The significance of this behavior is unclear, although it tends to favor the clustering of activity. Also, where data exist, faults are only weakly time predictable at best (Murray and Segall, 2002). The lack of strong time predictability suggests that stressing rate is not the dominant factor in the timing of earthquake events. Variations in fault strength through time and or triggering mechanisms must play a significant role.

4. Conclusions

We explore the empirical scaling relationships of SSE source parameters that provide some insight into the source process of this phenomenon. We find that the static stress drop is independent of event size, consistent with that found for earthquakes. However, the strong inverse dependence of average rupture velocity on seismic moment and the smaller ratio of duration over rise time indicate that some aspects of the underlying rupture process are different between SSEs and earthquakes. The scaling laws

presented here and their comparisons with earthquakes highlight the similarities and differences of these two phenomena.

Although the implications of these SSE scaling laws are still not fully understood, the heterogeneity of fault properties appears to be important for a comprehensive interpretation of these characteristics. We find that the source zone of SSEs is consistent with an asperity model where small patches of locally high strength are distributed within a broader zone of low strength. The shear strength over the entire region is significantly less than seismogenic faults because of near-lithostatic pore pressure. The low shear strength also limits the static stress drop. We propose that tremor ruptures the small asperities, whose small size results in fast rupture velocities and short rise times relative to aseismic slip. The strain on the surrounding fault is released by aseismic slip in a less pulse-like mode of rupture than do earthquakes. The presence of fluids facilitates low stress drops, and the interaction of the fluids with the fault zone may delay the healing process after the passage of the rupture front but more effectively help to strengthen the fault in the long term.

CHAPTER VI

CONCLUSIONS

In this dissertation I described my research related to two major projects. One part is to interpret the seismic signatures related to the long-term, large-scale tectonics of the Pacific Northwest of the United States, using the pattern of seismic anisotropy of the upper mantle in eastern Oregon and the construction of a high-resolution 3D seismic velocity model of the crust and uppermost mantle in the northwestern United States. My second focus is to study the characteristics of short-term, small-scale aseismic faulting on the plate interface by resolving the time-dependent slip histories of slow slip events on the Cascadia subduction zone in the last decade. I then expand the study to explore the general scaling and recurrence patterns of slow slip events worldwide. In this chapter, I summarize the results and implications of this work.

In Chapter II, I analyzed the upper-mantle azimuthal anisotropy of eastern Oregon and its surrounding areas with SKS-splitting program by combining the EarthScope Transportable Array, the Wallowa flexible array and the High Lava Plains project. I showed that the shear-wave splitting trends in High Lava Plains are fairly uniform and the fast polarization directions tend to align approximately E-W with delay times ~ 1.8 s on average. This contrasts with the more complex splitting directions and small delay times in the Blue and Wallowa Mountain regions. I infer that the observed splitting pattern in the High Lava Plains reflects strong mantle flow beneath this area in an approximately E-W direction. The region with large delay times correlates spatially well with where the mantle wavespeed is slow and where the Holocene volcanism occurs. The

interpretation is that the anisotropic layer beneath this area is thicker than average resulting in abnormally large delay times. The complex splitting pattern in NE Oregon is interpreted as evidence for weaker and more complex azimuthal anisotropy, suggesting that both active mantle flow in the asthenosphere and lithospheric anisotropy contribute to the shear-wave splitting pattern. The splitting measurements place a very strong constraint on present-day mantle flow beneath the studied area.

Overall, this study illustrates the azimuthal anisotropy pattern of the upper-mantle in eastern Oregon. This study provides a constraint on the tectonic evolution of this area, and I hope these results will prompt further study on the origin of anisotropy in the crust and mantle lithosphere.

In Chapter III, I present the ambient noise tomography results of the isotropic fundamental-mode Rayleigh-wave using data from the EarthScope Transportable Array, the Wallowa flexible array, a portion of the High Lava Plains project and seven permanent stations from 2006-2009. I show that the seismic velocity structure is complex but geologically coherent in the U.S. Pacific Northwest. Accretion of the Siletzia oceanic lithosphere to continental North America ~50 Ma resulted in a major and geologically well-recorded magmatic and tectonic reorganization of the plate margin whose structure is largely preserved in the seismically imaged crust and upper mantle. The geometry of western Columbia Basin in south-central Washington is well imaged with an abnormally slow sedimentary layer underlied by very fast lower-crust, which is interpreted to be the underplated crust of Siletzia lithosphere. The under-accreted distribution and boundaries of Siletzia, beneath eastern Washington, north-central Oregon and westernmost Idaho, are supported by high velocities in the lower crust. The competitive contribution of

temperature and composition to seismic velocity is well illustrated along the Cascade arc with temperature-dominant in the magmatically active Oregon Cascades and composition-dominant in the Washington part. Eruption of the Columbia River Flood Basalt in NE Oregon appears to have removed a piece of Siletzia lithosphere near its margin.

Overall, this study seismically reconstructs the subduction history of the oceanic Siletzia lithosphere and the consequent tectonic evolution of the Pacific Northwest with its accretion. I hope this study provides a high-resolution crustal model for others, and the seismic complexity in the source region of the Columbia River Flood Basalt will motivate a further study in this area for a better understanding of the geologic structures.

I then resolve the time-dependent slip histories of slow slip events on the Cascadia subduction zone from 1998-2008 using the Extended Network Inversion Filter in Chapter IV. The greatest cumulative fault slip is centered beneath Port Angeles in the northern Cascadia subduction zone, showing ~ 2.5 cm on average. This slip patch correlates well with the along-strike bending geometry of the subducting plate. This coherence may indicate that the geometry of the plate interface plays a critical role in controlling the occurrence of slow slip events and their spatial slip patterns. There is no systematic propagation pattern found for these 16 slow slip events along strike, and the average along-strike propagation velocity is ~ 6.0 km/day. The slip patterns and event statistics inferred from our inversion results will help to test models proposed for the occurrence of slow slip events.

Overall, this study illustrates the kinematic slip distributions of Cascadia slow slip events. This study contributes to the estimate of the onshore range of the seismically

locked zone and the comparison of the occurrence depth between slow slip events and non-volcanic tremor that occurred temporally and spatially coherent with slow slip events.

Built on this study, I then broadened my research to explore the general characteristics of slow slip phenomena by analyzing source parameter scaling laws collected from subduction zones and other tectonic environments (Chapter V). The scaling laws presented here and their comparisons with earthquakes highlight the similarities and differences of these two phenomena. The strong inverse dependence of average rupture velocity on seismic moment and the smaller ratio of duration over rise time indicate that some aspects of the underlying rupture process are different between SSEs and earthquakes. We propose that the heterogeneity of fault properties may be important for a comprehensive explanation of these characteristics.

This work demonstrates the need for a systematic methodology to solve the source parameters of slow slip events on different areas. Without a catalog of events that I used in this study, it would not have been possible to define the general scaling laws of source parameters for slow slip phenomena, nor to compare with those found for earthquakes.

In summary, my dissertation constructs a high-resolution seismic velocity model of the crust and uppermost mantle in the Pacific Northwest, as well as addresses the general characteristics of slow slip phenomenon. This work illustrates the close coherence of seismic features with the geologic history in this studied area. Also, my dissertation illustrates the similarities and differences between slow slip phenomenon and

earthquakes in order to better understand the physical mechanism of slow slip phenomenon.

REFERENCES CITED

Chapter II

- Becker, T. W., V. Schulte-Pelkum, D. K. Blackman, J. B. Kellogg, and R. J. O'Connell (2006), Mantle flow under the western United States from shear wave splitting, *Earth Planet. Sci. Lett.* 247, 235–251.
- Ben Ismaïl, W., and D. Mainprice (1998), A statistical view of the strength of seismic anisotropy in the upper mantle based on petrofabric studies of ophiolite and xenolith samples, *Tectonophysics*, 296, 145–157.
- Burdick, S., C. Li, V. Martynov, T. Cox, J. Eakins, T. Multer, L. Astiz, F. L. Vernon, G. L. Pavlis, R. D. van der Hilst (2008), Upper mantle heterogeneity beneath North America from travel time tomography with global and USArray Transportable Array data, *Seismol. Res. Lett.* 79, 384–387.
- Camp, V. E., and M. E. Ross (2004), Mantle dynamics and genesis of mafic magmatism in the intermontane Pacific Northwest, *J. Geophys. Res.* 109, B08204. doi:10.1029/2003JB002838.
- Carlson, R. W., and W. K. Hart (1987), Crustal genesis on the Oregon Plateau, *J. Geophys. Res.* 92, 6191–6206.
- Chevrot, S. (2006), Finite-frequency vectorial tomography: a new method for high resolution imaging of upper mantle anisotropy, *Geophys. J. Int.* 165, 641–657.
- Christiansen, R. L., and E. H. McKee (1978), Late Cenozoic volcanic and tectonic evolution of the Great Basin and Columbia inter-montane regions, *Geol. Soc. Am. Mem.* 152, 283–311.
- Christiansen, R. L., G. R. Foulger, and J. R. Evans (2002), Upper mantle origin of the Yellowstone hot spot, *Geol. Soc. Am. Bull.* 114, 1245–1256.
- Cross, T. A., and R. H. Pilger (1978), Constraints on absolute motion and plate interaction inferred from Cenozoic igneous activity in the western United States, *Am. J. Sci.* 278, 865–902.
- Fouch, M. J., and K. M. Fischer (1998), Shear wave anisotropy in the Mariana subduction zone, *Geophys. Res. Lett.* 25, 1221–1224.
- Fouch, M. J., and S. Rondenay (2006), Seismic anisotropy beneath stable continental interiors, *Phys. Earth Planet. Inter.* 158, 292–320.

- Fouch, M. J., and J. D. West, in preparation. The mantle flow field beneath western North America.
- Greve, S. M., and M. K. Savage (2009), Modelling seismic anisotropy variations across the Hikurangi subduction margin, New Zealand, *Earth Planet. Sci. Lett.* 285, 16–26.
- Greve, S. M., M. K. Savage, and S. D. Hoffman (2008), Strong variations in seismic anisotropy across the Hikurangi subduction zone, North Island, New Zealand, *Tectonophysics* 462, 7–21.
- Hales, T. C., D. L. Abt, E. D. Humphreys, and J. J. Roering (2005), A lithospheric instability origin for Columbia River flood basalts and Wallowa Mountains uplift in northeast Oregon, *Nature* 438, 842–845.
- Holtzman, B., D. L. Kohlstedt, M. E. Zimmerman, F. Heidelbach, T. Hiraga, and J. Hustoft (2003), Melt segregation and strain partitioning: implications for seismic anisotropy and mantle flow, *Science* 301, 1227–1230.
- Hooper, P. R., V. E. Camp, S. P. Reidel, M. E. Ross (2007), The origin of the Columbia River flood basalt province: plume versus nonplume models. In: Foulger, G.R., Jurdy, D.M. (Eds.), Plates, plumes, and planetary processes: *Geol. Soc. Am. Special Paper*, 430, 635–668.
- Humphreys, E. D., and D. D. Coblenz (2007), North American dynamics and western U.S. tectonics, *Rev. Geophys.* 45. doi:10.1029/2005RG000181.
- Humphreys, E. D., K. G. Deuker, D. L. Schutt, and R. B. Smith (2000), Beneath Yellowstone: evaluating plume and nonplume models using teleseismic images of the upper mantle, *GSA Today* 10, 1–7.
- Jordan, B. T. (2005), Age-progressive volcanism of the Oregon High Lava Plains: overview and evaluation of tectonic models. In: Foulger, G.R., et al. (Ed.), Plates, Plumes, and Paradigms: *Geological Society of America Memoir*, 388, 503–515.
- Jordan, B. T., A. L. Grunder, R. A. Duncan, and A. L. Deino (2004), Geochronology of age-progressive volcanism of the Oregon High Lava Plains: implications for the plume interpretation of Yellowstone, *J. Geophys. Res.* 109, B10202. doi:10.1029/2003JB002776.
- Jung, H., W. Mo, and H. W. Green (2009), Upper mantle seismic anisotropy resulting from pressure-induced slip transition in olivine, *Nature Geosci.* 2, 73–77.
- Karato, S., H. Jung, I. Katayama, and P. Skemer (2008), Geodynamic significance of seismic anisotropy of the upper mantle: new insights from laboratory studies, *Annu. Rev. Earth Planet. Sci.* 36, 59–95.

- Kincaid, C., K. Druken, and R. Griffiths (2008), Laboratory models of three-dimensional mantle flow and plume dispersion driven by rollback subduction and back-arc extension, *International Geological Congress, Oslo, Norway*.
- Leeman, W. P., J. S. Oldow, and W. K. Hart (1992), Lithosphere-scale thrusting in the western U.S. Cordillera as constrained by Sr and Nd isotopic transitions in Neogene volcanic rocks, *Geology* 20, 63–66.
- Li, X., X. Yuan, R. Kind (2007), The lithosphere-asthenosphere boundary beneath the western United States, *Geophys. J. Int.* 170, 700–710.
- Lipman, P. W., H. J. Prostka, and R. L. Christensen (1972), Cenozoic volcanism and plate tectonic evolution of the western United States, *I. Phil. Trans. Roy. Soc. London, Ser. A* 271, 217–248.
- Long, M. D., and P. G. Silver (2009), Shear wave splitting and mantle anisotropy: measurements, interpretations, and new directions, *Surv. Geophys.* 30, 407–461.
- Long, M. D., and R. D. van der Hilst (2005), Estimating shear wave splitting parameters from broadband recordings in Japan: a comparison of three methods, *Bull. Seismol. Soc. Am.* 95, 1346–1358.
- Long, M. D., M. V. de Hoop, and R. D. van der Hilst (2008), Wave-equation shear wave splitting tomography, *Geophys. J. Int.* 172, 311–330.
- Lowry, A. R., and R. B. Smith (1995), Strength and rheology of the western U.S. Cordillera, *J. Geophys. Res.* 100, 17,947–17,963.
- Mainprice, D. (2007), Seismic anisotropy of the deep Earth from a mineral and rock physics perspective. In: Schubert, G (Ed.), *Treatise on Geophysics* 2, 437–492.
- Mainprice, D., and P. G. Silver (1993), Interpretation of SKS waves using samples from the subcontinental lithosphere, *Phys. Earth Planet. Inter.* 78, 257–280.
- Marson-Pidgeon, K., and M. K. Savage (1997), Frequency-dependent anisotropy in Wellington, New Zealand, *Geophys. Res. Lett.* 24, 3297–3300.
- McCaffrey, R., M. D. Long, C. Goldfinger, P. C. Zwick, J. L. Nabelek, C. K. Johnson, and C. Smith (2000), Rotation and plate locking at the southern Cascadia subduction zone, *Geophys. Res. Lett.* 27, 3117–3120.
- McCaffrey, R., A. I. Qamar, R. W. King, R. Wells, G. Khazaradze, C. A. Williams, C. W. Stevens, J. J. Vollick, and P. C. Zwick (2007), Fault locking, block rotation and crustal deformation in the Pacific Northwest, *Geophys. J. Int.* 169, 1315–1340.

- Pierce, K. L., and L. A. Morgan (1992), The track of the Yellowstone hot spot: volcanism, faulting, and uplift. In: Link, K., Kuntz, M.A., Platt, L.B. (Eds.), Regional Geology of Eastern Idaho and Western Wyoming: Mem. *Geol. Soc. Am.* 179, 1–53.
- Roth, J. B., M. J. Fouch, D. E. James, and R. W. Carlson (2008), Three-dimensional seismic velocity structure of the northwestern United States, *Geophys. Res Lett.* 35, L15304. doi:10.1029/2008GL034669.
- Saltzer, R. L., J. Gaherty, and T. H. Jordan (2000), How are vertical shear wave splitting measurement affected by variations in the orientation of azimuthal anisotropy with depth? *Geophys. J. Int.* 141, 374–390.
- Savage, M. K. (1999), Seismic anisotropy and mantle deformation: what have we learned from shear wave splitting? *Rev. Geophys.* 37, 65–106.
- Schellart, W. P., D. R. Stegman, and J. Freeman (2008), Global trench migration velocities and slab migration induced upper mantle volume fluxes: constraints to find an Earth reference frame based on minimizing viscous dissipation, *Earth Science Rev.* 88, 118–144.
- Sigloch, K., N. McQuarrie, and G. Nolet (2008), Two-stage subduction history under North America inferred from multiple-frequency tomography, *Nature Geosci.* 1, 458–462.
- Silver, P. G. (1996), Seismic anisotropy beneath the continents: probing the depths of geology, *Annu. Rev. Earth Planet. Sci.* 24, 385–432.
- Silver, P. G., and W. W. Chan (1991), Shear wave splitting and subcontinental mantle deformation, *J. Geophys. Res.* 96, 16,429–16,454.
- Silver, P. G., and W. E. Holt (2002), The mantle flow field beneath western North America, *Science* 295, 1054–1057.
- Silver, P. G., and M. K. Savage (1994), The interpretation of shear-wave splitting parameters in the presence of two anisotropic layers, *Geophys. J. Int.* 119, 949–963.
- Smith, A. D. (1992), Back-arc convection model for Columbia River Basalt genesis, *Tectonophysics* 207, 269–285.
- Vachez, A., A. Tommasi, G. Barruol, and J. Maumus (2000), Upper mantle deformation and seismic anisotropy in continental rifts, *Phys. Chem. Earth (A)* 25, 111–117.
- Waff, H. S., and U. H. Faul (1992), Effects of crystalline anisotropy on fluid distribution in ultramafic partial melts, *J. Geophys. Res.* 97, 9003–9014.

- Warren, L. M., J. A. Snoke, and D. E. James (2008), S-wave velocity structure beneath the High Lava Plains, Oregon, from Rayleigh-wave dispersion inversion, *Earth Planet. Sci. Lett.* 274, 121–131.
- Wernicke, B., G. J. Axen, and J. K. Snow (1988), Basin and Range extensional tectonics at the latitude of Las Vegas, Nevada, *Geol. Soc. Am. Bull.* 100, 1738–1757.
- West, J. D., M. J. Fouch, J. B. Roth, and L. T. Elkins-Tanton (2009), Seismic detection of vertical mantle flow from a lithospheric drip, *Nature Geosci.* 2, 439–444.
- Wustefeld, A., and G. Bokelmann (2007), Null detection in shear-wave splitting measurements, *Bull. Seismol. Soc. Am.* 97, 1204–1211.
- Wustefeld, A., G. Bokelmann, G. Barruol, and C. Zaroli (2007), Splitlab: a shear-wave splitting environment in Matlab, *Comput. Geosci.* 34, 515–528.
- Xue, M., and R. M. Allen (2006), Origin of the Newberry hotspot track: evidence from shearwave spitting, *Earth Planet. Sci. Lett.* 244, 315–322.
- Zandt, G., and E. Humphreys (2008), Toroidal mantle flow through the western U.S. slab window, *Geology* 36, 295–298.
- Zimmerman, M. E., S. Zhang, D. L. Kohlstedt, and S. Karato (1999), Melt distribution in mantle rocks deformed in simple shear, *Geophys. Res. Lett.* 26, 1505–1508.

Chapter III

- Bensen, G. D., M. H. Ritzwoller, M. P. Barmin, A. L. Levshin, F. Lin, M. P. Moschetti, N. M. Shapiro, and Y. Yang (2007), Processing seismic ambient noise data to obtain reliable broad-band surface wave dispersion measurements, *Geophys. J. Int.* 169, 1239-1260, doi:10.1111/j.1365-246x.2007.03374.x.
- Blackwell, D. D., J. L. Steele, M. K. Frohme, C. F. Murphey, G. R. Priest, and G. L. Black (1990a), Heat flow in the Oregon Cascade Range and its correlation with regional gravity, Curie point depths, and geology, *J. Geophys. Res.* 95, 19,475-19,493.
- Blackwell, D. D., J. L. Steele, and S. Kelley (1990b), Heat flow in the state of Washington and thermal conditions in the Cascade range, *J. Geophys. Res.* 95, 19,495-19,516.
- Brandon, M. T., M. K. Roden-Tice, and J. I. Garver (1998), Late Cenozoic exhumation of the Cascadia accretionary wedge in the Olympic Mountains, northwest Washington State, *Geol. Soc. Am. Bull.* 110, 985-1009.

- Brandon, A. D., and G. G. Goles (1988), A Miocene subcontinental plume in the Pacific Northwest: Geochemical evidence, *Earth Planet. Sci. Lett.* 88, 273-283.
- Brocher, T. M. (2005), Empirical relations between elastic wavespeeds and density in the Earth's crust, *Bull. Seism. Soc. Am.* 95(6), 2081-2092.
- Brunet, M.-F., M. V. Korotaev, A. V. Ershov, and A. M. Nikishin (2003), The South Caspian Basin: a review of its evolution from subsidence modeling, *Sedimentary Geology*, 156, 119-148.
- Burchfiel, B. C., D. S. Cowan, and G. A. Davis (1992), Tectonics overview of the Cordilleran Oregon in the western United States, in *Burchfiel, B.C., Lipman, P.W., and Zoback, M.L., eds., The Cordilleran Orogen: Conterminous U.S.:* Boulder, Colorado. *Geol. Soc. Am. The Geology of North America*, G-3.
- Burdick, S., C. Li, V. Martynov, T. Cox, J. Eakins, T. Mulder, L. Astiz, F. L. Vernon, G. L. Pavlis, R. D. van der Hilst (2008), Upper mantle heterogeneity beneath North America from travel time tomography with global and USArray transportable array data, *Seism. Res. Lett.* 79, 384-392.
- Calkins, J. A., G. A. Abers, G. Ekstrom, K. G. Creager, and S. Rondenay (2009), Imaging the slab-continent interface beneath Washington with spectral ambient noise tomography, *Eos Trans. AGU*, U53A-0059.
- Camp, V. E., M. E. Ross, and W. E. Hanson (2003), Genesis of flood basalts and Basin and Range volcanic rocks from Steens Mountain to the Malheur River Gorge, Oregon, *Geol. Soc. Am. Bull.* 115, 105-128.
- Camp, V. E., and M. E. Ross (2004), Mantle dynamics and genesis of mafic magmatism in the intermontane Pacific Northwest, *J. Geophys. Res.* 109, B08204, doi:10.1029/2003JB002838.
- Campbell, N. P. (1989), Structural and stratigraphic interpretation of rocks under the Yakima fold belt, Columbia Basin, based on recent surface mapping and well data, *Geol. Soc. Am. Special Paper*, 239, 209-222.
- Campillo, M. and A. Paul (2003), Long-Range correlations in the diffuse seismic coda, *Science*, 299, 547-549.
- Carlson, R. W. (1984), Isotopic constraints on Columbia River flood basalt genesis and the nature of the subcontinental lithospheric mantle, *Geochim. Cosmochim. Acta* 48, 2357-2372.
- Carlson, R. W., and W. K. Hart (1987), Crustal genesis on the Oregon Plateau, *J. Geophys. Res.* 92, 6191-6206.

- Catchings, R. D., and W. D. Mooney (1988), Crustal structure of the Columbia Plateau; Evidence for continental rifting, *J. Geophys. Res.* *93*, 459-474.
- Christiansen, R. L., and R. L. Yeats (1992), Post-Laramide geology of the U.S. Cordillerian region, in *Burchfiel, B.C., Lipman, P.W., and Zoback, M.L., eds., The Cordilleran Orogen: Conterminous U.S.: Geol. Soc. Am. The Geology of North America*, G-3, 241-406.
- Coney, P. J., and S. J. Reynolds (1977), Flattening of the Farallon slab, *Nature*, *270*, 403-406.
- Coney, P. J., and T. A. Harms (1984), Cordilleran metamorphic core complexes: Cenozoic extensional relics of Mesozoic compression, *Geology*, *12*, 550-554.
- Duncan, R. A. (1982), A captured island chain in the Coast Range of Oregon and Washington, *J. Geophys. Res.* *87*, 10,827-10,837.
- Eagar, K. C., M. J. Fouch, and D. E. James (2010), Receiver function imaging of upper mantle complexity beneath the Pacific Northwest, United States, *Earth Planet. Sci. Lett.* doi:10.1016/j.epsl.2010.06.015.
- Evans, J. E. (1994), Depositional history of the Eocene Chumstick Formation — Implications of tectonic partitioning for the history of the Leavenworth and Entiat-Eagle Creek fault system, Washington, *Tectonics*, *13*, 1425-1444, doi:10.1029/94TC01321.
- Feeley, T. C. (1993), Crustal modification during subduction-zone magmatism: Evidence from the southern Salar de Uyuni region (20°-22°S), central Andes, *Geology*, *21*, 1019-1022.
- Fleck, R. J., and R. E. Criss (1985), Strontium and oxygen isotopic variations in Mesozoic and Tertiary plutons of central Idaho, *Contributions to Mineralogy and Petrology*, *90*, 291-308.
- Foster, D. A., P. T. Doughty, T. J. Kalakay, C. M. Fanning, S. Coyner, W. C. Grice, and J. Vogl (2007), Kinematics and timing of exhumation of metamorphic core complexes along the Lewis and Clark fault zone, northern Rocky Mountains, USA, *Geol. Soc. Am. Special Papers*, *434*, 207-232.
- Fouch, M. J., F. Lin, M. H. Ritzwoller, and J. D. West (2008), Seismic azimuthal anisotropy beneath the western United States from ambient noise tomography and shear wave splitting, *Eos Trans. AGU*, *S32B-01*.

- Gaschnig, R. M., J. D. Vervoort, R. S. Lewis, and W. C. McClelland (2010), Migrating magmatism in the northern US Cordillera: in situ U-Pb geochronology of the Idaho batholith, *Contrib. Mineral Petrol.* 159, 863-883, doi:10.1007/s00410-009-0459-5.
- Geherls, G., and 16 others (2009), U-Th-Pb geochronology of the Coast Mountains batholith in north-coastal British Columbia: Constraints on age and tectonic evolution, *Geol. Soc. Am. Bull.* 121, 1341-1361.
- Gilbert, H. J., and M. Fouch (2007), Complex upper mantle seismic structures across the southern Colorado Plateau/Basin and Range II: Results from receiver function analysis, *Eos Trans. AGU*, 88(S41B-0558).
- Giorgis, S., B. Tikoff, and W. McClelland (2005), Missing Idaho arc: Transpressional modification of the $^{87}\text{Sr}/^{86}\text{Sr}$ transition on the western edge of the Idaho batholith, *Geology*, 33, 469-472.
- Godfrey, N. J., B.C. Beaudoin, S. L. Klemperer, and Mendocino working group (1997), Ophiolitic basement to the Great Valley forearc basin, California, from seismic and gravity data: Implications for crustal growth at the North American continental margin, *Geol. Soc. Am. Bull.* 109, 1536-1562, doi:10.1130/00167606.
- Grand, S. P., and D. V. Helmberger (1984), Upper mantle shear structure of North America, *Geophys. J. R. Soc. London*, 76, 399-438.
- Gurnis, M., (1992), Rapid continental subsidence following the initiation and evolution of subduction, *Nature*, 255, 1556-1558.
- Hales, T. C., D. L. Abt, E. D. Humphreys, J. J. Roering (2005), A lithospheric instability origin for Columbia River flood basalts and Willowa Mountains uplift in northeast Oregon, *Nature*, 438(8), doi:10.1038/nature04313.
- Hooper, P. R., G. B. Binger, and K. R. Lees (2002), Constraints on the relative and absolute ages of the Steens and Columbia River basalts and their relationship to extension-related calc-alkaline volcanism in eastern Oregon, *Geol. Soc. Am. Bull.* 114, 43-50.
- Hughes, S. S., and E. M. Taylor (1986), Geochemistry, petrogenesis, and tectonic implications of central High Cascade mafic platform lavas, *Geol. Soc. Amer. Bull.* 97, 1024-1036.
- Humphreys, E. D. (1995), Post-Laramide removal of the Farallon slab, western United States, *Geology*, 23, 987-990.

- Jones, C. H., L. J. Sonder, and J. R. Unruh (1998), Lithospheric gravitational potential energy and past orogenesis: Implications for conditions of initial Basin and Range and Laramide deformation, *Geology*, 26, 639-642.
- Levander, A., F. Niu, M. S. Miller, Y. Zhai, K. Liu, and X. Cheng (2008), Receiver function images of the lithosphere in the western U.S. from USArray, *Geophys. Res. Abstracts*, 10, EGU2008-A-12372.
- Lin, F., M. P. Moschetti, and M. H. Ritzwoller (2008), Surface wave tomography of the western United States from ambient seismic noise: Rayleigh and Love wave phase velocity maps, *Geophys. J. Int.*, doi:10.1111/j.1365-246X.2008.03720.x.
- Long, M. D., H. Gao, A. Klaus, L. S. Wagner, M. J. Fouch, D. E. James, and E. D. Humphreys (2009), Shear wave splitting and the pattern of mantle flow beneath eastern Oregon, *Earth Planet. Sci. Lett.* doi:10.1016/j.epsl.2009.09.039.
- Magill, J. R., R. E. Wells, R. W. Simpson, and A. V. Cox (1982), Post-12 m.y. rotation of southwest Washington, *J. Geophys. Res.* 87, 3761-3776.
- Mann, G. M., and C. E. Meyer (1993), Late Cenozoic structure and correlations to seismicity along the Olympic-Wallowa Lineament, northwest United States, *Geol. Soc. Amer. Bull.* 105, 853-871.
- Masters, G., G. Laske, H. Bolton, and A. Dziewonski (2000), The relative behavior of shear velocity, bulk sound speed, and compressional velocity in the mantle: Implication for chemical and thermal structure, *Geophysical Monograph Series*, 117, 63-87.
- McCaffrey, R., M. D. Long, C. Goldfinger, P. C. Zwick, J. L. Nabelek, C. K. Johnson, and C. Smith (2000), Rotation and plate locking along the southern Cascadia subduction zone, *Geophys. Res. Lett.* 27, 3117-3120.
- McCaffrey, R., A. I. Omar, R. W. King, R. Wells, G. Khazaradze, C. A. Williams, C. W. Stevens, J. J. Vollick, and P. C. Zwick (2007), Fault locking, block rotation and crustal deformation in the Pacific Northwest, *Geophys. J. Int.*, doi:10.1111/j.1365-246X.2007.03371.x.
- Montagner, J.-P. (1986), Regional three-dimensional structures using long-period surface waves, *Annales Geophysicae*, 4, 283-294.
- Moschetti, M. P., M. H. Ritzwoller, F.-C. Lin, and Y. Yang (2010), Crustal shear wave velocity structure of the western United States inferred from ambient seismic noise and earthquake data, *J. Geophys. Res.*, doi:10.1029/2010JB007448, in press.
- Priest, G. R. (1990), Volcanic and tectonic evolution of the Cascade volcanic arc, central Oregon, *J. Geophys. Res.* 95, 19,583-19,599.

- Raisz, E. (1945), The Olympic-Wallowa lineament, *American Journal of Science*, 243-A, 479-485.
- Ramos, F. C., J. A. Wolff, and D. L. Tollstrup (2005), Sr isotope disequilibrium in Columbia River flood basalts: Evidence for rapid shallow-level open-system processes, *Geology*, 33, 457-460.
- Reidel, S. P., T. L. Tolan, P. R. Hooper, M. H. Beeson, K. R. Fecht, R. D. Bentley, and J. L. Anderson (1989), The Grande Ronde Basalt, Columbia River Basalt Group; Stratigraphic descriptions and correlations in Washington, Oregon, and Idaho, in *Reidel, S.P., and Hooper, P.R., eds., Volcanism and tectonism in the Columbia River flood-basalt province: Boulder, Colorado. Geol. Soc. Am. Special Paper 239.*
- Retallack, G. J., E. A. Bestland, and T. Fremd (2000), Eocene and Oligocene paleosols of central Oregon, *Geol. Soc. Am. Special Paper*, 344, 196.
- Riddihough, R. P., C. Finn, and R. Couch (1986), Klamath-Blue Mountain lineament, Oregon, *Geology*, 14, 528-531.
- Roth, J. B., M. J. Fouch, D. E. James, and R. W. Carlson (2008), Three-dimensional seismic velocity structure of the northwestern United States, *Geophys. Res. Lett.* 35, L15304, doi:10.1029/2008GL034669.
- Sambridge, M. (1999a), Geophysical inversion with a neighborhood algorithm-I. Searching a parameter space, *Geophys. J. Int.* 138, 479-494.
- Sambridge, M. (1999b), Geophysical inversion with a neighborhood algorithm-II. Appraising the ensemble, *Geophys. J. Int.* 138, 727-746.
- Schmandt, B., and E. D. Humphreys (2010), Complex subduction and small-scale convection revealed by body-wave tomography of the western United States upper mantle, *Earth Planet. Sci. Lett.* doi:10.1016/j.epsl.2010.06.047.
- Schmandt, B., and E. D. Humphreys (2011), Seismically imaged relict slab from the 55 Ma Siletzia accretion to the northwest United States, *Geology*, 39, 175-178.
- Schmidt, M. E., A. L. Grunder, and M. C. Rowe (2008), Segmentation of the Cascade Arc as indicated by Sr and Nd isotopic variation among diverse primitive basalts, *Earth Planet. Sci. Lett.* 266, 166-181.
- Shapiro, N. M., and M. Campillo (2004), Emergence of broadband Rayleigh waves from correlations of the ambient seismic noise, *Geophys. Res. Lett.* 31, L07614, doi:10.1029/2004GL019491.

- Sherrod, D. R., and J. G. Smith (1990), Quaternary extrusion rates of the Cascade Range, Northwestern United States and Southern British Columbia, *J. Geophys. Res.* 95, 19,465-19,474.
- Simpson, R. W., and A. Cox (1977), Paleomagnetic evidence for tectonic rotation of the Oregon Coast Range, *Geology*, 5, 585-589.
- Snavely, P. D., N. S. MacLeod, and H. C. Wagner (1968), Tholeiitic and alkalic basalts of the Eocene Siletz River volcanics, Oregon Coast Range, *Am. J. Sci.* 266, 454-481.
- Trehu, A. M., I. Asudeh, T. M. Brocher, J. H. Luetgert, W. D. Mooney, J. L. Nabelek, and Y. Nakamura (1994), Crustal architecture of the Cascadia forearc, *Science*, 266, 237-243, doi:10.1126/science.266.5183.237.
- Van der Pluijm, B. A., P. J. Vrolijk, D. R. Pevear, C. M. Hall, and J. Solum (2006), Fault dating in the Canadian Rocky Mountains: Evidence for late Cretaceous and early Eocene orogenic pulses, *Geology*, 34, 847-840.
- Wells, R. E., D. C. Engebretson, P. D. Snavely, and R. S. Coe (1984), Cenozoic plate motions and the volcano-tectonic evolution of western Oregon and Washington, *Tectonics*, 3, 275-294.
- Wells, R. E. (1990), Paleomagnetic rotations and the Cenozoic tectonics of the Cascade Arc, Washington, Oregon, and California, *J. Geophys. Res.* 95, B12, 19,409-19,417.
- Wells, R. E., C. S. Weaver, and R. J. Blakely (1998), Fore-arc migration in Cascadia and its neotectonic significance, *Geology*, 26, 759-762.
- Wells, R. E., and R. W. Simpson (2001), Northward migration of the Cascadia forearc in the northwestern U.S. and implications for subduction deformation, *Earth Planet Space*, 53, 275-283.
- Wolff, J. A., F. C. Ramos, G. L. Hart, J. D. Patterson, and A. D. Brandon (2008), Columbia River flood basalts from a centralized crustal magmatic system, *Nature Geoscience*, 1, 177-180.
- Yang, Y., M. H. Ritzwoller, F.-C. Lin, M. P. Moschetti, and N. M. Shapiro (2008), Structure of the crust and uppermost mantle beneath the western United States revealed by ambient noise and earthquake tomography, *J. Geophys. Res.* 113, B12310, doi:10.1029/2008JB005833.

Yao, H., R. D. van der Hilst, and M. V. de Hoop (2006), Surface-Wave array tomography in SE Tibet from ambient seismic noise and two-station analysis – I. Phase velocity maps, *Geophys. J. Int.* 166(2), 732-744, doi:10.1111/j.1365-246X.2006.03028.x.

Yao, H., C. Beghein, and R. D. van der Hilst (2008), Surface wave array tomography in SE Tibet from ambient seismic noise and two-station analysis - II. Crustal and upper-mantle structure, *Geophys. J. Int.* 173, 205-219, doi: 10.1111/j.1365-246X.2007.03696.x.

Zonenshain, L. P., and X. Pichon (1986), Deep basins of the Black Sea and Caspian Sea as remnants of Mesozoic back-arc basins, *Evolution of the Tethys*, 123, 181-211, doi:10.1016/0040-1951(86)90197-6.

Chapter IV

Altamimi, Z., X. Collilieux, J. Legrand, B. Garayt, and C. Boucher (2007), ITRF2005: A new release of the International Terrestrial Reference Frame based on time series of station positions and Earth Orientation Parameters, *J. Geophys. Res.* 112, B09401, doi:10.1029/2007JB004949.

Brudzinski, M., and R. M. Allen (2007), Segmentation in episodic tremor and slip all along Cascadia, *Geology* 35, 907–910.

Dong, D., P. fang, Y. Bock, M. K. Cheng, and S. Miyazaki (2002), Anatomy of apparent seasonal variations from GPS-derived site position time series, *J. Geophys. Res.* 107(B4), 2075, doi:10.1029/2001JB000573.

Dragert, H., X. Chen, and J. Kouba (1995), GPS monitoring of crustal strain in southwest British Columbia with the Western Canada Deformation Array, *Geomatica* 49, 301–313.

Dragert, H., K. Wang, and T. S. James (2001), A silent slip event on the deeper Cascadia subduction interface, *Science* 292, 1525–1528, doi:10.1126/science.1060152.

Herring, T. A., R. W King, and S. C. McClusky (2006), GPS analysis at MIT, Gamit reference manual, Release 10.3, Dep. of Earth Atmos. and Planet. Sci., Mass. Inst. of Technol., Cambridge.

Hirose, H., K. Hirahara, F. Kimata, N. Fujii, and S. Miyazaki (1999), A slow thrust slip event following the two 1996 Hyuganada earthquakes beneath the Bungo Channel, southwest Japan, *Geophys. Res. Lett.* 26, 3237–3240.

- Kanamori, H., and D. L. Anderson (1975), Theoretical basis of some empirical relations in seismology, *Bull. Seismol. Soc. Am.* 65, 1073–1095.
- Kao, H., S. Shan, G. Rogers, and H. Dragert (2007), Migration characteristics of seismic tremors in the northern Cascadia margin, *Geophys. Res. Lett.* 34, L03304, doi:10.1029/2006GL028430.
- Kodaira, S., T. Iidaka, A. Kato, J. Park, T. Iwasaki, and Y. Kaneda (2004), High pore fluid pressure may cause silent slip in the Nankai Trough, *Science* 304, 1295–1298, doi:10.1126/science.1096535.
- Liu, Y., and J. R. Rice (2005), Aseismic slip transients emerge spontaneously in three-dimensional rate and state modeling of subduction earthquake sequences, *J. Geophys. Res.* 110, B08307, doi:10.1029/2004JB003424.
- Lowry, A. R. (2006), Resonant slow fault slip in subduction zones forced by climatic load stress, *Nature* 442, 802–805, doi:10.1038/nature05055.
- Mazzotti, S., and J. Adams (2004), Variability of near-term probability for the next great earthquake on the Cascadia subduction zone, *Bull. Seismol. Soc. Am.* 94, 1954–1959.
- McCaffrey, R. (2009), Time-dependent inversion of three component continuous GPS for steady and transient sources in northern Cascadia, *Geophys. Res. Lett.* 36, L07304, doi:10.1029/2008GL036784.
- McCrory, P. A., J. L. Blair, D. H. Oppenheimer, and S. R. Walter (2004), Depth to the Juan de Fuca slab beneath the Cascadia subduction margin: A 3-D model for sorting earthquakes, *U.S. Geol. Surv. Data Ser. DS-91*.
- McGuire, J. J., and P. Segall (2003), Imaging of aseismic fault slip transients recorded by dense geodetic networks, *Geophys. J. Int.* 155, 778–788.
- Melbourne, T. I., W. M. Szeliga, M. M. Miller, and V. M. Santillan (2005), Extent and duration of the 2003 Cascadia slow earthquake, *Geophys. Res. Lett.* 32, L04301, doi:10.1029/2004GL021790.
- Miller, M. M., D. J. Johnson, C. M. Rubin, H. Dragert, K. Wang, A. Qamar, and C. Goldfinger (2001), GPS determination of along-strike variations in Cascadia margin kinematics: Implications for relative plate motion, subduction zone coupling, and permanent deformation, *Tectonics* 20, 161–176.

- Miller, M. M., T. Melbourne, D. J. Johnson, and W. Q. Sumner (2002), Periodic slow earthquakes from the Cascadia subduction zone, *Science* 295, 2423.
- Miyazaki, S., J. J. McGuire, and P. Segall (2003), A transient subduction zone slip episode in southwest Japan observed by the nationwide GPS array, *J. Geophys. Res.* 108(B2), 2087, doi:10.1029/2001JB000456.
- Murray, J. R., and P. Segall (2005), Spatiotemporal evolution of a transient slip event on the San Andreas fault near Parkfield, California, *J. Geophys. Res.* 110, B09407, doi:10.1029/2005JB003651.
- Nadeau, R. M., and L. R. Johnson (1998), Seismological studies at Parkfield VI: Moment release rates and estimates of source parameters for small repeating earthquakes, *Bull. Seismol. Soc. Am.* 88, 790–814.
- Obara, K. (2002), Nonvolcanic deep tremor associated with subduction in southwest Japan, *Science* 296, 1679–1681.
- Rogers, R., and H. Dragert (2003), Episodic tremor and slip on the Cascadia subduction zone: The chatter of silent slip, *Science* 300, 1942–1943, doi:10.1126/science.1084783.
- Royle, G. T., A. J. Calvert, and H. Kao (2006), Observations of nonvolcanic tremor during the northern Cascadia slow-slip event in February 2002, *Geophys. Res. Lett.* 33, L18313, doi:10.1029/2006GL027316.
- Rubinstein, J. L., M. La Rocca, J. E. Vidale, K. C. Creager, and A. G. Wech (2008), Tidal modulation of nonvolcanic tremor, *Science* 319, 186–189.
- Sammis, C. G., and J. R. Rice (2001), Repeating earthquakes as lowstress-drop events at a border between locked and creeping fault patches, *Bull. Seismol. Soc. Am.* 91, 532–537.
- Schwartz, S. Y., and J. M. Rokoşky (2007), Slow slip events and seismic tremor at circum-Pacific subduction zones, *Rev. Geophys.* 45, RG3004, doi:10.1029/2006RG000208.
- Segall, P., and M. Matthews (1997), Time-dependent inversion of geodetic data, *J. Geophys. Res.* 102, 22,391–22,409.
- Segall, P., R. Bürgmann, and M. Matthews (2000), Time-dependent triggered afterslip following the 1989 Loma-Prieta earthquake, *J. Geophys. Res.* 105, 5615–5634.

- Shen, Z. K., Q. L. Wang, R. Bürgmann, Y. G. Wan, and J. Y. Ning (2005), Pole-tide modulation of slow slip events at circum-Pacific subduction zones, *Bull. Seismol. Soc. Am.* *95*, 2009–2015.
- Shibazaki, B., and Y. Iio (2003), On the physical mechanism of silent slip events along the deeper part of the seismogenic zone, *Geophys. Res. Lett.* *30(9)*, 1489, doi:10.1029/2003GL017047.
- Szeliga, W., T. I. Melbourne, M. M. Miller, and V. M. Santillan (2004), Southern Cascadia episodic slow earthquakes, *Geophys. Res. Lett.* *31*, L16602, doi:10.1029/2004GL020824.
- Szeliga, W., T. Melbourne, M. Santillan, and M. Miller (2008), GPS constraints on 34 slow slip events within the Cascadia subduction zone, 1997–2005, *J. Geophys. Res.* *113*, B04404, doi:10.1029/2007JB004948.
- Thomas, A. L. (1993), Poly3D: A three-dimensional, polygonal element, displacement discontinuity boundary element computer program with applications to fractures, faults, and cavities in the earth's crust, M.S. thesis, 221 pp., Stanford Univ., Stanford, Calif.
- Tichelaar, B. W., and L. J. Ruff (1993), Depth of seismic coupling along subduction zones, *J. Geophys. Res.* *98*, 2017–2037.
- Wang, K., J. He, H. Dragert, and T. S. James (2001), Three-dimensional viscoelastic interseismic deformation model for the Cascadia subduction zone, *Earth Planets Space* *53*, 295–306.
- Wang, K., H. Dragert, H. Kao, and E. Roeloffs (2008), Characterizing an “uncharacteristic” ETS event in northern Cascadia, *Geophys. Res. Lett.* *35*, L15303, doi:10.1029/2008GL034415.
- Weaver, C. S., and K. M. Shedlock (1996), Estimates of seismic source regions from the earthquake distribution and regional tectonics in the Pacific Northwest: in *Assessing Earthquake Hazards and Reducing Risk in the Pacific Northwest*, edited by A. M. Roger et al., *U.S. Geol. Surv. Prof. Pap.* *1560*, 285–306.
- Wech, A. G., and K. C. Creager (2007), Cascadia tremor polarization evidence for plate interface slip, *Geophys. Res. Lett.* *34*, L22306, doi:10.1029/2007GL031167.
- Wells, R. E., and R. W. Simpson (2001), Northward migration of the Cascadia forearc in the northwestern U.S. and implications for subduction deformation, *Earth Planets Space* *53*, 275–283.

Chapter V

- Aki, K. (1979), Characterization of barriers on an earthquake fault, *J. Geophys. Res.* 84, 6140-6148.
- Anagnos, T., and A. S. Kiremidjian (1984), Stochastic time-predictable model for earthquake occurrences, *Bull. Seism. Soc. Am.* 74, 2593-2611.
- Audet, P., M. G. Bostock, N. I. Christensen, and S. M. Peacock (2009), Seismic evidence for overpressured subducted oceanic crust and mega-thrust fault sealing, *Nature* 457, 76-78.
- Beeler, N. M., and T. E. Tullis (1996), Self-healing slip pulse in dynamic rupture models due to velocity-dependent strength, *Bull. Seism. Soc. Am.* 86, 1130-1148.
- Beroza, G. C., and P. Spudich (1988), Linearized inversion for fault rupture behavior: application to the 1984 Morgan Hill, California, earthquake, *J. Geophys. Res.* 93, 6275-6296.
- Beroza, G. C., and T. Mikumo (1996), Short slip duration in dynamic rupture in the presence of heterogeneous fault properties, *J. Geophys. Res.* 101, 22449-22460.
- Brown, K. M. *et al.* (2005), Correlated transient fluid pulsing and seismic tremor in the Costa Rica subduction zone, *Earth Planet. Sci. Lett.* 238, 189–203.
- Day, S. M. (1982), Three-dimensional finite difference simulation of fault dynamics: Rectangular faults with fixed rupture velocity, *Bull. Seism. Soc. Am.* 72, 705-727.
- Dragert, H., K. Wang, and T. S. James (2001), A silent slip event on the deeper Cascadia subduction interface, *Science* 292, 1525-1528.
- Geller, R. J. (1976), Scaling relations for earthquake source parameters and magnitudes, *Bull. Seism. Soc. Am.* 66, 1501-1523.
- Hanks, T. C., and W. H. Bakun (2002), A bilinear source-scaling model for M-log A observations of continental earthquakes, *Bull. Seism. Soc. Am.* 92, 1841-1846.
- Heaton, T. H. (1990), Evidence for and implications of self-healing pulses of slip in earthquake rupture, *Phys. of the Earth and Planetary Interiors* 64, 1-20.
- Hirose, H., and K. Obara (2005), Repeating short- and long-term slow slip events with deep tremor activity around the Bungo channel region, southwest Japan, *Earth Planet. Sci. Lett.* 57, 961- 972.

- Houston, H. (2001), Influence of depth, focal mechanism, and tectonic setting on the shape and duration of earthquake source time functions, *J. Geophys. Res.* 106, 11,137- 11,150.
- Houston, H. (2010), Reconciling the diverse spectro-spatio-temporal patterns of ETS and earthquakes, *EarthScope Institute on the Spectrum of Fault Slip Behaviors*.
- Ide, S., G. C. Beroza, D. Shelly, and T. Uchide (2007), A scaling law for slow earthquakes, *Nature* 447, 76-79.
- Ide, S. *et al.* (2008), Bridging the gap between seismically and geodetically detected slow earthquakes, *Geophys. Res. Lett.* 35, L10305.
- Ito, Y., and K. Obara (2006), Very low frequency earthquakes within accretionary prisms are very low stress-drop earthquakes, *Geophys. Res. Lett.* 33, L09302.
- Ito, Y. *et al.* (2007), Slow earthquakes coincident with episodic tremors and slow slip events. *Science* 315, 503-506.
- Johnson, L. R., and R. M. Nadeau (2002), Asperity model of an earthquake: Static problem, *Bull. Seism. Soc. Am.* 92, 672-686.
- Kanamori, H., and D. L. Anderson (1975), Theoretical basis of some empirical relations in seismology, *Bull. Seism. Soc. Am.* 65, 1073-1095.
- Kostoglodov, V. *et al.* (2003), A large silent earthquake in the Guerrero seismic gap, Mexico, *Geophys. Res. Lett.* 30, doi:10.1029/2003GL017219.
- Linde, A. T. *et al.* (1996), A slow earthquake sequence on the San Andreas fault, *Nature* 383, 65-68.
- Liu, Y., and J. R. Rice (2009), Slow slip predictions based on granite and gabbro friction data compared to GPS measurements in northern Cascadia, *J. Geophys. Res.* 114, B09407.
- Liu, Y., and A. M. Rubin (2010), Role of fault gouge dilatancy on aseismic deformation transients, *J. Geophys. Res.* 115, B10414.
- Marone, C. J., C. H. Scholz, and R. Bilham (1991), On the mechanics of earthquake afterslip, *J. Geophys. Res.* 96, 8441-8452.
- McCausland, W. A., K. C. Creager, M. L. Rocca, and S. D. Malone (2010), Short-term and long-term tremor migration patterns of the Cascadia 2004 tremor and slow slip episode using small aperture seismic arrays, *J. Geophys. Res.* 115, B00A24.

- Miller, M., T. Melbourne, D. J. Johnson, and W. Q. Sumner (2002), Periodic slow earthquakes from the Cascadia subduction zone, *Science* 295, 2423.
- Montgomery-Brown, E. K., P. Segall, and A. Miklius (2009), Kilauea slow slip events: Identification, source inversions, and relation to seismicity, *J. Geophys. Res.* 114, B00A03.
- Murray, J., and P. Segall (2002), Testing time-predictable earthquake recurrence by direct measurement of strain accumulation and release, *Nature* 419, 287-291.
- Nadeau, R. M., and A. Guilhem (2009), Nonvolcanic tremor evolution and the San Simeon and Parkfield, California, Earthquakes, *Science* 325, 191-193.
- Obara, K. (2002), Nonvolcanic deep tremor associated with subduction in southwest Japan, *Science* 296, 1679-1681.
- Obara, K., H. Hirose, F. Yamamizu, and K. Kasahara (2004), Episodic slow slip events accompanied by non-volcanic tremors in southwest Japan subduction zone, *Geophys. Res. Lett.* 31, L23602.
- Obara, K. (2010), Phenomenology of deep slow earthquake family in southwest Japan: Spatiotemporal characteristics and segmentation, *J. Geophys. Res.* 115, B00A25.
- Ohta Y., J. T. Freymueller, S. Hreinsdóttir, and H. Suito (2006), A large slow slip event and the depth of the seismogenic zone in the south central Alaska subduction zone, *Earth Planet. Sci. Lett.* 247, 108-116.
- Rogers, G., and H. Dragert (2003), Episodic tremor and slip on the Cascadia subduction zone: The chatter of silent slip, *Science* 300, 1942-1943.
- Rubinstein, J. L. *et al.* (2007), Non-volcanic tremor driven by large transient shear stresses, *Nature* 448, 579-582.
- Schmidt, D. A., and H. Gao (2010), Source parameters and time-dependent slip distributions of slow slip events on the Cascadia subduction zone from 1998 to 2008, *J. Geophys. Res.* 115, B00A18, doi:10.1029/2008JB006045.
- Segall, P. *et al.* (2006), Earthquakes triggered by silent slip events on Kilauea volcano, Hawaii, *Nature* 442, 71-74.
- Sekine, S., H. Hirose, and K. Obara (2010), Along-strike variations in short-term slow slip events in the southwest Japan subduction zone, *J. Geophys. Res.* 115, B00A27.

- Shelly, D. R., G. C. Beroza, H. Zhang, and C. H. Thurber (2006), High-resolution subduction zone seismicity and velocity structure beneath Ibaraki Prefecture, Japan, *J. Geophys. Res.* *111*, B06311.
- Shelly, D. R., G. C. Beroza, and S. Ide (2007), Complex evolution of transient slip derived from precise tremor locations in western Shikoku, Japan, *Geochem. Geophys. Geosyst.* *8*, Q10014.
- Shibazaki, B., S. Bu, T. Matsuzawa, and H. Hirose (2010), Modeling the activity of short-term slow slip events along deep subduction interfaces beneath Shikoku, southwest Japan, *J. Geophys. Res.* *115*, B00A19.
- Shimazaki, K., and T. Nakata (1980), Time-predictable recurrence model for large earthquakes, *Geophys. Res. Lett.* *7*, 279-282.
- Shimazaki, K. (2002), Long-term probabilistic forecast in Japan and time-predictable behavior of earthquake recurrence, *Seismotectonics in Convergent Plate Boundary*, Eds. Y. Fujinawa and A. Yoshida, 37-43.
- Wallace, L. M. and J. Beavan (2006), A large slow slip event on the central Hikurangi subduction interface beneath the Manawatu region, North Island, New Zealand, *Geophys. Res. Lett.* *33*, L11301.
- Weldon, R., T. Fumal, and G. Biasi (2004), Wrightwood and the earthquake cycle: What a long recurrence record tells us about how faults work, *GSA Today* *14*, 4-10.